Analysis of PV/T air combi-panels with a semi-transparent absorber

Mollen, J.W.

Award date:
2005

Analysis of PV/T air combi-panels with a semi-transparent absorber

J.W. Mollen

MSc. Thesis
Reportnumber WET 2005.07

Supervisors: Prof.dr.ir. R.Ch.J. van Zolingen
Dr.ir. C.C.M. Rindt

Eindhoven University of Technology
Department of Mechanical Engineering
Division Thermo Fluid Engineering

Samenvatting

Voor de conversie van zonlicht in elektriciteit of thermische energie, is het gebruikelijk om twee aparte systemen te gebruiken. Het is ook mogelijk om zonnecollectoren en fotovoltaïsche cellen. Te combineren, zodat een systeem ontstaat waarmee tegelijkertijd warmte en elektriciteit geproduceerd kan worden. Als thermische en fotovoltaïsche omzetting worden gecombineerd, wordt dat een PV/T combipaneel genoemd.

Nieuwe dunne film zonnecel technologieën bieden de mogelijkheid om een deel van de instraling van het zonlicht dat de cel bereikt door te laten. Dit deel zal voor een groot deel bestaan uit straling met een lange golflengte, dat door de bandafstand van het zonnecel materiaal niet omgezet kan worden in elektriciteit. Deze doorgelaten instraling kan omgezet worden in thermische energie door een tweede absorber aan het paneel toe te voegen. Wanneer we nu een collector medium tussen de twee absorbers door laten stromen kan een deel van deze warmte hiernaar worden overgedragen. Er is gekozen om lucht te gebruiken als collector medium om de grote statische drukken bij het gebruik van water te voorkomen. Door de relatief slechte warmte overdracht eigenschappen van lucht is het van belang een groot warmtewisselend oppervlak te creëren.

Allereerst zijn enkele algemene overwegingen over de configuratie van het paneel onderzocht. Het bleek dat het goed zou zijn voor de thermische efficiency om een cover toe te voegen. Het toevoegen van een tweede cover zou de thermische efficiency maar licht laten stijgen, terwijl de elektrische efficiency er ook onder te lijden heeft. Verder concludeerden we dat het toevoegen van vinnen in het kanaal een positief effect heeft op de thermische efficiency van het systeem.

Door gebruik te maken van de energie stromen van, naar en in de collector zijn er energie balansen over de verschillende delen van het paneel opgezet. Deze energie balansen kunnen in elkaar worden ingevuld om uitdrukkingen voor het temperatuurverloop over de lengte van verschillende delen van het paneel te verkrijgen. Om de convectieve warmteoverdracht in het hellende paneel te beschrijven is er naar Nusselt relaties gezocht. Ook zijn de drukval en het resulterende ventilator vermogen dat nodig is om het collector medium te laten stromen gedefinieerd. Op deze manier kunnen de thermische en netto efficiency van het paneel berekent worden. Enkele betrouwbaarheidstests hebben uitgewezen dat het model betrouwbare resultaten voor temperaturen, warmte overdracht coëfficiënten en de thermische en netto efficiency geeft.

Hierna is een gevoeligheidsanalyse van de verschillende modelparameters uitgevoerd om de invloed op het prestaties van het paneel te vinden. De parameters die belangrijk zijn voor de thermische verliezen van het systeem zijn de emissie coëfficiënt van de bovenkant van de eerste absorber, de absorptie en transmissie coëfficiënt van de eerste absorber, de windsnelheid en de dikte van het isolatie materiaal. De thermische opbrengst van de collector kan worden verhoogd door een verhoging van de warmte overdracht coëfficiënt in het kanaal. Dit kan worden verwezenlijkt door de massastroom lucht te verhogen of de kanaalhoogte af te laten nemen.
Omdat het beïnvloeden van thermische verliezen moeilijk blijkt, wordt de warmte overdracht coëfficiënt in het kanaal verhoogd door vinnen toe te voegen.

Er is gebruik gemaakt van een eenvoudig 1-dimensionaal benadering om continue en plaat vinnen aan het model toe te voegen. Beide vinsoorten zorgen voor een toename van convectieve warmte overdracht in het kanaal. De invloed op het thermisch en netto vermogen is echter klein, aangezien het toevoegen van vinnen de temperatuur van de eerste absorber maar enigszins beïnvloeden. Ook is te zien dat de drukval over het collector medium kanaal voor snelheden die meestal in thermische zonnecollectoren wordt gebruikt maar relatief klein is.
Het wordt aanbevolen om te proberen de warmte overdracht coëfficiënt van de eerste absorber naar het collector medium te verhogen. Dit kan met behulp van smalle vinnen, of door het toevoegen van swirls aan de tweede absorber.

Abstract

Nowadays it is most common to use two separate systems to convert sunlight into electricity or thermal energy. It is also possible to combine solar heat collectors with photovoltaic cells to form hybrid energy units that simultaneously produce heat and electricity. When thermal and photovoltaic conversion is combined, it is called a PV/T combi-panel.

New thin film solar cell technologies offer the possibility to transmit part of the solar irradiance that hits the cell. This part will mainly consist of longwave radiation that cannot be converted into electricity due to the bandgap of the solar cell material. We can convert this transmitted irradiance into thermal energy by adding a second absorber to the panel. When we force a collector medium to flow between these two absorbers we can transfer part of the heat to the collector medium. We have chosen to use air as the collector medium to avoid the large static operating pressure of water. Because of its relatively poor heat transfer properties, it is essential to provide a large heat transfer area to remove the heat from the absorbers.

First a few general considerations for the panel configuration were investigated. It appeared to be beneficial to incorporate a cover to increase the thermal efficiency of the panel. The addition of a second cover will not increase the thermal efficiency very much, though it does provide an additional loss in electrical efficiency. We have also concluded that the addition of fins to the channel can be beneficial to increase the heat transfer to the collector medium.

Using the energy flows to from and inside the collector the energy balances over the various parts of the collector can be set up. These energy balances can be substituted in one another and in this way expressions for the temperatures over the length of the panel are formulated. Nusselt numbers have been found to help describe the convective heat transfer of an inclined solar panel. Also the pressure drop and resulting fan power that is needed to force the air through the collector and its support system has been specified. In this way the thermal and net efficiency of the channel can be calculated. Reliability tests show that the model gives reliable results for the calculation of temperatures, heat transfer coefficients and efficiencies.

A sensitivity analysis for the various parameters of the panel was performed in order to find out what parameters have what influence on the collector performance. Of importance for the thermal losses inside the panel is the emission coefficient of the top of the first absorber, the absorption and transmission coefficient of the first absorber, the wind speed and the insulation thickness.
The yield of the collector is influenced positively by an increase in heat transfer inside the collector medium channel. This can either be obtained by increasing the mass flow, or by decreasing the height of the channel.
Since it is hard to influence the thermal losses of the panel, the heat transfer coefficient inside the collector medium channel will be altered using fins.

A simple one-dimensional approach to try and model the addition of both continuous and offset fins to the second absorber was incorporated. It can be seen both continuous and offset fins provide an increase in the convection from the back absorber to the collector medium. The influence on the thermal and net yield is however marginal since the first absorber temperature can be made only slightly smaller through the use of fins. We can also see the additional pressure drop caused by the fins in the speed range normally used in solar air collectors does not cause a very large fan power increase.
It is recommended to increase the heat transfer from the first absorber to the collector medium in order to further lower the first absorber temperature. This can either be done by the addition of small fins directly to the first absorber or by adding swirls to the second absorber.

Nomenclature

Roman characters

A	area	[m^2]
B	cross section shape number	[-]
$C_{f,x}$	dimensionless skin friction coefficient	[-]
c_p	specific heat at constant pressure	[J/kg.K]
D_h	hydraulic diameter	[m]
E_g	bandgap	[eV]
E_p	photon energy	[eV]
f	friction factor	[-]
F'	collector efficiency factor	[-]
g	gravitational acceleration	[m/s^2]
Gr	Grasshof number	[-]
Gz	Greatz number	[-]
h	planck's constant	[Js]
h	heat transfer coefficient	[W/m^2K]
H	height	[m]
H_a	absorbed solar irradiance of the first absorber	[W/m^2]
H_b	absorbed solar irradiance of the second absorber	[W/m^2]
I_s	solar irradiance	[W/m^2]
k	thermal conductivity	[W/mK]
l	length	[m]
L	length	[m]
m	mass flow rate	[kg/s]
Nu	Nusselt number	[-]
p	perimeter	[m]
P	pressure	[N/m^2]
Pr	Prandtl number	[-]
q	heat transfer rate	[W]
Q	heat transfer	[J]
Ra	Rayleigh number	[-]
S	spacing between cover and absorber	[m]
T_b	temperature	[K]
V	velocity	[m/s]
U	loss coefficient	[W/m^2K]
U	velocity	[m/s]
w	width	[m]
W	work transfer rate	[W]
x	Cartesian coordinate	[m]

Greek characters

α	thermal diffusivity	[m^2/s]
α_1	absorption coefficient of the cover	[-]
α_2	absorption coefficient of the first absorber	[-]
α_3	absorption coefficient of the second absorber	[-]
β	coefficient of volumetric thermal expansion	[K^{-1}]
β	inclination angle	[°]
ε_1	emission coefficient of the cover	[-]
ε_2	emission coefficient of the first absorber	[-]
ε_3	emission coefficient of the second absorber	[-]
η	efficiency	[-]
ν	frequency	[s^{-1}]
ν	kinematic viscosity	[m^2/s]
ρ	density	[kg/m^3]
ρ_1	reflection coefficient of the cover	[-]
ρ_1	reflection coefficient of the first absorber	[-]

ρ_1	reflection coefficient of the second absorber	[-]
σ	Stefan-Boltzmann constant	[W/m^2K^4]
τ	skin friction coefficient	[N/m^2]
τ_1	transmission coefficient of the cover	[-]
τ_2	transmission coefficient of the first absorber	[-]
τ_3	transmission coefficient of the second absorber	[-]
ϕ	inclination angle	[°]

Subscripts

$()_a$	ambient
$()_b$	second absorber
$()_{ba}$	back
$()_c$	cover
$()_{conv}$	convection
$()_{cm}$	collector medium
$()_{coll}$	collector
$()_{Dh}$	hydraulic diameter
$()_e$	edge
$()_{el}$	electric
$()_{in}$	in
$()_L$	total loss
$()_{max}$	maximal
$()_{min}$	minimal
$()_{out}$	out
$()_p$	first absorber
$()_r$	radiation
$()_{ref}$	reference
$()_s$	sky
$()_t$	top
$()_{th}$	thermal
$()_u$	useful
$()_w$	wall
$()_{21}$	top of the first absorber
$()_{22}$	bottom of the first absorber
$()_\infty$	free stream

1 Introduction

1.1 General introduction

Radiation from the sun can be used to supply energy around the world. A few ways exist to convert solar energy into useable energy. Solar irradiation can be converted into electricity with solar cells. This is called photovoltaic conversion. Solar irradiation can also be converted into heat, which is called thermal conversion. Both conversion methods can be applied in one system. In this way we get a photovoltaic/thermal or PV/T panel.

Photovoltaic conversion
The generation of electricity from solar irradiation can be done using solar cells. The working principle of a solar cell will be explained using figure (1.1) (Zolingen, 2003):

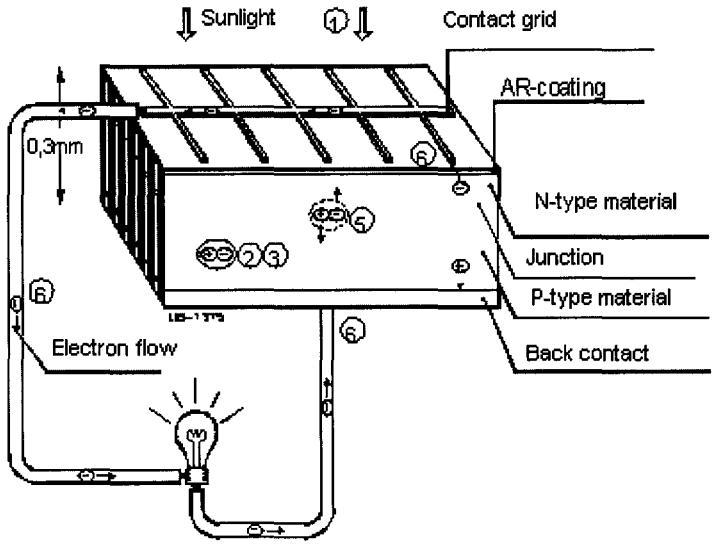

Figure 1.1: Construction and working principle of a photovoltaic solar cell.

The solar cell is made of semiconductor material, usually silicon, which is doped with impurities to create an extrinsic semiconductor. Dopants like phosphorus and arsenic create n-type material and dopants like boron or gallium create p-type material.
At the top of the cell a contact grid is applied to collect the power that is generated by the solar cell. Also an anti-reflection (AR) coating is applied at the top of the cell to minimize reflection from the cell. At the back of the cell a metal surface or contact grid is applied.

Light consists of photons, which are small particle-like packets that have energy and momentum but no mass. The energy of a photon is given by:

$$E_p = h\nu \tag{1.1}$$

where *(h)* is the Planck constant (6.625×10^{-34} (J·s)) and *(ν)* is the frequency.
When sunlight hits the solar cell, the photons will penetrate the material. Whether a photon is absorbed depends on the bandgap of the material.

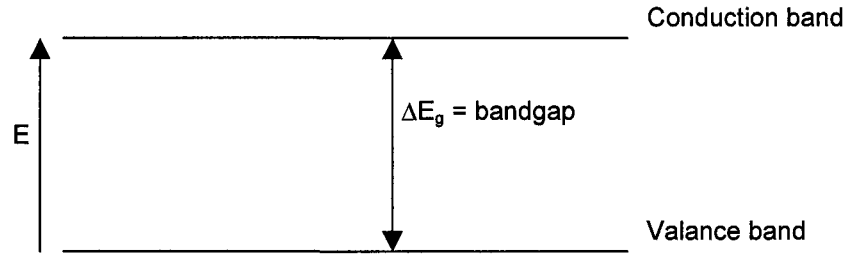

Figure 1.2: Valance and conduction band of a semi conductor.

The bandgap of a semiconductor is the energy difference between the valance band and the conduction band. The valance band is the band that is fully filled with electrons. The next band of permitted energy levels is called the conduction band.
Photons with energy higher than the bandgap *($h\nu \geq \Delta Eg$)* are absorbed. During the absorption of a photon, an electron from the valance band jumps into the conduction band. A hole in the valance band is left behind. The absorption of a photon thus creates an electron-hole pair.

A photon with an energy that is smaller than the bandgap *(ΔE_g)*:

$$h\nu < \Delta E_g \tag{1.2}$$

is not able to generate an electron-hole pair. This means that the solar energy for that part of the spectrum is lost for photovoltaic conversion, but could be used for generation of heat. These photons can also fall through the solar cell if a non-metallic back contact is used.

A photon with an energy that is equal or larger than the bandgap of the material:

$$h\nu \geq \Delta E_g \tag{1.3}$$

will be absorbed and will deliver an electron-hole pair. Losses will however also occur for every photon with $h\nu > \Delta E_g$. A photon can only create one electron-hole pair. The excess energy $h\nu - \Delta E_g$ of the photon will be converted into heat.

There are however more losses inside the solar cell, like recombination of the electron hole pair, which will be released in the form of heat.

Solar thermal conversion
Solar irradiation can also be used to produce thermal energy. The basic principle is that solar irradiance hits a sheet of material, usually metal, where it is absorbed and converted to heat. The heat that is generated in this way is then transferred to a collector medium. The medium can flow past the absorber directly or through tubes containing the collector medium attached to the absorber. One or more covers can be added to the panel to decrease the thermal losses to the environment.
The collector medium is usually water or air. Most solar thermal collectors use water as the collector medium because of its high density, large heat capacity and large heat conductivity compared to air. Water collectors therefore have good heat transfer properties. The disadvantages are the high operating pressure and the fact that water freezes and boils and is very sensitive to leaking. The collector medium can be used to heat tap water or ventilation air or can be stored for future use.

PV/T panels
Inside a combi-panel (PV/T or Photovoltaic/Thermal panel) both electrical and thermal energy are collected. A lot of combi-panel concepts are imaginable. The type of solar technology that is used and the kind of collector medium determine the choice of a combi-panel concept. In this particular report, air will be used as the collector medium and the concept of a second absorber will be examined.
Combi-panels have several advantages in that an area covered with combi-panels produces more electrical and thermal energy than a corresponding area partially filled with conventional PV systems and partially filled with conventional thermal collectors. Also the installation costs are reduced.

1.2 Problem definition

New solar cell technologies offer different possibilities for the realization of combi-panel concepts. As explained in § 1.1 photons with an energy smaller than the bandgap ($h\nu < \Delta E_g$), will not be absorbed, but, in the case of a non-metallic back contact, will be transmitted.
The bandgap for a singular thin-film amorphous silicon solar cell is relatively high. This means that the contribution of non-absorbed longwave radiation in this type of solar cell is in the order of 30 %. This radiation can be caught by a second absorber.
In a two-absorber combi-panel, the solar cell is considered as the first absorber and the second absorber is used to capture the longwave radiation, which wasn't absorbed by the first one. A schematic overview of a two-absorber concept is shown in figure (1.3).

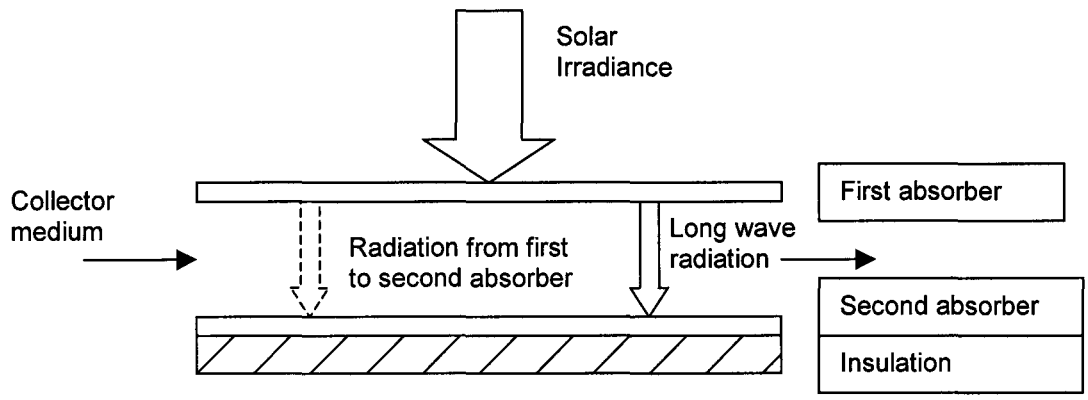

Figure 1.3: Schematic representation of a situation with two absorbers.

The principle of the application of a second absorber can be explained using this figure. Part of the solar energy that hits the first absorber will be absorbed by the solar cell. Part of the photons will be converted into electricity. Another part will however be converted into heat (through recombination and excess energy photons), allowing the temperature of the first absorber to rise. The temperature difference with the second absorber will cause radiative heat transfer from the first to the second absorber. Also the non-absorbed longwave radiation will fall through the first absorber directly onto the second, causing the second absorber to heat up. By situating the second absorber in the air channel behind the first absorber, the captured heat can be transferred to the collector medium.

The problem can be subdivided into the following subjects:
- The assessment of suitable two-absorber combi-panel configurations, featuring air as the collector medium.
- Determine what a suitable second absorber would be.
- Build a general model for the heat transfer in a suitable combi-panel concept with an air channel behind the first absorber.

- Find out what parameters influence the performance of a PV/T panel in what way.

1.3 Outline of the report

The report will discuss different concepts for PV/T air solar collectors in chapter 2. Examples are concepts with different amounts of top covers, the addition of fins inside the collector medium channel and a different type and location of the second absorber.
In chapter 3 a thermal model is developed for a basic two-absorber panel. After defining the efficiencies, the energy balance over the different parts of the panel is described, together with the solution procedure, in order to calculate the relevant temperature profiles and the resulting efficiency. To solve this model, the relevant Nusselt numbers and pressure drop over the collector will be defined. Finally a few tests will be performed to validate the reliability of the model.
In chapter 4, the results obtained with the basic two-absorber model will be presented. First the model output parameters will be defined. Next a sensitivity analysis of the model input parameters will be performed. This will determine which parameters have the largest influence on the performance of the collector.
Chapter 5 focuses on the modeling of the two-absorber panel with fins attached to the second absorbers. These fins should improve the heat transfer to the collector medium. The model as described in chapter 3 will be altered and new Nusselt relationships and pressure drop relations will be presented. Sensitivity analysis for the different finned configurations will be performed and the differences with the model described in chapter 3 will be noted.
Chapter 6 will feature the discussion of the results obtained from the different models.

2 Different PV/T configurations

Until now combi-panels mostly use water as the collector medium. In this research however air will be used as the collector medium and the effect of (semi) transparent absorbers will be researched. In this chapter different considerations for PV/T configurations featuring air as the collector medium will be treated. In this way suitable configurations for such a PV/T panel can be deduced. First the basic concepts of a PV/T will be explained using figure (2.1):

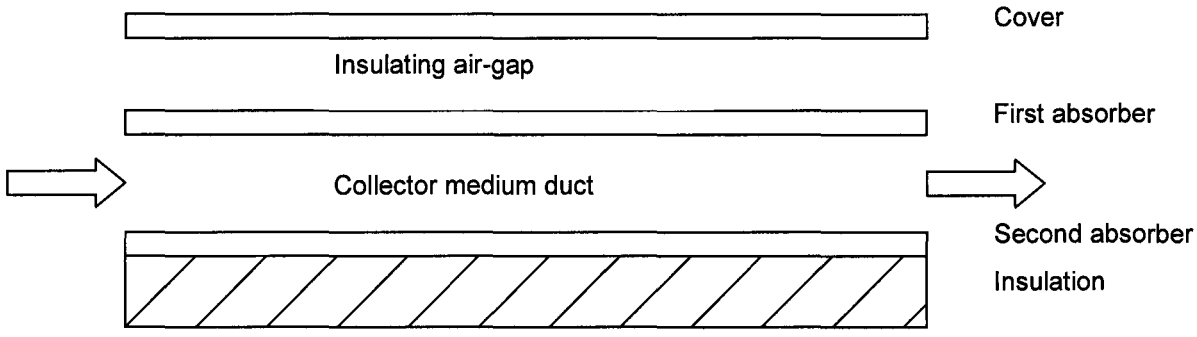

Figure 2.1: Schematic overview of a basic PV/T panel.

A basic PV/T panel consists of one or more covers of transparent material, like glass or plastic. The cover(s) provide an insulating air-gap between the first absorber and the cover(s). This means the convection from the top will be reduced. The cover however also reflects part of the solar irradiance, which is lost for both photovoltaic and thermal conversion.
Between the first and second absorber a duct exists through which the collector medium flows. The collector medium then enters the support system, which directs the air to the location where it can be either stored or used for space heating or crop drying. The air is forced through the collector and support system by a fan. The collector medium will collect part of the heat that is thermally converted from solar irradiation by both absorbers. The PV/T panel is insulated on all sides except the top to minimize heat losses to the ambient.
For a better understanding of the optical processes inside a PV/T panel, the reflection, absorption and transmission inside the collector will be treated.

2.1 General considerations for PV/T configurations

The panel shown in figure (2.1) can be altered in a few ways:

- The amount of top covers can be altered.
- Tubes containing the collector medium can be attached to the absorber instead of letting it flow directly past the absorber. This is called a sheet and tube configuration.
- Fins can be added to the absorbers to increase the heat transfer to the collector medium.
- The type, material and location of the absorbers may vary.

2.1.1 Covers

The purpose of a transparent cover is to transmit the short wavelength radiation from the sun (300 to 2500 [nm]) and block the long wavelength re-radiation from the absorber plate. Figure (2.2) shows the transmission as a function of the wavelength for a suitable cover (Goswami 2000):

Figure 2.2: Transmission (τ) vs. wavelength of a glass cover.

A transparent cover also reduces the heat loss by convection from the top of the absorber plate. In order to minimize the upward heat loss from the collector, more than one transparent glazing may be used. The increase in number of plates will however lead to a decrease in transmission. The reflection from a cover is about 8 to 10 % of the total irradiance. Figure (2.3) shows the total transmission of a cover vs. the angle of incidence of the solar radiation (Goswami, 2000). It also illustrates the transmission reduction by an increased number of covers.

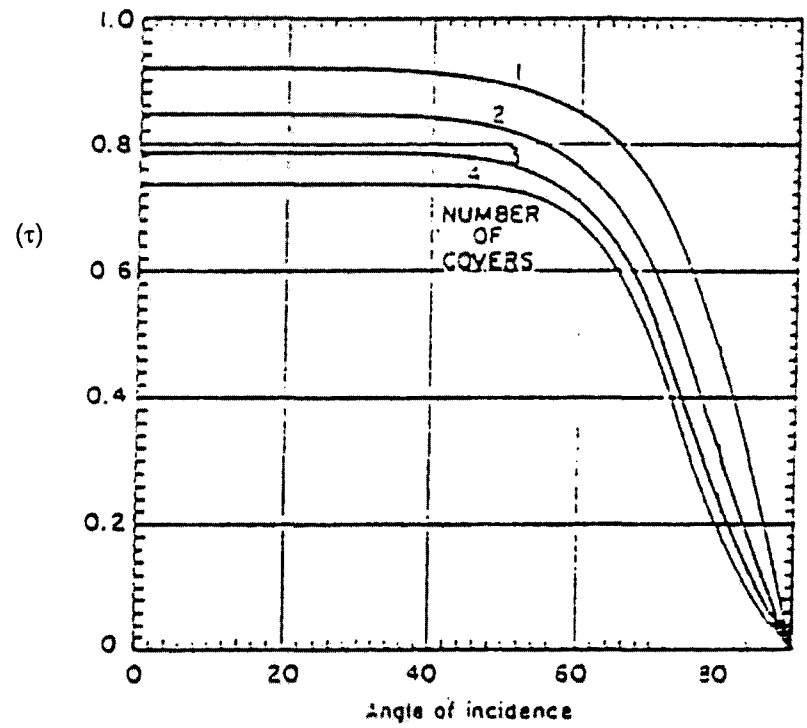

Figure 2.3: Transmission (τ) vs. angle of incidence for different amount of covers (θ).

Adding additional covers to the configuration can lead to a better thermal performance. The electrical output shall however decrease with every added cover.
The addition of one cover will deliver a large addition in thermal output and a small drop in electrical output. The addition of a second cover will provide a small addition in thermal performance and another drop in electrical output. Therefore the optimal configuration is assumed to have one transparent cover.

2.1.2 Channel construction vs. sheet and tube configuration

The basic air-cooled collector differs from the liquid based collectors because of the relatively poor heat transfer properties of air. A sheet and tube configuration consists of a plate with tubes attached to it through which the collector medium flows. Figure (2.4) shows the difference between the two types of configurations schematically:

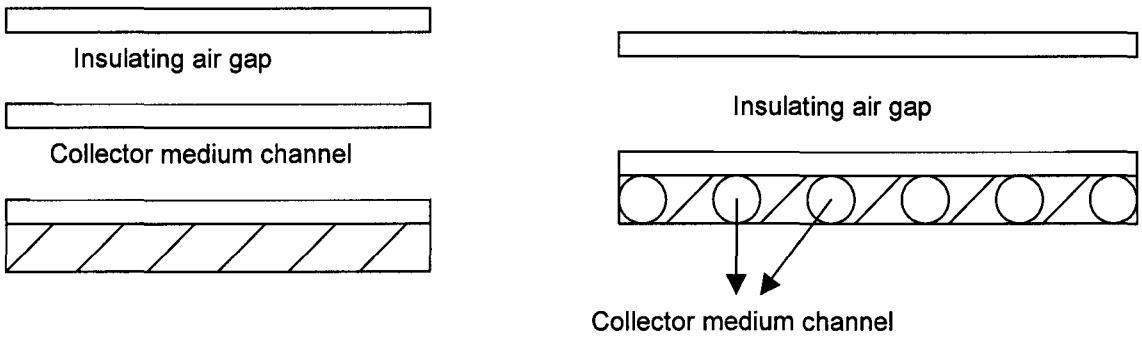

Figure 2.4: Schematic view of a channel construction and a sheet and tube configuration.

Liquid based collectors often use the sheet and tube design because the static operating pressure would become too high in a narrow water channel configuration. Air based collectors however are not constrained by the high pressure experienced in liquid based collectors. The most common way to achieve adequate heat transfer is to flow air over the entire surface of the absorber, thus making the surface for heat exchange as large as possible. A flat plate collector with channel construction is therefore preferable and will be used.

2.1.3 Addition of fins to the absorber

As mentioned in § 2.1.2 heat has to be transferred effectively from the absorber to the collector medium to accomplish high thermal efficiencies. This will decrease the temperature of the first absorber and thus the heat losses through the cover. There are a few ways to increase the heat transfer inside the collector medium channel, like roughening the surface and adding fins. Roughening the surface leads to an increase of the Reynolds number. Since most Nusselt-relationships depend on the Reynolds number, the heat transfer coefficient will increase. As the friction factor also depends on the Reynolds number, the required fan power will also increase. The fins can be classified as either continuous or offset strip fins.

Continuous fins are fins that exist along the entire length of the channel. A schematic front view of such a finned 2-absorber model is shown in figure (2.3).
The collector medium in this case flows out of the paper. The advantage of continuous fins is a larger heat exchange area and thus a higher thermal output.
The disadvantage is that measures that provide an increase in heat transfer generally increase the pressure drop. The fan power needed will therefore increase. In order to reduce the electrical power necessary to pump the air through the collector the pressure drop inside the panel has to be minimized.

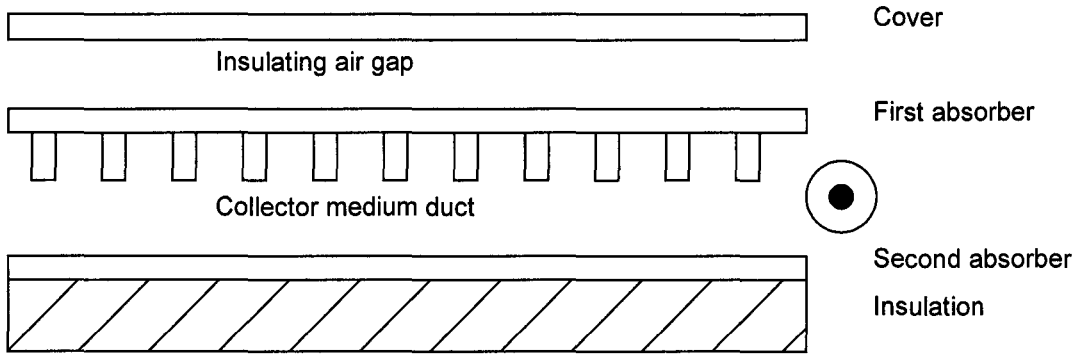

Figure 2.5 Schematic side and top view of a channel with continuous fins.

Offset strip fins are usually oriented in the flow direction. Because boundary layers vanish and redevelop periodically in the channel, the heat transfer coefficient will be high. There is off course an associated increase in pressure drop due to the increased friction. An example of a possible configuration for offset fins is shown in figure 2.4

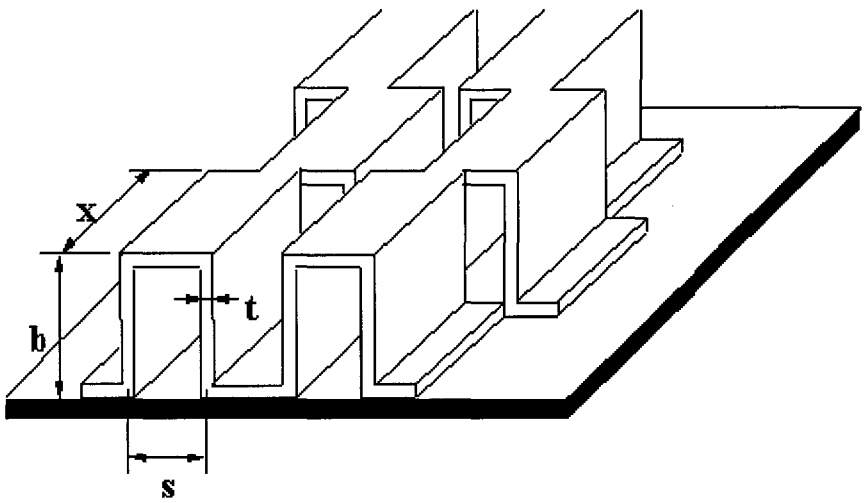

Figure 2.6: Possible configuration of offset strip fins inside a channel.

The simulations in chapter 5 will determine whether the addition of both continuous and offset strip fins has a positive effect on the output of the 2-absorber panel.

2.1.4 Considerations concerning the absorbers

The first absorber can differ in a few ways. This mainly depends on the type of solar cells used, because this determines what part of the solar irradiance is reflected, what part is absorbed (for PV or thermal application) and, if the solar cell has a transparent back encapsulment, what part is transmitted.
The second absorber can differ in material choice, type of absorber and location of the absorber. The purpose of the second absorber is to absorb as much of the incident solar radiation as possible and to allow efficient heat transfer to the collector medium. Generally a metal like aluminum or copper is used, because of its high absorption factor.

There are a few ways in which the basic PV/T configuration from figure (2.1) can be altered.
A variation on the PV/T-air solar panel design is shown in figure (2.7):

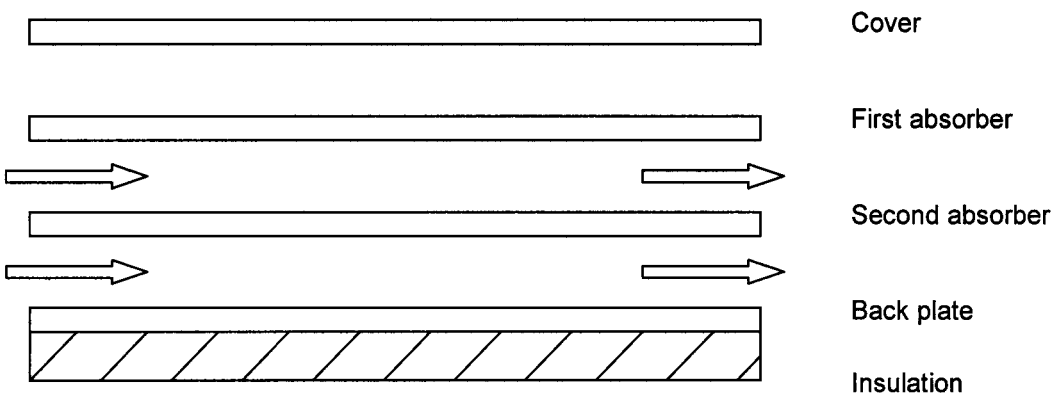

Figure 2.7: Schematic representation of a configuration with the second absorber halfway the collector channel.

Here the second absorber is placed halfway the collector medium channel. A back plate now acts as a third absorber. A research by Tripanagnostopoulos (2001) states this has a positive effect on the heat output of the collector. This type of panel will however not be included in the present research.

The second absorber can also be taken as a porous absorber. The advantage of a porous absorber is the large heat exchange area, compared to flat plate channel configuration. The disadvantages are the limited velocities and the sensitivity to fouling. The choice of a porous absorber should therefore be taken based on several boundary conditions: Averaged irradiation, the subsequent absorbed heat and the pressure drop. Although the porous absorber might have a positive impact on the yield of the collector, it will not be discussed in further detail in this report

2.2 Reflection, absorption and transmission inside the collector

When radiation hits a body in general three things can happen.

- A portion can be absorbed, defined with the total absorptivity α.
- A portion can be reflected, defined with the total reflectivity ρ.
- A portion can be transmitted, defined with the total transmissivity τ.

Because the energy inside the system must be conserved, the added value of these free components will be equal to one:

$$\alpha + \rho + \tau = 1 \qquad (2.1)$$

Figure (2.8) gives a schematic presentation of these processes when solar irradiance hits a basic PV/T panel. Solar irradiance of intensity I_s hits the cover. When the solar irradiance hits the cover at a right angle, as much as 92 % is transmitted (τ_1). A large part of the remaining irradiance will be reflected (ρ_1) a small part is absorbed (α_1). The transmitted irradiance through the cover then falls onto the first absorber. How much of the irradiance is absorbed (α_2) for conversion in electricity and heat depends on the type of solar cell used.

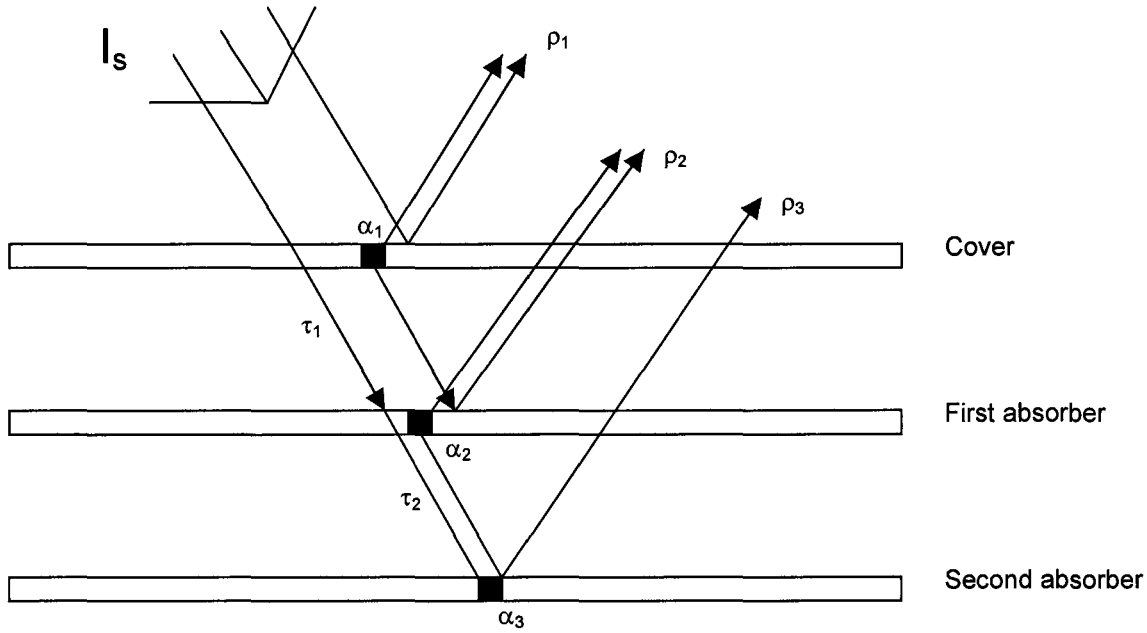

Figure 2.8: Schematic representation of solar irradiance on a PV/T collector.

If the back encapsulates of the cell is not opaque ($\tau = 0$) part of the non-absorbed long wave radiation will be transmitted (τ_2) and part will be reflected (ρ_2). It is assumed that the reflection from all surfaces inside the collector will be lost to the environment (§2.1). Finally the second absorber shall absorb a large part of the longwave transmitted radiation through the first absorber (α_3) and a small part is reflected to the ambient again (ρ_3). The second absorber will be opaque, which means the transmissivity (τ_3) is zero

The amount of solar irradiance absorbed by a unity-squared area of the absorbers can be written as:

$$H_a = I_s \tau_1 \alpha_2 \tag{2.2}$$

$$H_b = I_s \tau_1 \tau_2 \alpha_3 \tag{2.3}$$

The amount of transmitted solar irradiance that hits the second absorber thus depends largely on the transmission and absorption of the first absorber. If the solar cells have non-transparent back contacts the transmission will be zero. This means no irradiance is transmitted to the second absorber.
If however the back of the solar cell is made transparent, transmittance coefficients of 0.1 can be reached with crystalline silicon solar cell and transmittance coefficients of 0.3 can be reached for a thin-film amorphous silicon solar cell. The sun thus heats the second absorber directly. A possible influence on the performance of a PV/T panel will be researched now by modeling a basic PV/T 2-absorber panel.

3. Modeling of a basic two-absorber PV/T panel

The two-absorber panel uses a semi-transparent PV laminate as a primary absorber and a plate with high absorption coefficient as secondary absorber. Because a part of the long wavelength light that hits the first absorber is transmitted, the operating temperature of this absorber will not be as high in the case of an opaque first absorber. In this chapter the basic two-absorber PV/T panel will be modeled. First a general description of the configuration will be given, with a definition of its efficiency. All heat flows to, from and inside the panel will be specified. The resulting temperatures can be obtained by writing the energy balance over the different parts of the collector. After that Nusselt relationships for convective heat transfer of an inclined panel will be specified. Also the pressure drop calculations and the resulting fan power will be given. After this a few reliability tests will be performed.

3.1 General description of a two-absorber configuration

The general two-absorber panel consists of a transparent cover, the first semi-transparent absorber containing the photovoltaic cells and a back plate that acts as a second absorber. The plates are secured by a casing. The edges and back of the panel are well insulated to minimize the heat losses through conduction.
Between the cover and first absorber a dead air channel consists, which suppresses the convective heat transfer to the environment from the top. Between the first and second absorber a second channel consists, which contains the collector medium. The collector medium is forced through the channel by a fan. After the collector medium leaves the collector, it is transported through the support system to be either stored or used directly. The support system is considered to consist of a round tube to transfer the collector medium air to the place where it is stored or used directly. The configuration is schematically drawn in figure (3.1):

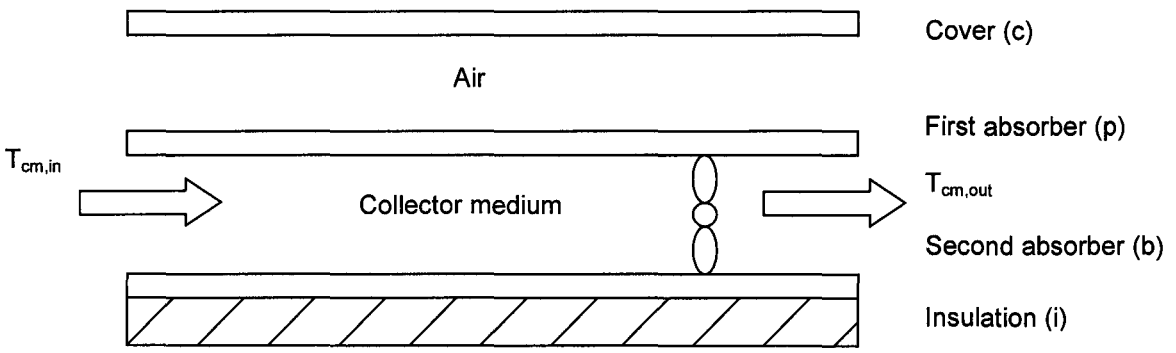

Figure 3.1: Schematic overview of the general two-absorber model.

3.1.1 Collector efficiency

The 'useful' power for a solar thermal collector is defined as the energy gain per second by the collector medium:

$$q_u = mc_{p,cm}\left(T_{cm,out} - T_{cm,in}\right) \tag{3.1}$$

Here m is the mass flow rate of the collector medium, $c_{p,cm}$ the heat capacity of the collector medium and $(T_{cm,out} - T_{cm,in})$ the temperature difference of the in and out flow. The solar energy

collection efficiency of a thermal collector is defined as the ratio of useful thermal power over the useable solar irradiance falling on the aperture area:

$$\eta_{th} = \frac{q_u}{A_{coll} I_s} \tag{3.2}$$

Here (A_{coll}) is the top area of the collector that is irradiated and (I_s) the solar irradiance. Combining equations (3.1) and (3.2) the equation for the collector efficiency becomes:

$$\eta_{th} = \frac{m_{cm} c_{p,cm} \left(T_{cm,out} - T_{cm,in}\right)}{A_{coll} I_s} \tag{3.3}$$

The first law of thermodynamics states that both electric and heat output are forms of energy. Thus a simplistic first law approach is to consider them of equal value. In this way a simple one-to-one energy approach to express the combined efficiency of thermal and electrical output is developed (Coventry, Lovegrove, 2003.
Since irradiance that has been used for photovoltaic conversion cannot be used to create thermal energy we must correct the absorption factor of the first absorber:

$$\alpha_2^{'} = \alpha_2 - \eta_{el} \tag{3.4}$$

Here (η_{el}) is the electrical efficiency of the cells and (α_2) the absorption factor of the semi-transparent absorber. In this research we will however assume all absorbed irradiance is converted into heat ($\alpha_2^{'} = \alpha_2$).

To obtain the net efficiency of the panel, we must take into account the fan power used to overcome the pressure drop inside the panel and its support system (W_{fan}). The net efficiency can now be defined as:

$$\eta_{net} = \frac{\dot{m}_{cm} c_{p,cm} \left(T_{cm,out} - T_{cm,in}\right) - W_{fan}}{A_{coll} I_s} \tag{3.5}$$

3.2 *Modeling of the two-absorber panel*

In this paragraph the energy balance over the various collector parts will be formulated. In order to do this the energy flows to, from and inside the collector will have to be specified (Garg, 1999). Using this balance a solution procedure to calculate the temperature distribution over the length of the channel will be given. Before the actual calculations can commence the Nusselt numbers, used to calculate the convective heat transfer coefficients, must be formulated. Also the pressure drop over the collector and its support system must be determined in order to calculate the net power output of the two-absorber panel. Finally the model will be subjected to some reliability tests.

With respect to the configuration shown in figure (3.1), a number of simplifying assumptions are made:

- The performance will be in steady state.
- There is no absorption of solar energy by covers (§ 2.2).
- The temperature difference in each part of the collector is dependent only on x, x being the flow direction. However heat conduction in x-direction is not accounted for.
- Reflected irradiance from a surface will be considered as lost to the environment.

3.2.1 Energy flows to, from and inside the collector

The energy flows that occur in the two-absorber panel are schematically drawn in figure (3.2).

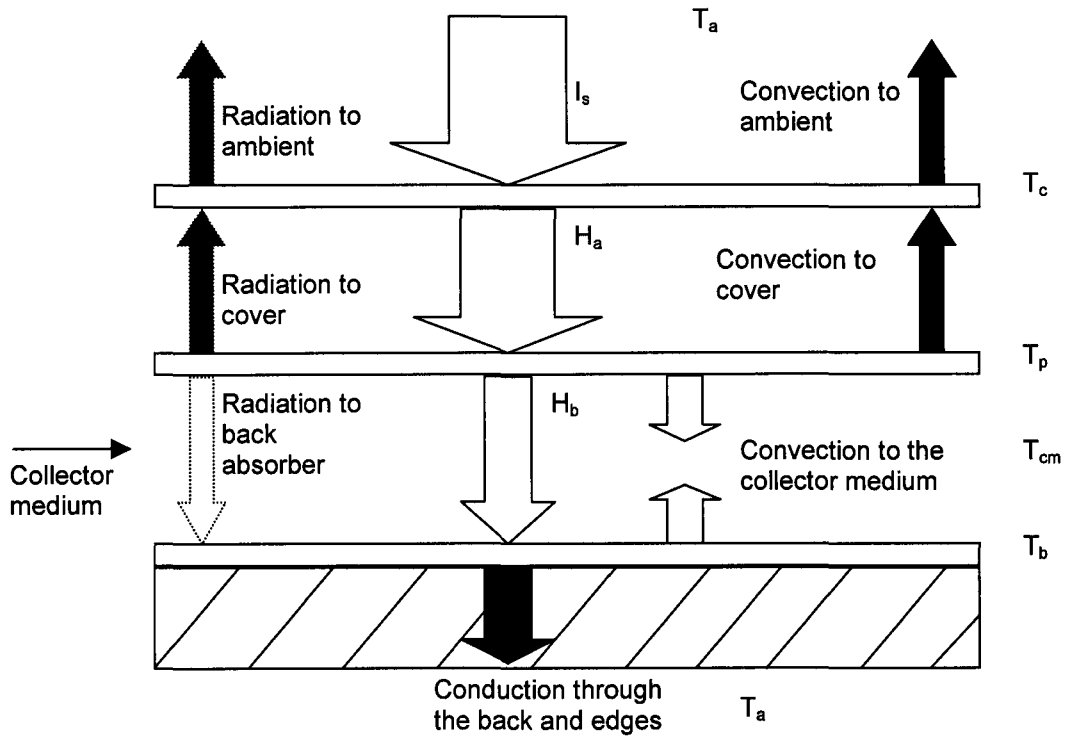

Figure 3.2: Schematic overview of the energy flows inside the two-absorber panel.

Solar irradiance hits the cover (I_s), where a large part is transmitted and a small part is reflected. The transmitted irradiance falls onto the first absorber, where a part is absorbed (H_a) and converted into heat and electricity, part is transmitted to the second absorber and part is reflected. A large part of the transmitted irradiance through the first absorber (H_b) will be converted into heat by the second absorber. A small part will be reflected.

As the first absorber heats up, part of its heat is lost due to radiation and convection to the cover. As a result, the cover will heat up and will transfer heat to the ambient through convection and to the sky through radiation.
The amount of solar irradiance that is absorbed combined with the losses experienced by both absorbers is usually not equal. The temperature of both absorbers will therefore differ, which means that radiative heat transfer between the first and second absorber will occur. Both absorbers will transfer heat to the collector medium via convection.
Although the panel is well insulated at the back and edges, conduction to the ambient will be inevitable.
Figure (3.2) also shows the symbols used to characterize the temperatures of the different parts of the collector: (T_c) is the cover temperature, (T_p) is the temperature of the first absorber, (T_{cm}) is the collector medium temperature, (T_b) is the second absorber temperature and (T_a) is the temperature of the ambient. A thermal network of the temperatures and the heat transfer coefficients in this system can be made.

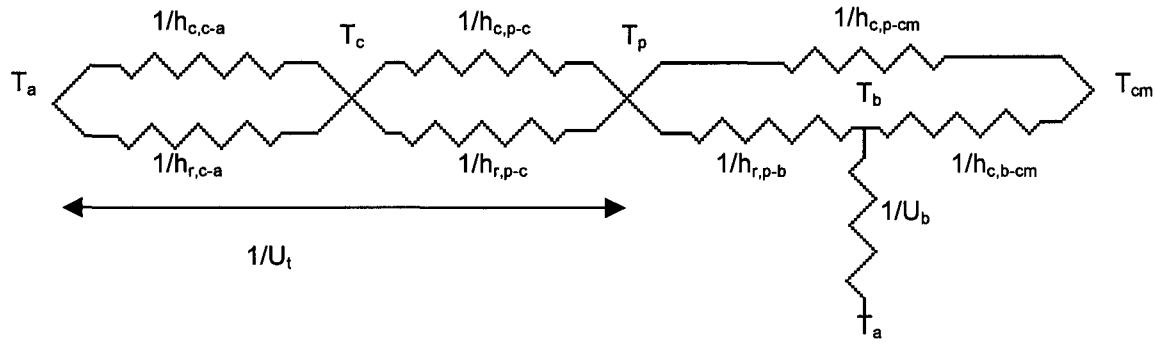

Figure 3.3: Thermal network of the two-absorber flat plate PV/T panel.

Figure (3.3) presents the heat flows from figure (3.2) as thermal resistances. We can see the temperatures are the same as those given in figure (3.2). The thermal resistances are defined as 1/h and 1/U.
Each heat transfer coefficient (h) has a subscript in which the heat transfer mechanism (c = convection, r = radiation) and the direction of the energy flow is given. For example $h_{c,c-a}$ is the heat transfer coefficient for convection between the cover and the ambient. The heat transfer coefficients (U) represent thermal loss mechanisms to the ambient and sky. U_b is the conductive heat transfer coefficient between the second absorber and the ambient. U_t is the top loss coefficient, which is a combination of the convective and radiative heat transfer from the first absorber to the cover and from the cover to the ambient.

Heat loss through the back and edges of the collector can be represented by two series of resistances. The first represents the resistance to conductive heat flow through the insulation and the second represents the convective and radiative heat flow resistance to the environment. The magnitudes of these two resistances is such that it is usually possible to assume the convective and radiative resistance is zero and all resistance to heat flow is due to insulation (Duffie, Beckman, 1980). The back loss coefficient U_{ba} can therefore be written as:

$$U_{ba} = \frac{k}{t_i} \tag{3.6}$$

Here *(k)* and *(t_i)* are the insulation thermal conductivity and thickness respectively. For most collectors the evaluation of edge losses is very complicated. In well-designed systems however, the edge losses are very small so they do not have to be predicted with great accuracy. It is assumed that the thickness of the bottom insulation is the same as that of the edges. In that case the altered back loss coefficient *(U_b)* can be written as a function of the edge losses *(U_e)* and the area of both the back *(A_b)* and edges *(A_e)* of the PV/T panel:

$$U_b = U_{ba} + \frac{A_e}{A_b} U_e \tag{3.7}$$

The top loss coefficient *(U_t)* describes the loss terms that exist between the first absorber and the ambient through the top. These terms can be seen in figure (3.2) as the four black arrows at the top of the panel and in figure (3.3) as the resistances from T_a on the left side to T_p. The top loss coefficient thus consists of radiative *($h_{r,p-c}$)* and convective *($h_{c,p-c}$)* heat transfer from the first absorber to the cover and radiative *($h_{r,c-a}$)* and convective *($h_{c,c-a}$)* heat transfer from the cover to the ambient:

$$U_t = \left(\frac{1}{h_{c,p-c} + h_{r,p-c}} + \frac{1}{h_{c,c-a} + h_{r,c-a}} \right)^{-1} \tag{3.8}$$

Convective heat transfer is the heat transfer process that is executed by the flow of a fluid. It can be either natural or forced. In natural convection the fluid flow is driven by the effect of buoyancy. In forced convection another entity pushes the medium past a solid body. The convective heat transfer rate can be written as:

$$q_c = A_{coll} h_c \Delta T \tag{3.9}$$

Here A_{coll} is the area of the collector, h_c is the convective heat transfer coefficient and ΔT is the difference in temperature between the wall and the fluid. The convective heat transfer coefficients inside the panel will be defined in § 3.2.4.

The radiative heat transfer coefficient between the first absorber and the cover can be given using the relationship for two infinite parallel plates (Bejan, 1993):

$$h_{r,p-c} = \frac{\sigma \left(T_p + T_c\right)\left(T_p^2 + T_c^2\right)}{\frac{1}{\varepsilon_p} + \frac{1}{\varepsilon_c} - 1} \tag{3.10}$$

Here (σ) is the Stefan Boltzmann coefficient, (ε_p) is the emission coefficient of the first absorber and (ε_c) is the emission coefficient of the cover.
From the top of the absorber, radiative heat transfer occurs between the cover and the sky. The radiative heat transfer coefficient in this situation can be given using the relationship for extremely large surfaces surrounding a convex surface (Bejan, 1993):

$$h_{r,c-a} = \frac{\sigma \varepsilon_c \left(T_c + T_s\right)\left(T_c - T_s\right)\left(T_c^2 + T_s^2\right)}{\left(T_c - T_s\right)} \tag{3.11}$$

(T_s) is considered as the sky temperature. The sky can be considered as a blackbody at some equivalent sky temperature. We will use the sky temperature for clear skies as proposed by Swinbank (1963), which relates the sky temperature to the local air temperature as:

$$T_s = 0.0552 T_a^{1,5} \tag{3.12}$$

The heat transfer from the first absorber to the second occurs through radiation. In this case again the relationship for two infinite parallel plates as described in formula (3.10) can be used:

$$h_{r,p-b} = \frac{\sigma \left(T_p + T_b\right)\left(T_p^2 + T_b^2\right)}{\frac{1}{\varepsilon_p} + \frac{1}{\varepsilon_b} - 1} \tag{3.13}$$

It is useful to develop the concept of an overall loss coefficient for a solar collector to simplify the mathematics. Energy can be lost trough the top, the bottom and the edges. Duffie and Beckman (1980) state that the overall loss coefficient (U_L) can be determined by adding the top, edge and back loss coefficients.
Therefore the total heat loss coefficient of a collector can be written as:

$$U_L = U_t + U_b \tag{3.14}$$

This is however not entirely true, because this is only the case when both absorbers have the same temperature. Both heat losses will be assumed to be dependable on the first absorber temperature (T_p). In § 3.3 the influence of this assumption on the collector performance will be checked.
It will also proof usefull to define a total heat transfer coefficient inside the collector medium channel. The heat transfer coefficients of the radiation from the first to the second absorber and the convection from both absorbers to the collector medium can be combined into:

$$h = h_{c,p-cm} + \left[\frac{1}{\frac{1}{h_{r,p-b}} + \frac{1}{h_{c,b-cm}}} \right] \tag{3.15}$$

Due to the assumptions made in formula (3.14) and (3.15) the thermal network can now be rearranged to:

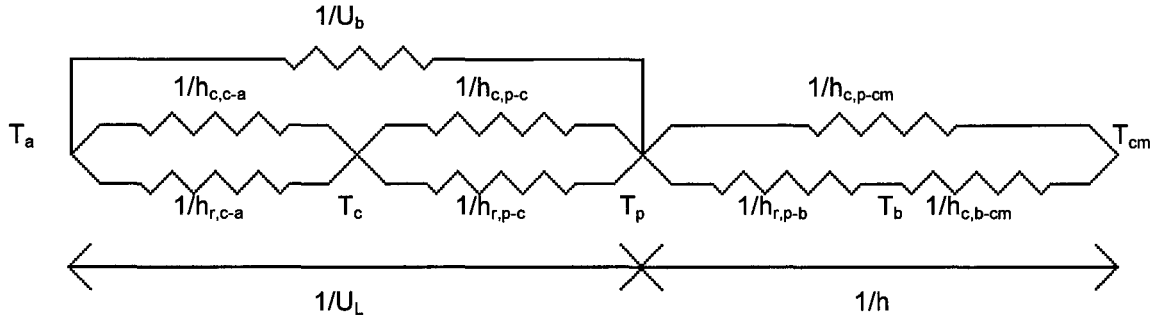

Figure 3.4: Altered thermal network of the two-absorber flat plate PV/T panel.

As can be seen in figure (3.4) the thermal network can now be considered to consists of two parts; $1/U_L$ and 1/h. The loss term $1/U_L$ consists of all resistances that are responsible for the losses in the system. It is of importance to keep this value low and with the help of the model the most influential heat transfer coefficients can be identified.
The value 1/h consist of the terms which eventually lead to the heat transfer to the collector medium. The value of h determines the yield that can be realized. An increase of this value can be achieved by the addition of fins to the absorber. The increase of thermal output will however be weight against the increase in fan power. This will be treated in chapter 5.

3.2.2 Energy balance over the various collector parts

Since all energy flows to, from and inside the collector are now known, an energy balance over the various collector parts can be formulated. The model is assumed to be quassi one-dimensional and therefore the energy balance will be given over een area (*dx.w*), where *dx* is a section over the length of the collector at a distance 'x' from the inlet of the collector and (w) is the collector width. The balances will be formulated using figure (3.2) and (3.4).

The energy balance over the first absorber consists of the absorbed solar irradiance (H_a) on the one side and the losses to the ambient, radiation to the second absorber and convection to the collector medium on the other:

$$H_a = U_L(T_p - T_a) + h_{c,p-cm}(T_p - T_{cm}) + h_{r,p-b}(T_p - T_b) \quad (3.16)$$

The energy balance over a small part of the collector medium consists of the convective heat transfer from both absorbers to the medium and the temperature rise that thus arises over an element *dx*:

$$\dot{m}c_p \frac{dT_{cm}}{dx} = h_{c,p-cm}(T_p - T_{cm}) + h_{c,b-cm}(T_b - T_{cm}) \quad (3.17)$$

Since the back losses are assigned to the overall losses, which originate from the first absorber, the energy balance at the back consists of the absorbed solar irradiance (H_b) and radiation from the first absorber to the second on one side and convection to the collector medium on the other:

$$H_b = h_{c,b-cm}(T_b - T_{cm}) + h_{r,p-b}(T_p - T_b) \quad (3.18)$$

3.2.3 Calculation of the temperatures

We now have a system of three equations, (3.16), (3.17) and (3.18) with three unknown temperatures T_{cm}, T_p and T_b. Rewriting the equations and substituting the expressions found for the temperatures should solve the system.

The temperature of the back plate can be rewritten from equation (3.18) to isolate the second absorber temperature:

$$T_b = \frac{h_{r,p-b}T_p + h_{c,b-cm}T_{cm} + H_b}{h_{r,p-b} + h_{c,b-cm}} \quad (3.19)$$

This expression for the temperature of the second absorber can be substituted in the balance of the absorber plate (3.16), which gives:

$$T_p(U_L + h) = H_a + \left(\frac{h_{r,p-b}}{h_{r,p-b} + h_{c,b-cm}}\right)H_b + U_L T_a + hT_{cm} \quad (3.20)$$

Here *h* is defined as in formula (3.15).
The expression for T_b, (3.19), can also be substituted in the energy balance equation of the collector medium (3.17):

$$h(T_p - T_{cm}) + \left(\frac{h_{c,b-cm}}{h_{r,p-b} + h_{c,b-cm}}\right)H_b = \dot{m}c_p \frac{dT_{cm}}{dx} \quad (3.21)$$

We now have 2 equations (3.20) and (3.21) with two unknown temperatures T_p and T_{cm}. Substituting equation (3.20) in (3.21) gives an expression for the medium temperature as a function of *x*, which is a function of the known parameters T_a, H_a and H_b:

$$\dot{m}c_p \frac{dT_{cm}}{dx} = F'\left[H_a + \left(\left(\frac{h_{r,p-b}}{h_{c,b-cm}} + 1 + \frac{U_L}{h}\right)\frac{h_{c,b-cm}}{h_{c,b-cm} + h_{r,p-b}}\right)H_b - U_L(T_{cm} - T_a)\right] \quad (3.22)$$

where

$$F' = \frac{h}{U_L + h} \tag{3.23}$$

The collector efficiency factor (F') is the ratio of the combined heat transfer coefficients inside the collector medium channel (h, formula 3.15) and the total heat transfer coefficient between the collector medium and the ambient air (U_L + h, see figure (3.4)) (Duffie & Beckman, 1980), (Goswami, 2000). At a particular location, F' represents the ratio of actual useful energy gain to the useful energy gain that would result if the two absorbers]q vad been at the local fluid temperature. It is essentially a constant for any collector design and fluid flow rate.

For every PV/T panel configuration F' can be deduced using the thermal network. This will also prove useful when fins are added to the absorbers (chapter 5).

The solution of the energy balance (3.22), a first order differential equation, can now be solved with the initial conditions $T_{cm}=T_{fluid,in}$ at x = 0 and the assumption that the heat transfer coefficients and material properties remain constant over the length x.

$$T_{cm} = \left[\frac{H_a}{U_L} + \left(\frac{1}{U_L} + \frac{1}{h}\frac{h_{c,b-cm}}{\left(h_{r,p-b} + h_{c,b-cm}\right)}\right)H_b + T_a\right] - \frac{1}{U_L}\left[H_a + \left(1 + \frac{U_L}{h}\frac{h_{c,b-cm}}{\left(h_{r,p-b} + h_{c,b-cm}\right)}\right)H_b - U_L\left(T_{fluid,in} - T_a\right)\right]\exp\left[\frac{-U_L F'}{\dot{m}c_p}x\right] \tag{3.24}$$

The energy loss through the top is the result of convection and radiation between two parallel plates. The energy transfer between the first absorber at T_p and the cover at T_c is equal to the energy lost to the surroundings from the cover. This can be written as:

$$q_{top} = A_{coll}U_t\left(T_p - T_{amb}\right) = A_{coll}\left(T_p - T_c\right)\left(h_{c,p-c} + h_{r,p-c}\right) \tag{3.25}$$

Formula (3.25) can be rewritten to obtain an expression for the cover temperature:

$$T_c = T_p - \frac{U_t\left(T_p - T_a\right)}{h_{c,p-c} + h_{r,p-c}} \tag{3.26}$$

We now have expressions for all temperatures over the length x of the collector, since all temperatures are calculated with the x-dependent collector medium temperature from formula (3.24). The only unknown parameters are the convective heat transfer coefficients of the model, which will be formulated in the next paragraph.

3.2.4 Definition of the convective heat transfer coefficients

The convective heat transfer coefficient is usually calculated using the dimensionless Nusselt number *(Nu)*. The Nusselt number is defined as the ratio of convective heat transfer to conduction heat transfer under the same conditions:

$$Nu_L = \frac{q(convection)}{q(conduction)} = \frac{hL}{k} \tag{3.27}$$

Here h is the convective heat transfer coefficient, L the characteristic length and k the thermal conductivity. The Nusselt numbers depend on the type of convection, natural or forced, and type of flow, laminar, transitional or turbulent flow.

Natural convection
Natural convection occurs when the fluid motion is driven by the effect of buoyancy. When heat is added to a gas, it expands, and thus changes density. If gravity is present this change in density induces a change in the body forces, and the forces may cause the fluid to move "by itself" without any externally imposed flow velocity. Nusselt correlations for natural convection are usually dependent on the dimensionless Rayleigh number *(Ra)*. This number is obtained if the momentum equation is solved in the case that buoyancy is balanced by friction. It is defined as:

$$Ra_L = \frac{g\beta(T_w - T_*)L^3}{\alpha\nu} \tag{3.28}$$

Where g is the gravitational acceleration, β is the coefficient of volumetric expansion, α is the thermal diffusivity, ν is the kinematic viscosity and T_w and T_* are the wall and free stream temperature respectively.

Forced convection
Forced convection occurs when an entity pushes the fluid past a solid body. Nusselt correlations for forced convection are dependent on the Reynolds number *(Re)*. This number is obtained when the momentum equation is solved in the case that inertia forces are balanced by friction and is defined as:

$$\mathrm{Re} = \frac{VL}{\nu} \tag{3.29}$$

Where V is the fluid velocity and ν is the kinematic viscosity of the fluid.

Both natural and forced convection can differ in flow regime.
There are in general three types of fluid flow:

- laminar
- turbulent
- transient

Laminar flow generally occurs when dealing with small length scales and low flow velocities. Laminar flow can be regarded as a series of smooth fluid blades of infinitesimal thickness, slipping past one another with different longitudinal speeds.

In turbulent flow vortices, eddies and wakes make the flow unpredictable. Turbulent flow happens in general at high flow rates and with larger pipes.

Transitional flow is a mixture of laminar and turbulent flow, with turbulence in the center of the pipe, and laminar flow near the edges. Each of these flows behave in different manners in terms of their frictional energy loss while flowing, and have different equations that predict their behavior.

The optimum angle with the earth for a solar collector in the Netherlands would be 37° with the earth in order to obtain a maximum yearly energy yield *(mysolar.com)* Therefore Nusselt numbers that satisfy this demand will be searched.

3.2.4.1 Convection from the cover to the ambient

Natural convection
At low wind speeds the convective heat transfer can be considered natural. The relevant Nusselt relationships shall differ with the inclination angle.

For a hot surface facing upwards, the Nusselt number varies as follows (Bejan, 1993):

$$Nu_L = 0.76 Ra_L^{1/4} \qquad \left(10^4 < Ra_L < 10^7\right) \tag{3.30}$$

$$Nu_L = 0.15 Ra_L^{1/3} \qquad \left(10^7 < Ra_L < 10^{10}\right) \tag{3.31}$$

where the characteristic length of the plane surface (L) is equal to the area of the plate (A) divided by the perimeter (p) of (A):

$$L = \frac{A}{p} \tag{3.32}$$

For inclined plates the definition of the Rayleigh number differs for turbulent and laminar flow [Bejan, 1993]. For turbulent natural flow the Rayleigh number defined in formula (3.28) can be used. For laminar flow however, a 'corrected' Rayleigh number is defined, dependent on the inclination angle φ:

$$Ra_L = \frac{(g\cos(\phi))\beta(T_w - T_*)L^3}{\alpha\nu} \tag{3.33}$$

For vertical plates the Nusselt number differs from formula (3.30) and (3.31). Duffie & Beckman (1980) give:

$$Nu_L = 0.59 Ra_L^{1/4} \qquad \left(10^4 < Ra_L < 10^7\right) \tag{3.34}$$

$$Nu_L = 0.13 Ra_L^{1/3} \qquad \left(10^7 < Ra_L < 10^{10}\right) \tag{3.35}$$

where the characteristic length (L) is the plate height. This is valid for inclination angles between 30° and 90°. If the angle is smaller then 30 °, the horizontal relationships from formula (3.30) to (3.32) should be used.

Forced convection
In the case of forced convection we have to differentiate between laminar and turbulent flow. Transition roughly takes place in the Reynolds regime from $6*10^4$ to $4*10^5$. Because the Reynolds numbers for solar collectors are generally larger then $4*10^5$, we will assume the Nusselt relation for turbulent forced convection from (Bejan, 1993):

$$Nu = 0.037\,\mathrm{Pr}^{1/3}\left(\mathrm{Re}_L^{4/5} - 23550\right) \tag{3.36}$$

The validity range of this relation is $5*10^5 < \mathrm{Re} < 1*10^8$, L is the plate length and *Pr>0*. Here the Prandtl number Pr gives the ratio between the thermal diffusivity α and the kinematic viscosity ν:

$$\mathrm{Pr} = \frac{\nu}{\alpha} \tag{3.37}$$

Mixed convection
To determine whether forced or free convection correlations applies, the quotient of the Grashof number *Gr* and Re^2 is calculated. For values for $GrRe^2$ around one the flow regime is called mixed convection. In this region the Churchill equation (Churchill, 1977) can be used:

$$Nu = (Nu_f^p + Nu_n^p)^{1/p} \tag{3.38}$$

Where Nu_f and Nu_n are the Nusselt number for forced and natural convection respectively. Churchill states the exponent *p* should be 3. If the flow is turbulent however, Kakaç (1987) recommend a value of 4 for *p*.

Wind speed dependent heat transfer coefficient
The heat transfer coefficient from the top can also be calculated directly from the wind speed (V_{wind}). Duffie and Beckman (1980) suggest heat transfer coefficients that are only dependent of the wind speed:

$$h_{c,c-a} = 2.8 + 3.0V_{wind} \tag{3.39}$$

Although this formula is often used, it is from data on a $0.5m^2$ plate.
Formula (3.39) is however generally accepted to give reliable results for roof mounted (and therefore inclined) solar collectors. The minimum value for the heat transfer coefficient with formula (3.39) will however be taken as 5 W/m^2K as this is recommended by Duffie and Beckman (1980).

Comparison
We can now plot the heat transfer coefficient vs. the wind speed for horizontal and inclined plates, as well as the direct wind speed coefficient from formula (3.39) in figure (3.5).

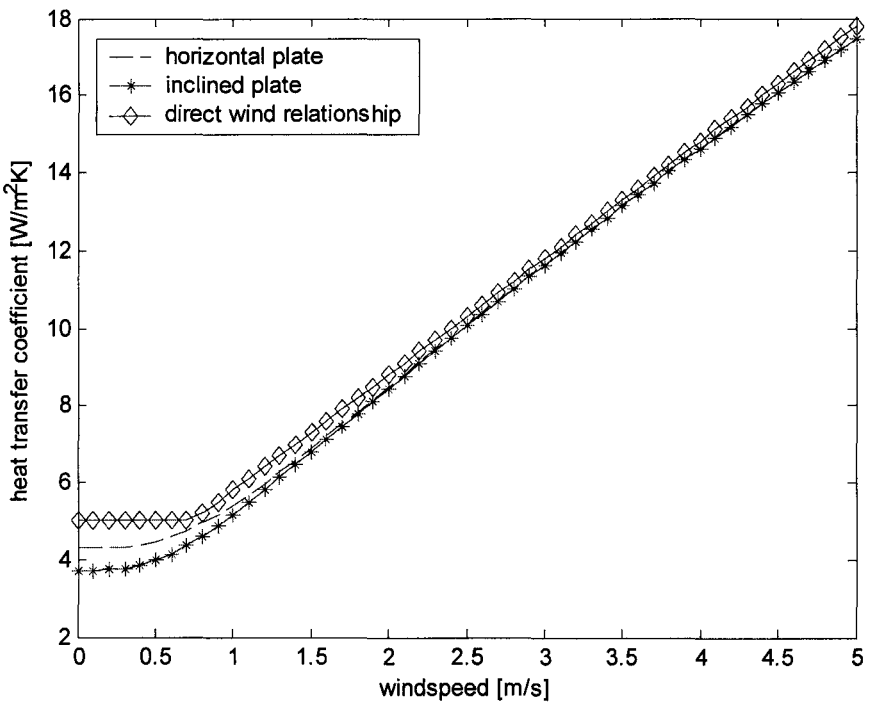

Figure 3.5: Heat transfer coefficient vs. windspeed

As can been seen in the figure there is a slight difference between horizontal and inclined plates. The direct wind relationship seems to predict the value of the heat transfer coefficient fairly well too. Since the assumption is that the collector has an angle with the earth of 37°, the inclined plate relationships from formula (3.31), (3.32), (3.33) and (3.35) will be used. If however the angle is made 30° or less the horizontal plate relationship must be used.

3.2.4.2 Heat transfer from the first absorber to the cover

For the convective heat transport in an inclined insulating air layer with the lower and upper boundaries at a uniform temperature Bejan (1993) recommends the following Nusselt relation valid for inclined angles (ϕ) between 0 en 75 ° with the earth and Raleigh numbers between 0 and 10^5:

$$Nu_L(\phi) = 1+1.44\left(1-\frac{1708}{Ra_L\cdot\cos(\phi)}\right)\left(1-\frac{\sin(1.8\phi)^{1/6}*1708}{Ra_L\cdot\cos(\phi)}\right)+\left(\left[\frac{Ra_L\cdot\cos(\phi)}{5830}\right]^{1/3}-1\right) \quad (3.40)$$

Here the Rayleigh number depends on the characteristic length L, which is the plate spacing and ϕ is the angle with the earth. Duffie and Beckman (1980) and De Vries (19..) use the same formula, although the latter states that it is only valid for tilt angles between 0 and 60°. This will however also suffice in the current model.

3.2.4.3 Heat transfer from both absorbers to the medium

Laminar convection
The convective heat transfer from the absorbers to the medium is forced.
When the flow is laminar and developed (Bejan, 1993, Lienhard, 2000) tells us that a constant Nusselt number, based on the hydraulic diameter D_h, applies of:

$$Nu_{Dh} = 4.364 \quad (3.41)$$

This is however only the case for the fully developed thermal region. In the thermal entrance region the following equation is used:

$$Nu_{Dh} = \left(4.364*\left[1+(Gz/29.6)^2\right]^{1/6}\right)\times \left[1+\left(\frac{Gz/19.04}{[1+(\mathrm{Pr}/0.0207)^{2/3}]^{1/2}[1+(Gz/29.6)^2]^{1/3}}\right)^{3/2}\right]^{1/3} \quad (3.42)$$

Where the new dimensionless group *Gz* is the Graetz number, which is defined as:

$$Gz = \frac{\pi}{4}\left(\frac{x/D_h}{\mathrm{Re}_{Dh}\,\mathrm{Pr}}\right)^{-1} \quad (3.43)$$

Here the characteristic length scale is the hydraulic diameter of the channel D_h.

Turbulent convection
When the flow becomes turbulent (Re > 2300) a Reynolds-dependent relationship is needed. [Goswami et al, 2000] give a suitable expression for the Nusselt number for a smooth air-heating collector and turbulent flow:

$$Nu_{Dh} = \frac{0.0192\,\mathrm{Re}_{Dh}^{3/4}\,\mathrm{Pr}}{1+1.22\,\mathrm{Re}_{Dh}^{-1/8}(\mathrm{Pr}-2)} \tag{3.44}$$

3.2.5 Pressure drop calculations

When the collector medium air is driven through the collector, it induces a pressure drop over the channel. There will also consist a pressure drop over the support system, mostly piping, of the heating system. To overcome this combined pressure drop, a fan is added to the system. The pressure drop will increase with increasing mass flow rate, which will lead to an increase in fan power. To determine the total fan power, the pressure drop over the system will have to be calculated. The pressure drop inside the channel can be calculated in terms of the friction factor, hydraulic diameter (D_h) and length of the channel (L), density (ρ) and velocity (U):

$$\Delta P = f\frac{4L}{D_h}\frac{1}{2}\rho U^2 \tag{3.45}$$

The friction factor will differ in laminar, mixed and turbulent flow. For laminar flow, the friction factor is written as:

$$f = \frac{C}{\mathrm{Re}_{Dh}} \tag{3.46}$$

The constant C appearing in the numerator depends on the shape of the duct cross section. Bejan (1993) introduces a cross section shape number:

$$B = \frac{\pi D_h^2/4}{A} \tag{3.47}$$

The purpose of this number is to measure the deviation of the actual shape form circular shape. B = 1 will therefore correspond to a round channel. A good approximation for the C-values is:

$$C \cong 16\exp\left(0{,}294B^2 + 0{,}068B - 0{,}318\right) \tag{3.48}$$

For the transition area, $2\times10^3 < \mathrm{Re}_{Dh} < 2\times10^4$, the friction factor is stated as:

$$f \cong 0.079\,\mathrm{Re}_{Dh}^{-1/4} \tag{3.49}$$

In the higher Reynolds number region, $2\times10^4 < \mathrm{Re}_{Dh} < 10^6$ the relation becomes:

$$f \cong 0.046\,\mathrm{Re}_{Dh}^{-1/5} \tag{3.50}$$

For the support system, added for a better approximation of the actual situation, these same relationships hold. For velocities normal to an air collector we will usually need formula (3.49). For very high or very low speeds the other two are needed.

The fan power can now be calculated using the fan efficiency, mass flow rate, density and pressure drop:

$$W_{fan} = \frac{1}{\eta_{fan}} \dot{m} \frac{1}{\rho} \Delta P \tag{3.51}$$

This will be needed to calculate the net efficiency of the panel, defined by formula (3.5)

3.2.6 Solution procedure

With the formulas defined in this chapter a model for the energy flows in a basic two-absorber PV/T panel has been set up. The consecutive steps are shown in figure (3.6) with a flow diagram.

First all model parameters, like geometries and velocities, and material properties, like emission coefficients, are specified. Then a first approximation of the temperatures inside the collector is made. This first temperature approximation is constant over the length of each part of the collector. Next one of the parameters or properties inside the model is varied. This means that for every value of the varied parameter all temperatures, efficiencies and energy output will be calculated. This is practical because it allows us to recognize the influence of this parameter on the panel performance.
The panel, with length L, is now subdivided into elements of length *dx*, where n is de number of increments. The averaged temperature over the increments of each part of the collector is now determined with which an approximate value of the temperature dependent material properties inside the model is calculated.
With the first, constant temperature approximation, the heat transfer coefficient of each increment *dx* is now calculated. The first approximation of the heat transfer coefficient will thus also be constant over the length of each part of the collector. With the first approximation of the heat transfer coefficients of each increment, the new temperature of each increment over the length of the two absorbers, the collector medium and the top cover will be calculated. This new temperature distribution is used to calculate the new temperature dependent material properties and heat transfer coefficients.
When this process is repeated 15 times, experience with the model learns that the temperature difference between two consecutive steps is in the order of 10^{-4} °C per increment. The final solution for the temperatures at this value of the varied parameter is then reached and the efficiencies and other output are stored in a matrix.
At this point the second value of the varied parameter is taken and the process is repeated.
When the temperatures, efficiencies and other model output of all values of the varied parameter have been calculated, the results can be compared in figures derived by the model.

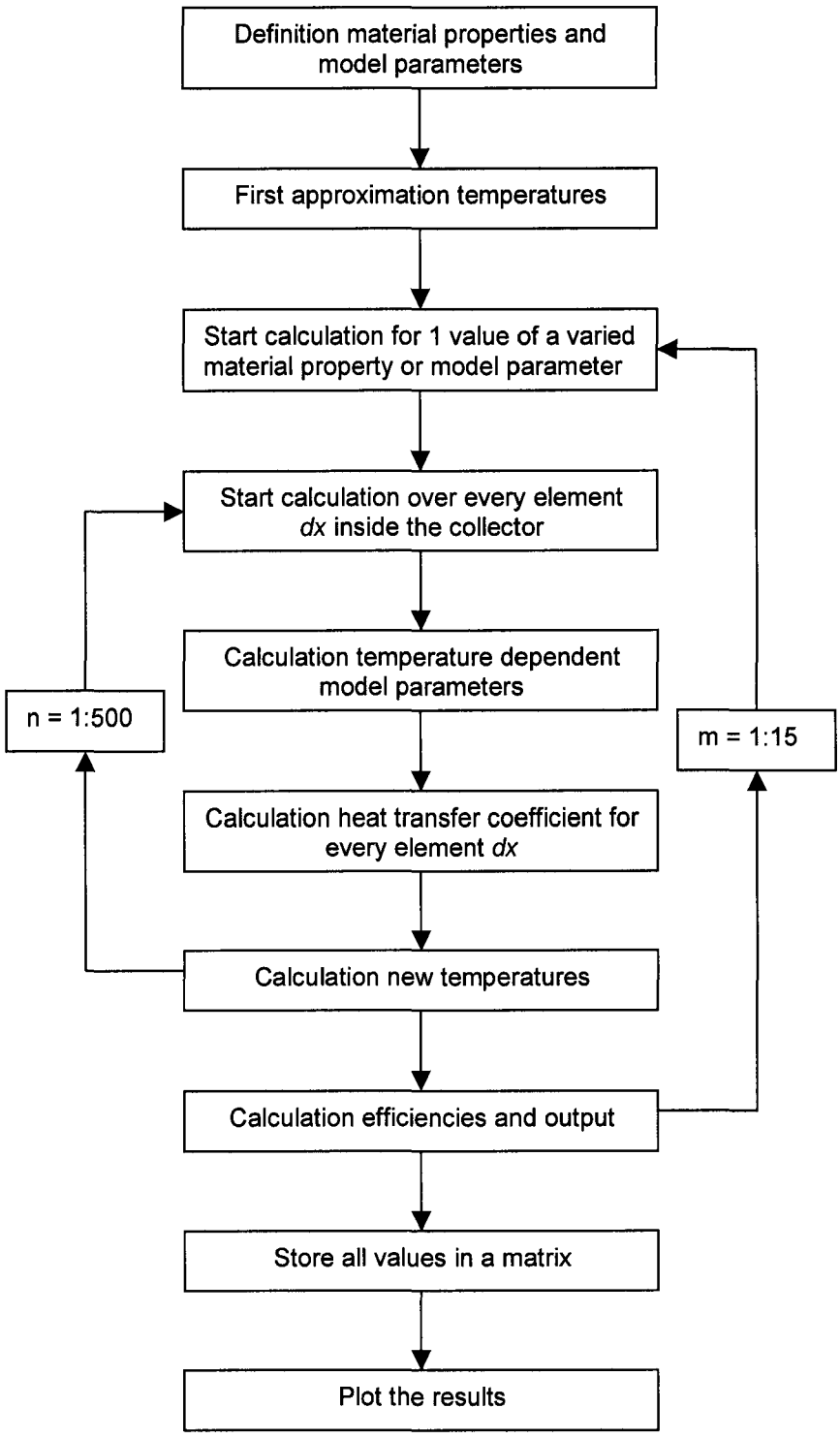

Figure 3.6: flow diagram of the formulated matlab file.

3.3 *Model reliability testing*

The model will now be subjected to some simple tests to validate its reliability.

Heat output when losses are set to zero.
In this first test the heat loss coefficient U_L shall be made zero. This would mean in steady state that no heat is lost to the environment (ambient and sky) and that the amount of solar irradiance absorbed by the absorbers should be equal to the amount of heat removed by the collector medium.
The amount of absorbed solar irradiance at each absorber can be calculated using formula (2.2) and (2.3). The assumptions made in this test are:

- The solar irradiance (I_s) is 500 [W/m^2].
- The collector surface is 5 [m^2].
- The transmission coefficient of the cover (τ_1) is 0.92.
- The transmission coefficient of the first absorber (τ_2) is 0.26.
- The absorption coefficient of the first absorber (α_2) is 0.70.
- The absorption coefficient of the second absorber (α_3) is 0.96.

Substituting these values in formula (2.2) and multiplying with the collector surface the amount of solar irradiance absorbed by the first absorber is 1610 [W]. Substituting in formula (2.3) and multiplying with the collector surface the amount of solar irradiance absorbed by the second absorber is 574.08 [W]. This means the total absorbed solar irradiance is 2184.08 [W].
The model output gives:

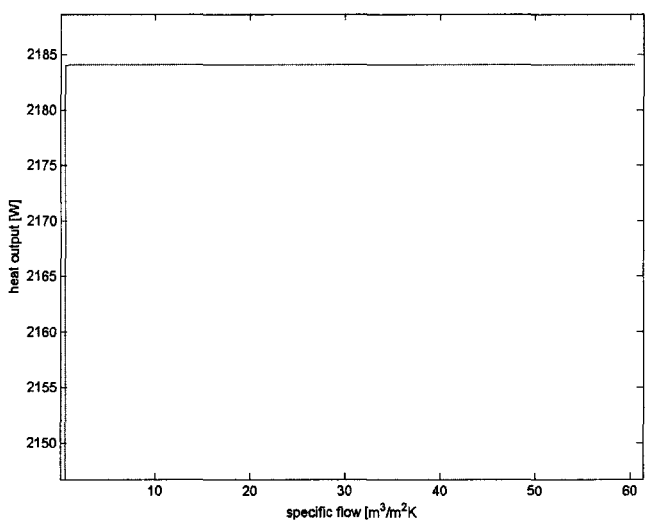

Figure 3.7: Heat output vs. specific flow with U_L = 0.

In Figure (3.7) the heat output is set against the specific flow inside the absorber. The specific flow is defined as the volume flow of collector medium divided by the collector area of the collector. It provides comparisment of the velocity of the collector medium for solar panels with different collector area. When the specific flow is made zero (there is no flow) there will be no heat output, which can be seen in the figure. When the collector medium does flow, the heat output is constant at 2184 [W]. This means all absorbed irradiance is removed and the model projection is correct.

Heat output at constant heat transfer coeffcients

In the next test the heat transfer coeffcients inside the model will be made constant. Both the heat transfer coeffcients inside the collector medium channel ($h_{c,p-cm}$, $h_{c,b-cm}$ en $h_{r,pb}$) and the total loss coeffcient (U_L in formula 3.17) will be set at 3 [W/m^{2}K]. The total heat transfer coeffcient inside the collector medium channel can now be calculated with formula (3.18), which tells us that h = 4.5. The mass flow rate will be 0.1 [kg/s], the ambient temperature and channel medium inflow temperature are 283 and 285 respectively and the specific heat is 1006 [J/kgK]. The temperature of the collector medium at the exit of the channel can now be calculated when the absorbed irradiance of the first absorber (H_a) and second absorber (H_b) are calculated at 322 and 114.816 [W/m^2]. These values are substituted in formula (3.27). With the collector medium outflow, the other temperatures at L = 5 can also be calculated using formula (3.22), (3.23) and (3.28). The model will now run with these same input parameters and should give approximately the same results. This proves wheter the calculations inside the model are executed correctly:

	T_{cm} (°K)	T_p (°K)	T_b (°K)	T_c (°K)
Model prediction	298.3812	342.8165	339.7348	309.9607
Direct calculation	298.3865	342.7796	339.7191	309.9589

Table 3.1: Comparison between temperatures of model and direct calculations at constant heat loss and transfer coefficients.

Table (3.1) shows the hand calculations correspond to the model results very well. The calculations inside the model can thus be assumed to be correct.

Comparison in top loss coefficient
To find out whether the model gives reliable results, the averaged top loss coefficient over the length of the panel will be compared to calculations in Duffie & Beckman (1980) at specific values of a variaty of model parameters. The cover spacing (S) is 25 [mm], the ambient temperature (T_a) is made 313, 283 and 263 °K, the emittance coefficient at the top of the top absorber (ε_{21}) is 0.95 and 0.1, the inclination angle (β) is 45° and the convective heat transfer coeffcient due to wind from the cover to the ambient ($h_{c,c-a}$) is 5, 10 and 20 [W/m^{2}K]. The predictions of the model compared to the values in Duffie and Beckman (1980) are summarized in table (3.2):

	U_t from Duffie and Beckman	U_t from Model prediction
$h_{c,c-a}$ = 5, Tamb = 283, ε_{21} = 0.95	4.3	4.2
$h_{c,c-a}$ = 10, Tamb = 283, ε_{21} = 0.95	5.0	5.0
$h_{c,c-a}$ = 20, Tamb = 283, ε_{21} = 0.95	5.8	5.8
$h_{c,c-a}$ = 5, Tamb = 313, ε_{21} = 0.95	5.0	5.0
$h_{c,c-a}$ = 5, Tamb = 263, ε_{21} = 0.95	3.9	3.8
$h_{c,c-a}$ = 5, Tamb = 283, ε_{21} = 0.1	2.5	2.4

Table 3.2: Predictions of the top loss coefficient.

The values in table (3.2) correspond within a small error range. The model can thus be assumed to give reliable results.

Altered top loss coefficient
In paragraph 3.2.1 both *(U_t)* and *(U_b)* are made dependent of de first absorber temperature *(T_p)*, so formula (3.14) would be valid. This was done to simplify the mathematics. An indication of the influence of this assumption can be obtained by calculating the altered total loss coefficient. This total loss coefficient (U_{LL}) can be calculated using the formula:

$$U_{LL} = \frac{\overline{U}_t(\overline{T}_p - T_a) + \overline{U}_b(\overline{T}_b - T_a)}{(\overline{T}_p - T_a)} \qquad (3.53)$$

The difference between U_L and U_{LL} is thus the factor $\overline{U}_b \frac{\left(\overline{T}_b - T_a\right)}{\left(\overline{T}_p - T_a\right)}$. When the averaged second absorber temperature is in the range of the averaged first absorber temperature, the error will be small. It will however increase with increasing temperature difference. An indication of the error can now be obtained by plotting both U_L and U_{LL} for a varied specific flow:

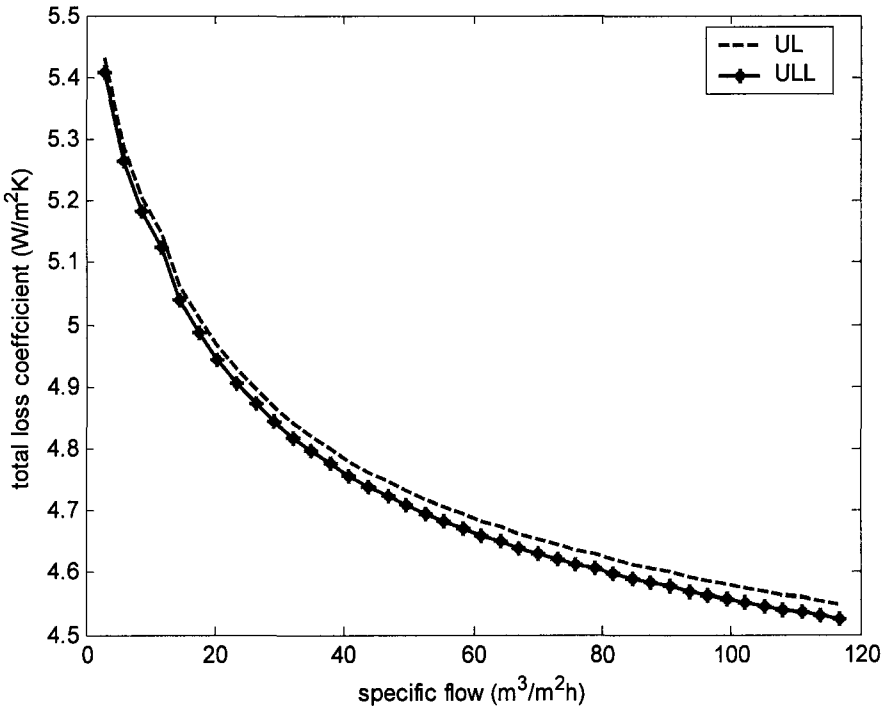

Figure 3.8: U_L and U_{LL} plotted against the specific flow in the collector.

Figure (3.8) shows the assumption has an increasing influence with increasing specific flows. The influence on the total loss coefficient at a specific flow of 120 [m^3/m^2h], which is high for an air thermal collector, is about 1%. We will therefore assume that the influence of making the back and edge loss coefficient dependent of the first absorber does not have any influence on the results obtained with the model.

4 Results of the two-absorber configuration model

In this chapter results obtained with the model described in chapter 3 will be presented. First a base case will be specified, with an explanation of its base values. An introduction on the various results that can be obtained with the model will be given and a reference value for the efficiency of the base case will be determined. Next a number of model and material parameters will be varied to determine the sensitivity of these parameters on the thermal and net efficiency of the model. This information can be used to alter the panel design to obtain a higher efficiency.

4.1 Definition of the base model

In this paragraph a base case of the two-absorber panel will be defined. The relevant model parameters can be classified in parameters that are determined by the environment and parameters that can be modified in the panel design. The parameters that can be influenced can be classified as material or, important in this model, optical parameters and geometrical parameters together with the collector medium speed. This is shown in figure (4.1):

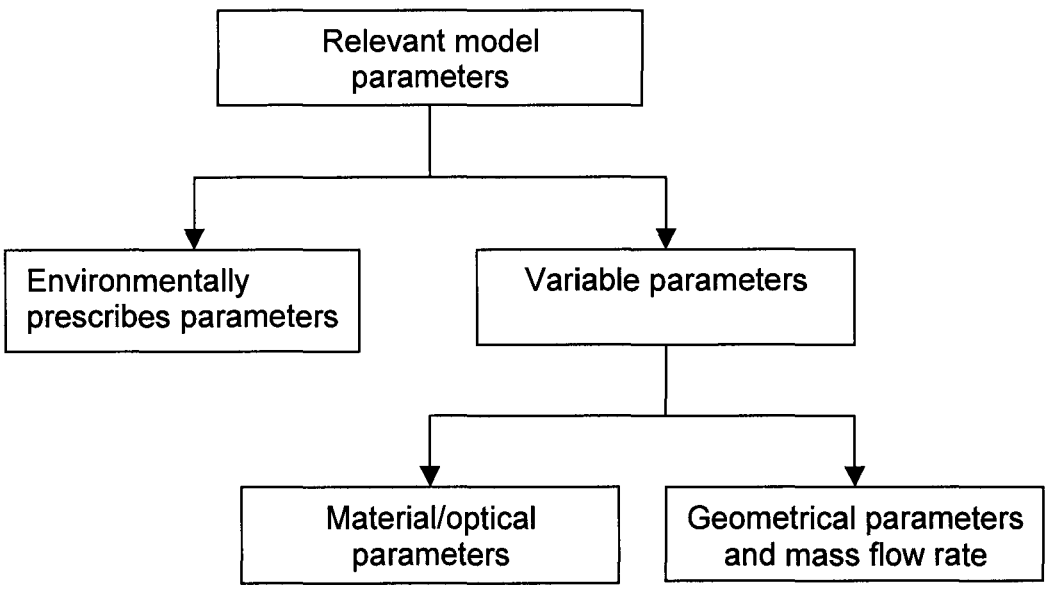

Figure 4.1: Classification of the relevant model parameters.

4.1.1 Geometrical parameters and collector medium velocity

Figure (4.2) shows a schematic representation of the panel with several of its geometrical parameters. (S) is the spacing between the top cover and the first absorber, (H) is the collector medium channel height, (L) is the length of the channel, (W) is the width of the collector and (v) is the velocity of the collector medium.

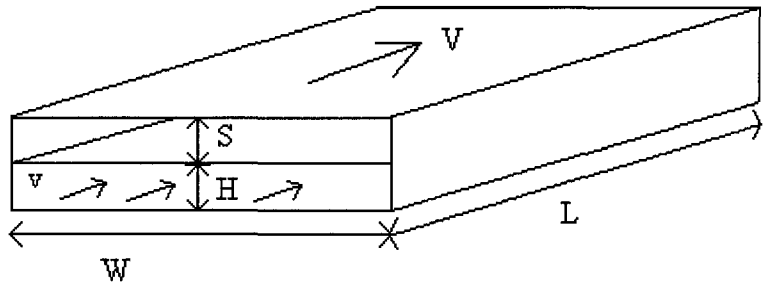

Figure 4.2: Schematic representation of the two-absorber panel.

Other geometrical parameters are the insulation thickness (t_i), the inclination angle of the panel (β) and the diameter of the piping of the support system (D_{hs}). The values of the length and width of the panel and height of the collector medium channel can be chosen freely. For moderately sized panels, values could be:

Parameter description	Value
Panel length (L)	5 [m]
Panel width (W)	1 [m]
Collector medium channel height (H)	0.02 [m]
Spacing cover – first absorber (S)	0.04 [m]
Hydraulic diameter support system (D_{hs})	0.1 [m]
Support system length (L_s)	5 [m]
Insulation thickness (t_i)	0.1 [m]
Inclination angle (β)	37 [°]
Mass flow rate (m)	0.1 [kg/s]

Table 4.1: Base case values of the geometrical parameters and mass flow rate.

A few remarks about the base case values that were chosen:

- The panel length, panel width, collector medium channel height, length of the support system and insulation thickness were chosen using the values we came across in the literature for moderately sized panels.
- Figure (6.4.5) in Duffie and Beckman (1980) shows the spacing between first absorber and cover in a classical thermal collector has little influence on collector performance when it is made larger then 2 [mm]. In this research it will be set to 4 [mm].
- The hydraulic diameter of the piping system must be big enough to reduce the pressure drop over the support system. On the other hand it can't be made too big because this would take up much space. The hydraulic diameter will be set at 0.1 [m]
- The inclination angle was already defined in chapter 3.2.4 as 37°.
- A literature study also reveals that the specific flow value for air solar thermal collectors lies between 20 and 120 [m^3/m^2h]. We will take a base specific flow value of 60 [m^3/m^2h]. The density, although temperature dependent, will be about 1.2 [kg/s], which means the mass flow rate is 0.1 [kg/s].

4.1.2 Material/Optical parameters

The cover, first absorber and second absorber are all made of different materials. Of the properties these materials have, the optical properties are important for the model. Therefore the optical parameters of each of the absorbers and cover will be specified. The parameters needed are the absorption factor α, the transmission factor τ, the reflection factor ρ and the emission factor ε, as discussed in § 2.2.

Cover
The cover will be modeled with optical parameters for glass.

Optical properties of the cover	Value
Absorption coefficient (α_1)	0 [-]
Transmission coefficient (τ_1)	0.92 [-]
Reflection coefficient (ρ_1)	0.08 [-]
Emission coefficient (ε_1)	0.90 [-]

Table 4.2: Base case values of the optical properties of the cover.

First absorber
The first absorber of the base model consists of thin film amorphous silicon solar cells without back contact. Van Poppel (2002) gives values for α, ρ and τ of these cells at the AM 1.5 solar spectrum. The back and top of the cell are made of glass and therefore the emission coefficient of this material will be taken:

Optical properties of the first absorber	Value
Absorption coefficient (α_2)	0.40 [-]
Transmission coefficient (τ_2)	0.36 [-]
Reflection coefficient (ρ_2)	0.24 [-]
Emission coefficient (ε_2)	0.9 [-]

Table 4.3: Base case values of the optical properties of the first absorber.

It is noted that the optical values for the solar cell in the work of van Poppel (2002) apply for solar cells with a planar structure. When textured solar cells are used, the absorption coefficient becomes approximately 0.1 [-] larger and the reflection coefficient becomes approximately 0.1 [-] smaller.

Second absorber
The second absorber can be made of a lot of materials. The demands are that the material is opaque (no transmission) and has a high emission coefficient when the first absorber temperature is higher and a low emission coefficient when it is lower. With the optical parameters chosen as in the base case the first absorber temperature will be lower, thus the second absorber will be modeled with a low emission coefficient:

Optical properties of the second absorber	Value
Absorption coefficient (α_3)	0.96 [-]
Transmission coefficient (τ_3)	0 [-]
Reflection coefficient (ρ_3)	0.04 [-]
Emission coefficient (ε_3)	0.1 [-]

Table 4.4: Base case values of the optical properties of the second absorber.

4.1.3 Parameters prescribed by the environment

Some parameters cannot be influenced, because they are prescribed by the environment. For the base model the calculations will be performed for meteorological and operational conditions in what will be called the reference situation.

Parameters prescribed by the environment	Value
Solar irradiance (I_s)	500 [W/m^2]
Collector medium inflow temperature ($T_{cm,in}$)	283 [K]
Wind speed	2 [m/s]

Table 4.5: Base case values of the parameters prescribed by the environment.

4.2 Results obtained with the model

When the parameters from § 4.1.1, 4.1.2 and 4.1.3 are substituted inside the model, it will render a variety of plots, which present the results obtained with the model. The plots of the results obtained with the model will be shown with a variation in mass flow rate.

Temperature distribution over the absorber length
First the temperature distribution over the length of the cover, the absorbers and the collector medium are plotted. This is shown in figure (4.3).

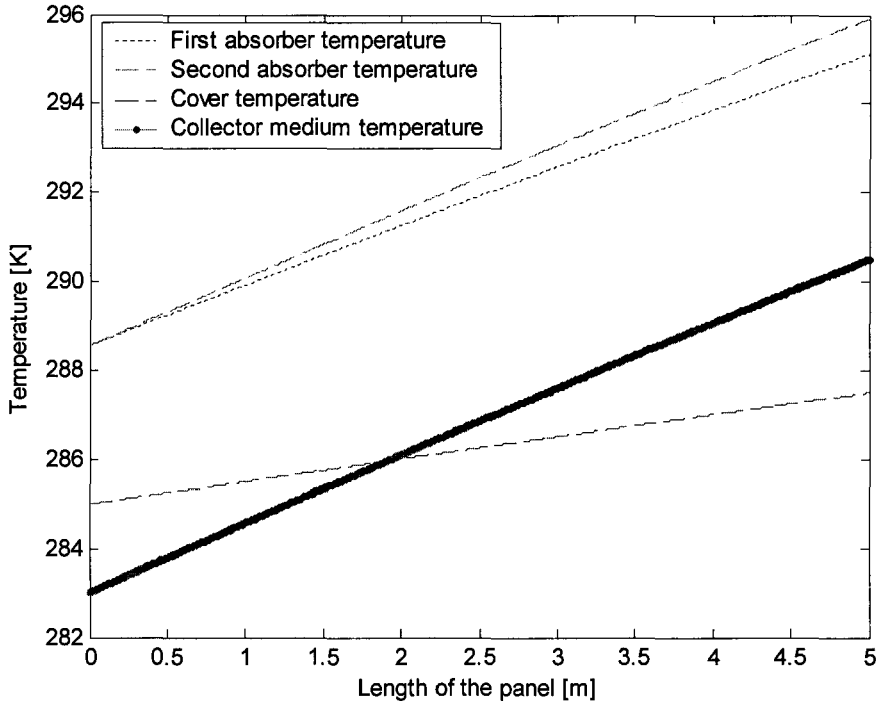

Figure 4.3: Temperature of the collector medium, absorbers and cover vs. the collector length for the base case.

We can see the second absorber temperature is higher than that of the first one. It would thus be beneficial to keep de emission coefficient of the second absorber low, because the radiative heat transfer to the first absorber will be small in this way. Since we assume that all heat losses to the environment are suffered from the first absorber, this would improve the efficiency of the panel. The figure also reveals the collector medium outflow temperature, which is convenient when a minimum temperature rise for the air must be obtained. When the air is used for direct space heating or crop drying it is convenient to control the temperature using the collector medium velocity.
We can also see the first absorber temperature increases much slower than that of the collector medium and second absorber. This gives us a first impression of the importance of the losses from the first absorber. Although the absorption coefficient of the first absorber is larger than that of the second absorber the temperature of the second absorber is larger over the entire length of the panel. This means the influence of the losses at these base case conditions is still fairly large.

Thermal efficiency vs. specific flow
The thermal efficiency of the panel, as defined in formula (3.3), can be plotted for all varied values of the mass flow. The mass flow will however be rewritten as the specific flow for these

dimensions of the collector (length 5 [m], width 1 [m]) to simplify the comparison for collectors with different collector area. The thermal efficiency vs. the specific flow of the collector is shown in figure (4.4):

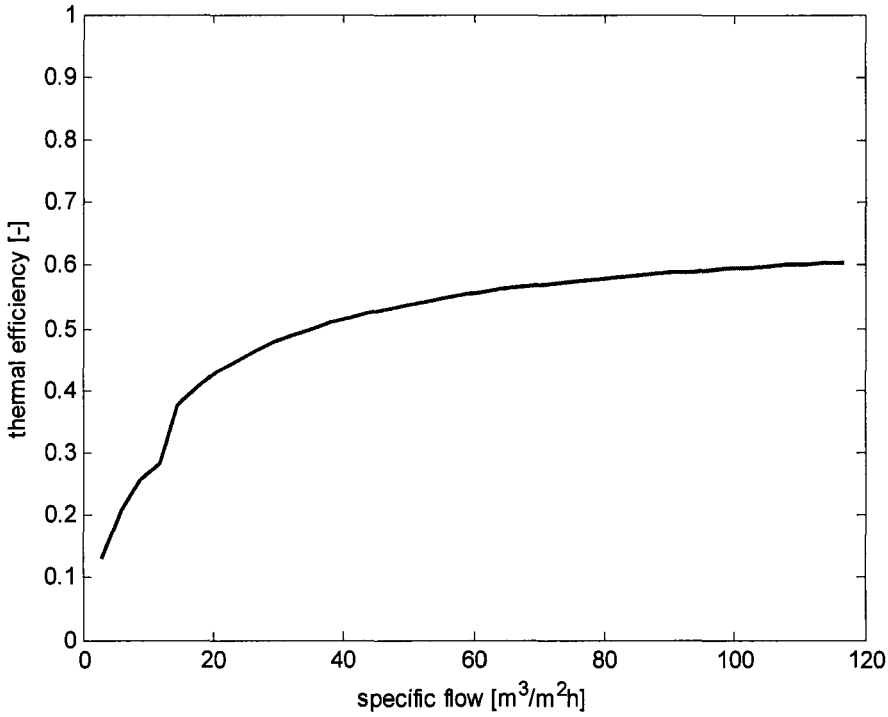

Figure 4.4: Thermal efficiency of the collector vs. specific flow for the base case.

As to be expected, the thermal efficiency rises with the specific flow, since the convective heat transfer coefficients inside the collector medium channel increase with the collector medium velocity. At a specific flow of approximately 12 [m^3/m^2h] the thermal efficiency jumps from 0.32 to 0.37. This is caused by the transition from laminar to turbulent flow inside the channel. We have chosen to add a direct transition in the model when the Reynolds number inside the channel reaches the value of 2300. This is the approximate value when the turbulent regime takes over. This means the transition range, between approximately $2000 < Re < 2300$, has not been taken into account.

Figure (4.4) shows the thermal efficiency of the panel seems to go to a limit value. This value will be reached when the collector medium velocity is made very large and will be treated in more detail in § 4.3.1.

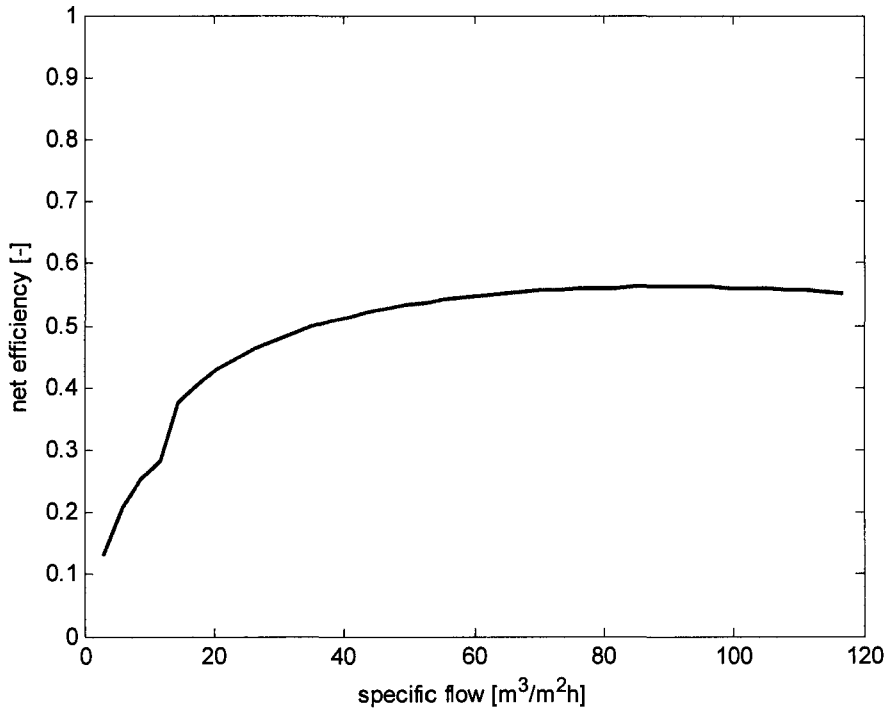

Figure 4.5: Net panel efficiency vs. the specific flow for the base case.

Net efficiency vs. specific flow
The model also calculates the net collector efficiency defined in formula (3.5). The net efficiency is the total output of the collector minus the fan power and divided by the solar irradiance. It is shown in figure (4.5).
The net efficiency increases until it reaches a maximum at approximately 90 [m^3/m^2h]. From this point the extra fan power needed to increase the velocity is larger than the extra heat yield it provides. The net output will thus decrease. The figure thus indicates that we cannot infinitely increase the collector medium velocity to obtain better net efficiencies.

4.3 Sensitivity analysis

A sensitivity analysis is used to identify the parameters that have a large influence on the performance of the two-absorber model. This will be achieved by varying one of the base parameters and see what influence it will have on the efficiencies of the collector.
First the range of the varied parameters will be given. Next we will calculate the optical efficiency and compare it to the limit value that is reached at large velocities. After this the sensitivity analysis will commence. The resulting plots will be shown with an explanation for its trends.

4.3.1 Varied parameters

To determine which parameters inside the model should be varied we must look at figure (3.2), which describes the energy flows present inside the collector panel. Varying one or more parameters can influence each of these energy flows.

$\dot{m}$	Mass flow of the collector medium	0 - 0.2 [kg/s]
g	Height collector channel	0.003 – 0.1 [m]
s	Height between cover and absorber	0.005 – 0.1 [m]
ε_{21}	Emission top of the first absorber	0.05 – 0.95 [-]
ε_{22}	Emission bottom of the first absorber	0.05 – 0.95 [-]
ε_3	Emission top of the second absorber	0.05 – 0.95 [-]
V	Wind speed	0 – 10 [m/s]
α_2	Absorption coefficient first absorber	0.05 – 0.76 [-]
τ_2	Transmission through first absorber	$\alpha_2 \cdot \tau_2 = 0.76$[-]
I_s	Irradiance on the collector	0 – 1000 [W/m^2]
t_i	Thickness of the insulation	0.01 – 0.15 [m]

Table 4.6: Varied parameters and their values.

Table (4.1) shows all parameters that will be varied with its description and variation. The influence of a varied parameter shall be determined by comparing the thermal and net efficiency of the collector. To better rate the variety in performance a maximum, minimum and reference value of the thermal efficiency will be calculated. First however we will calculate the theoretical thermal efficiency value that is reached when the losses to the environment are made zero, which means the only losses inside the system are optical losses. This value is calculated by adding the total absorbed irradiance of the first and second absorber and dividing it by the total solar irradiance:

$$\eta_{th,\max} = \frac{H_a + H_b}{I_s} = 0.686 \qquad (4.1)$$

This value will never be reached in practice, since there will always be some radiative losses to the sky. The sky temperature, as defined in formula (3.12), is always smaller than the ambient temperature. The maximum practical value will be calculated with the model at base case values, but with the mass flow rate made extremely large.
We will also define a reference efficiency value, which is the value achieved with the parameter values of the base model from § 4.1. The minimum thermal efficiency is zero when the mass flow rate is made equal to zero. The minimum, reference and practical maximum value of the thermal efficiency thus become:

- $\eta_{\min} = 0$; $\dot{m} = 0$ [kg/s]
- $\eta_{ref} = 0.555$; $\dot{m} = 0.1$ [kg/s]
- $\eta_{\max} = 0.661$; $\dot{m} = 1$ [kg/s]

4.3.2 Varying the mass flow rate of the collector medium

The mass flow rate (m) of the collector medium is varied between 0 and 0.2 [kg/s], which results in specific flows between 0 and +/- 120 [m^3/m^{2}h]. By varying the mass flow, the collector medium velocity changes. The Reynolds number, which depends on the collector medium velocity, determines the Nusselt number inside the channel (§ 3.2.4.3) and therefore the convective heat transfer coefficient inside the channel. The efficiencies that are plotted in figure (4.6) are the combined efficiencies from figure (4.4) and (4.5):

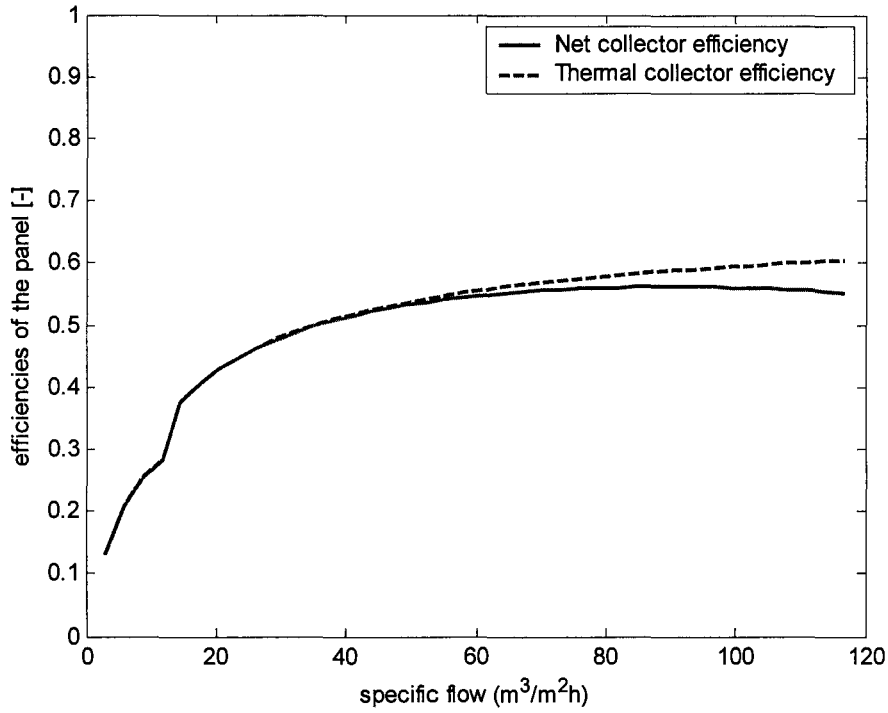

Figure 4.6: Efficiencies vs. specific flow

The thermal collector efficiency is increasing with increasing specific flow. The net collector efficiency however increases until it reaches its maximum value around 90 [m^3/m^2h]. After that it decreases with every increase in mass flow. This means that from there the fan power needed to increase the velocity is larger than the thermal power profit it induces. The mass flow rate can therefore not be infinitely increased.

4.3.3 Varying the collector medium channel height

The collector medium channel height will be varied between a very small value of 0.005 [m] and a large value of 0.1 [m]. Similar to the variation in mass flow rate, the convective heat transfer inside the collector medium channel (§ 3.2.4.3) will be directly influenced, because of the change in collector medium velocity. The efficiencies are plotted in figure (4.7).

A similar trend to the one in § 4.3.2 can be recognized. The thermal performance will increase with decreasing height (velocity increase). The net efficiency will however reach a maximum because the velocity increase also means an increasing pressure drop.

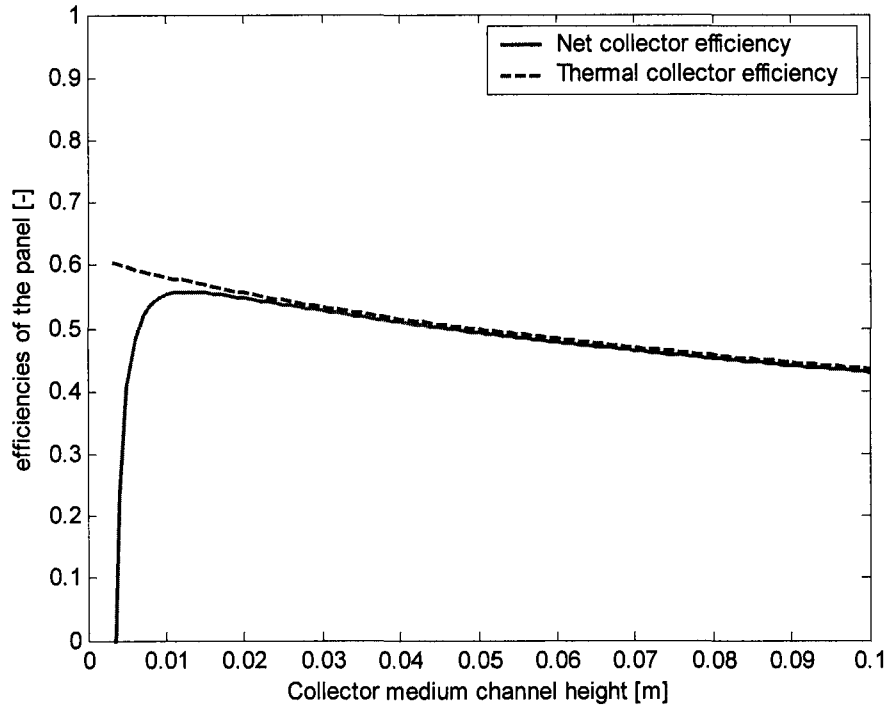

Figure 4.7: Efficiencies vs. collector medium channel height.

4.3.4 Varying the height between the cover and first absorber.

The cover height (S) will be varied between 0.005 and 0.1 [m]. Most conventional thermal solar collectors have cover heights between 0.02 and 0.05 [m]. The spacing cannot be made too small because the losses will increase rapidly. It can on the other hand not be made too large because this is not practical during transport and installation. The efficiencies are shown in figure (4.8). The trend satisfies the typical trend for variation in the spacing between cover and absorber seen in figure 6.4.5 in Duffie and Beckman (1980). For very small plate spacing convection is suppressed and the heat transfer mechanism through the gap is by conduction and radiation. In this range the top loss coefficient decreases rapidly as the plate spacing increases until a maximum efficiency is reached at about 0.01 to 0.015 [m] plate spacing. When fluid motion first begins to contribute to the heat transfer process the efficiency decreases until a minimum is reached at approximately 0.025 [m]. Further increase in plate spacing causes only a small reduction in top loss coefficient. The influence on the thermal performance is marginal when the spacing is greater than 0.025 [m].

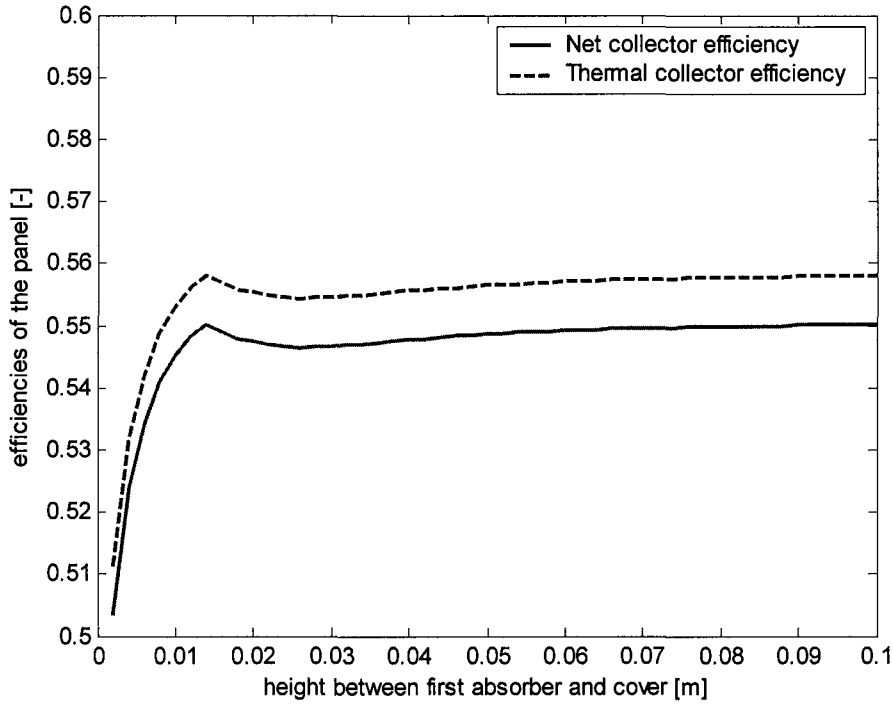

Figure 4.8: Efficiencies vs. height between cover and absorber.

4.3.5 Varying the different emission coefficients

The emission coefficients of the absorbers and cover directly influence the radiative heat transfer between the two absorbers, the first absorber to cover and the radiation to the sky.

Emission coefficient of the top of the first absorber
From formula (3.11) it can be seen that the emission coefficient from the top of the first absorber directly influences the radiative heat transfer coefficient between the first absorber and the cover. A low emission coefficient will render a low heat transfer coefficient. Since this is a loss term, a low emission coefficient should increase the thermal efficiency. The results are plotted in figure (4.9).
The results show a low emission coefficient would be beneficial for the output of the collector. This means a thermal selective surface should be applied to the first absorber. This type of coating provides low long-wave emission, but at the same time a high solar absorption. This would however mean the electric output would become considerably lower, since the coating would already absorb most of the solar irradiance. Also the transmittance of solar irradiance by the cell would become small. The application of a thermal selective surface on the first absorber is therefore not suitable for PV/T-panels.

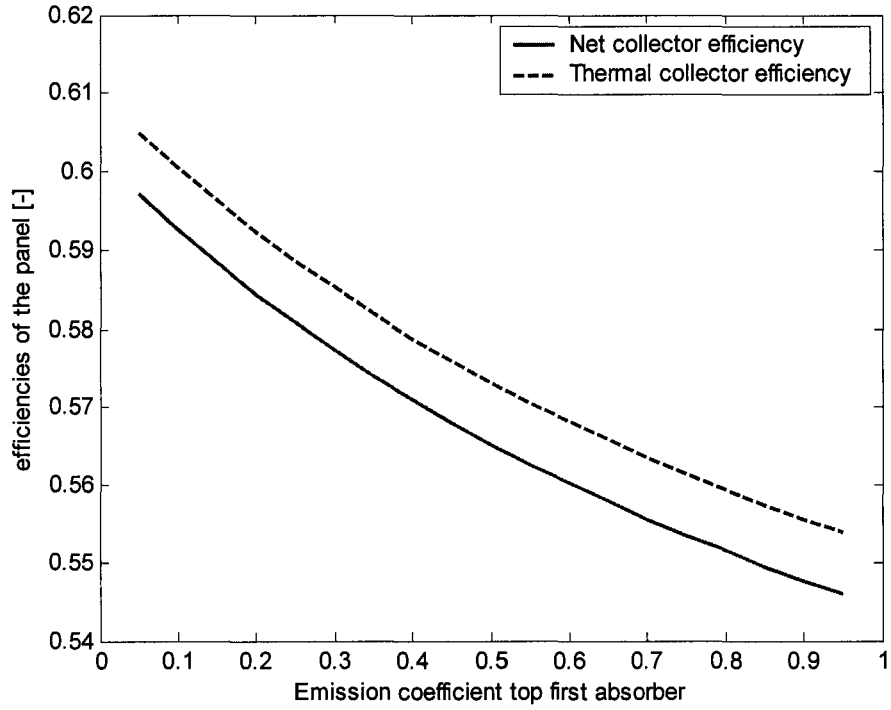

Figure 4.9: Efficiencies vs. emission coefficient from the top of the first absorber.

Emission coefficient of the bottom of the first absorber
The emission coefficient of the bottom of the first absorber was 0.9 [-] in the base case. The results of varying the coefficient will depend on the temperature of the first and second absorber.

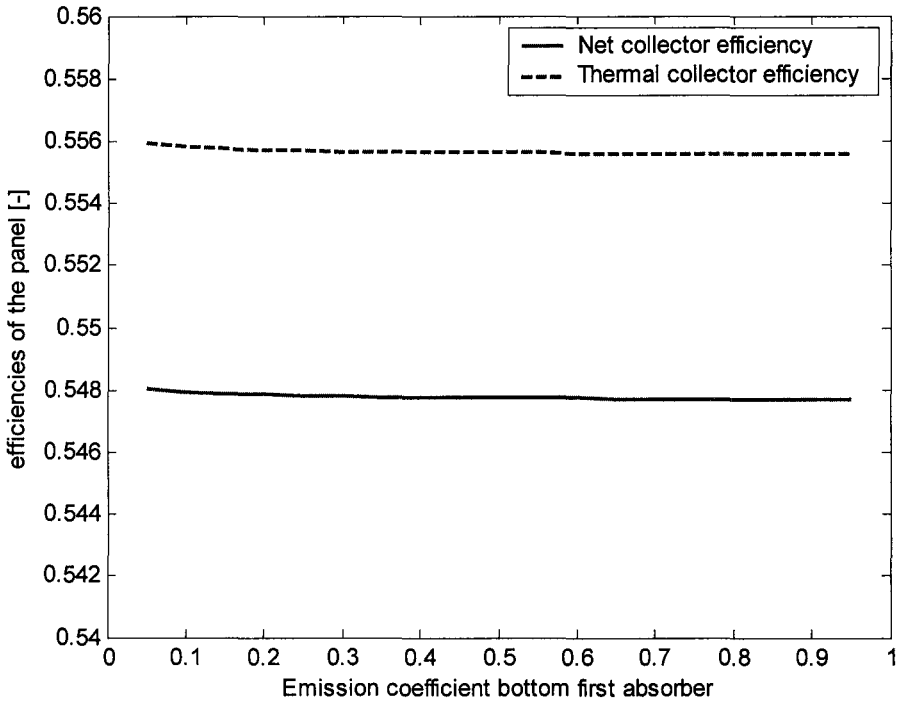

Figure 4.10: Efficiencies vs. emission coefficient from the bottom of the first absorber.

When the second absorber temperature is smaller than that of the first the radiative heat transfer between the two absorbers should be large to decrease the first absorber temperature and vice versa. The results of the variation of the bottom of the first absorber are shown in figure (4.10) We can see the influence of the emission coefficient on the efficiencies of the panel is very small. This is due to the fact that the base case value of the emission coefficient of the second absorber has been made 0.1. This small value suppresses radiative heat transfer between the two surfaces, making its influence on the collector performance very small.

Emission coefficient of the second absorber
The base value of the emission coefficient of the second absorber is 0.1. The consequence of this small value is a reduction in radiative heat transfer between the two absorbers. When we vary the emission coefficient we can determine its influence on the collector performance.

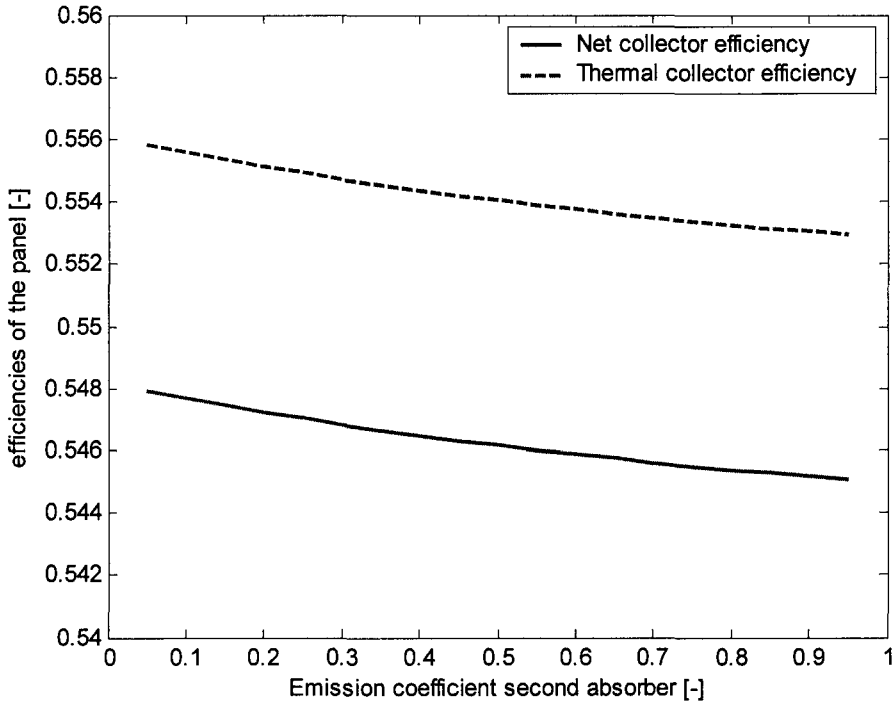

Figure 4.11: Efficiencies vs. emission coefficient from the second absorber.

Again we see the influence of the emission coefficient on the panel efficiencies is very small. This is due to the fact that the temperatures of the first and second absorber are almost the same. When we influence the temperature of the first and second absorber, for example by changing the absorption and transmission coefficient of the first absorber, we will see the emission coefficients inside the collector medium channel will have a larger influence on the panel performance.

4.3.6 Varying the wind speed

The wind speed is a parameter that is prescribed by the environment as was explained in § 4.1.3. It would nonetheless be interesting to see what influence the wind speed and the resulting convective heat transfer have on the collector performance. The results of the variation are plotted in figure (4.12).
Figure (4.12) shows the influence of wind over the panel is approximately 0.04 over the domain. From 0 to 0.7 [m/s] the flow over the cover is considered natural and the resulting heat transfer coefficient is fairly constant over this region. From 0.7 [m/s] forced convection will dominate the

heat transfer. Due to the convective heat transfer coefficient from the cover to the ambient, the total loss coefficient will initially increase very fast. The Nusselt number, formulated in formula (3.40), increases with $Re^{0.8}$, which provides the trend in figure (4.12).

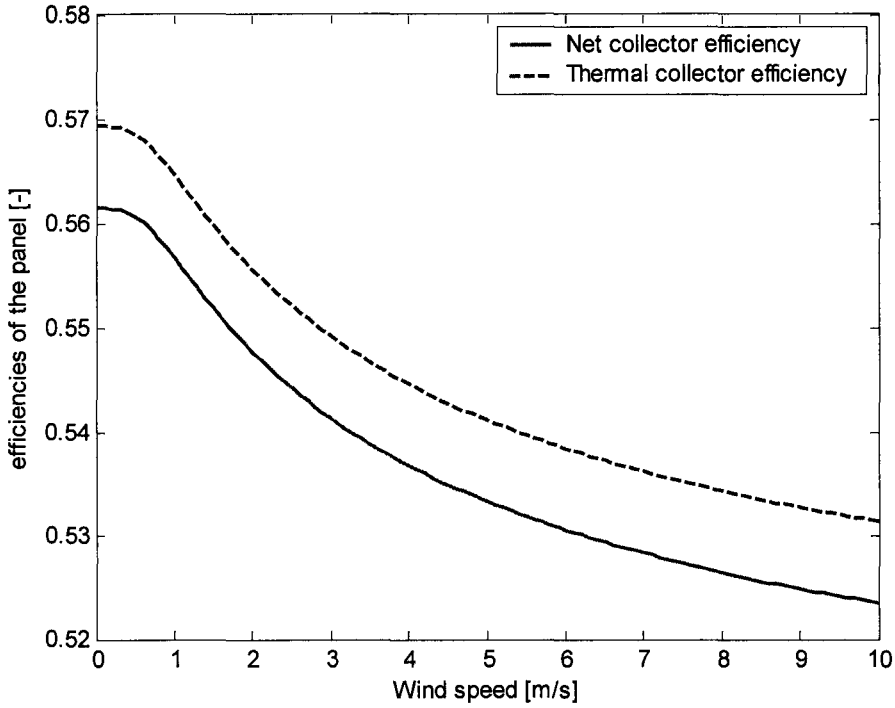

Figure 4.12: Efficiencies vs. wind speed.

4.3.7 Varying the transmission and absorption of the first absorber

The absorption coefficient of the first absorber will be varied between 0 and 1-ρ, in this case 0.76. It will be assumed that the reflection coefficient will stay constant at 0.24 over the entire variation range. This means the transmission coefficient can be calculated with $\tau = (1-\rho)-\alpha$. The resulting efficiency plot is shown in figure (4.13).
Figure (4.13) shows the efficiencies drop with increasing absorption factor. The temperature of the first absorber will increase with increasing absorption factor. Since the heat losses inside the collector are assumed to be dependent of the first absorber temperature only this is what we would expect. The influence of the absorption factor proves to be 10% absolute over the absorption range. This may however differ when the emission coefficients are varied.

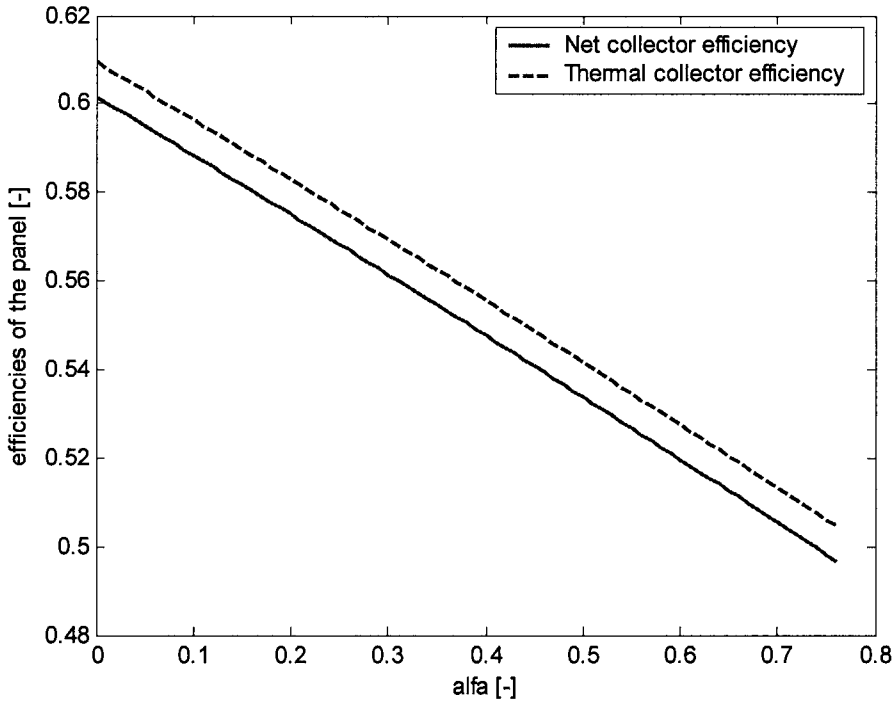

Figure 4.13: Efficiencies vs. absorption factor of the first absorber.

4.3.8 Varying the solar irradiance

The solar irradiance on the collector will be varied between 0 [W/m^2] and 1000 [W/m^2] for clear skies. The panel efficiencies are plotted in figure (4.14).

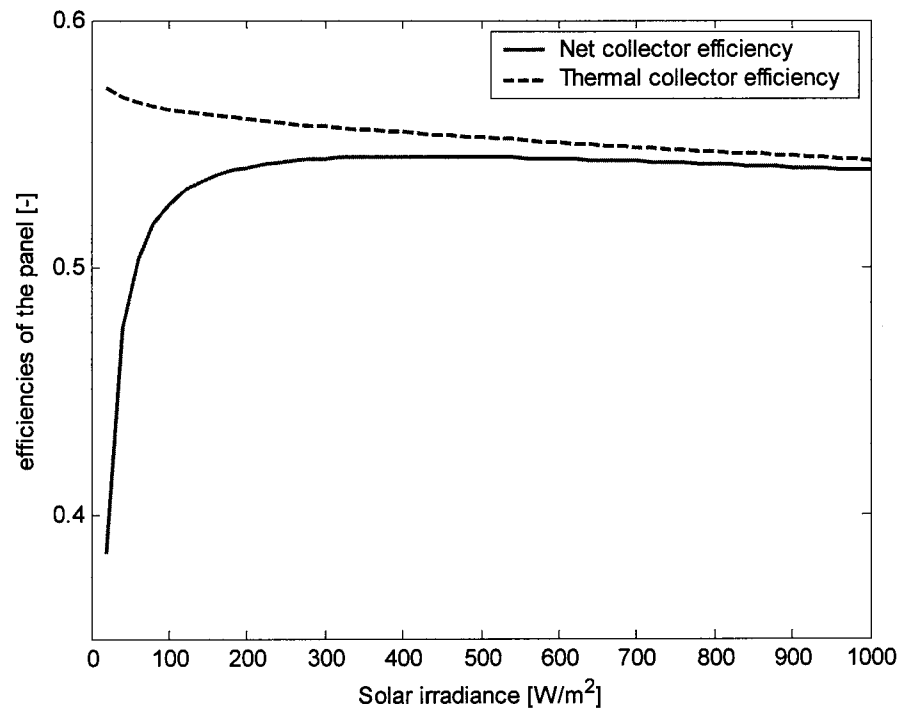

Figure 4.14: Efficiencies vs. the solar irradiance.

The thermal collector efficiency shows a decreasing trend with increasing solar irradiance. The model shows the collector medium output temperature, the only variable in determining the thermal efficiency (formula 3.3), does not increase linear. Every increase in solar irradiance gives a slightly smaller increase in outflow temperature in comparison to the previous. This means that for every increase in solar irradiance the increase in total heat loss coefficient (U_L) will be larger than that of the total heat transfer coefficient inside the collector (h). We can see that the collector efficiency factor (formula 3.26) decreases from F' = 0.849 at I_s = 20 [W/m^2] to F' = 0.820 at I_s = 1000 [W/m^2].

The net efficiency initially increases very fast. In this initial part the fan power (approximately 20 [W]) is of great influence on the efficiency. This influence quickly becomes smaller and when it approaches the thermal collector efficiency curve it will reach an optimum and follow the trend of this curve. The difference between the two curves will become slightly smaller with every increase in solar irradiance and the difference will approach the limit value of the fan power when the solar irradiance is infinitely increased.

4.3.9 Varying the insulation thickness

Finally the thickness of the insulation at the back and edges of the collector will be varied between 0.01 and 0.1 [m]. The results are plotted in figure (4.15):

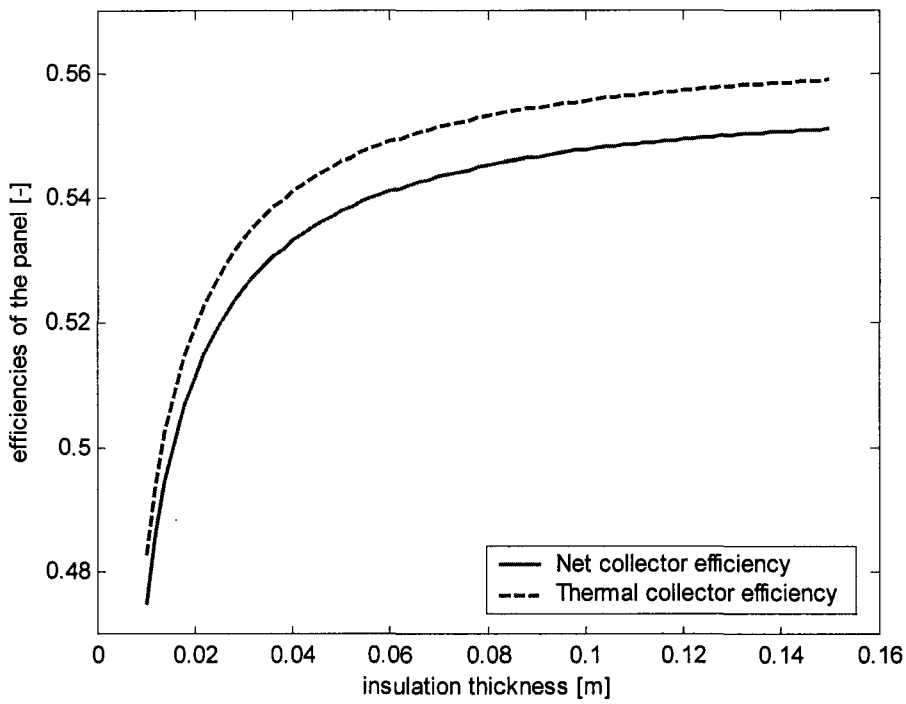

Figure 4.15: Efficiencies vs. insulation thickness of the back and edges of the collector.

Figure (4.15) shows the influence of insulation thickness is important for values to 0.05 [m]. After that the influence on the total heat loss coefficient is only small. The insulation can thus have considerable influence on the panel performance. When it however is made sufficiently thick its influence will be very small.

4.4 Conclusions of the sensitivity analysis

The sensitivity analysis was set up to gain knowledge about which parameters have what influence on the collector performance. In this way, approaches to improve the collector performance can be considered. When the basic two-absorber panel described in chapter three is considered, the losses inside the system can be made smaller by:

- Increasing the insulation thickness.
- Adding a selective coating to the top of the first absorber, to minimize the emission coefficient.
- Increasing the height between the cover and absorber.

The effect of increasing the thickness of the insulation and height between first absorber and cover have little effect however when increased from the base situation. The addition of a selective coating to the top of the first absorber will influence the electrical production of the solar cells and transmission of solar irradiance to the second absorber.

It seems hard to increase the collector performance by altering the losses in the system. A better performance will therefore have to be obtained by increasing the heat transfer inside the collector medium channel. Figure (4.6) and (4.7) shows the heat transfer rate inside the channel can be altered by varying the collector medium velocity and collector medium height. Another way to increase the heat transfer would be to situate fins inside the channel. This will provide a larger area to exchange heat. In this way the thermal collector efficiency (the dotted line in figure 4.6 and 4.7) will increase. This is illustrated by figure (4.16).

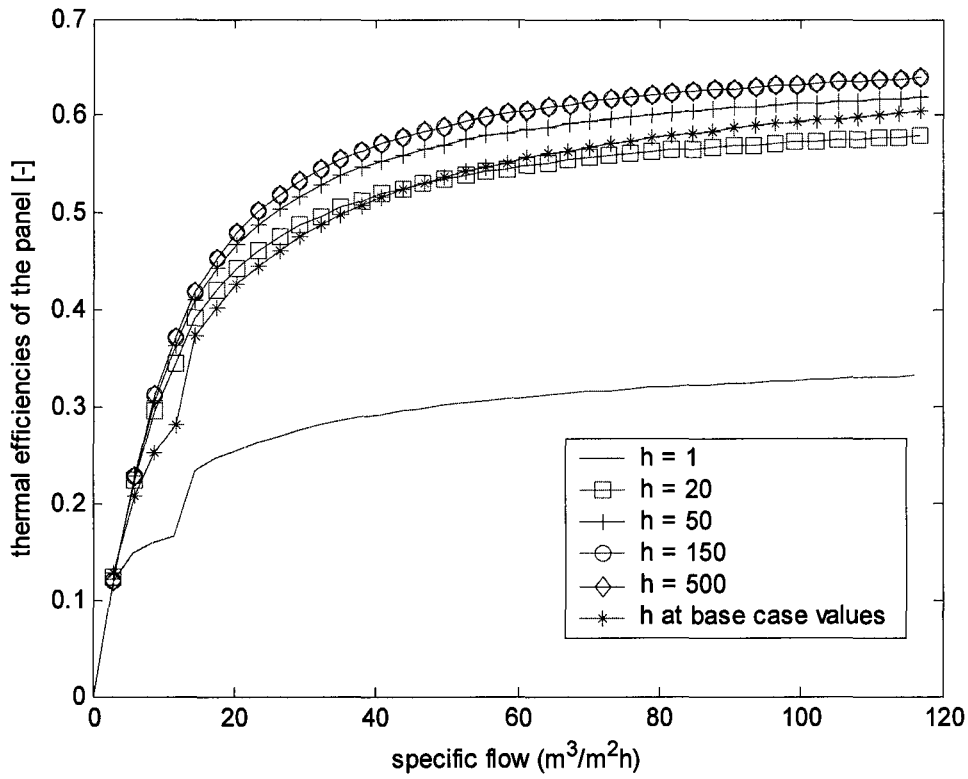

Figure 4.16: Variation of the heat transfer coefficient h inside the collector medium channel over the specific flow range.

In figure (4.16) the heat transfer coefficient inside the collector medium channel (h) was plotted for constant values. The green line represents the base case with increasing specific flow. We can see the base case value for the line with h = 150 has a better thermal efficiency over the

entire specific flow range. For example it is 0.08 larger at 20 [m^3/m^2h] and 0.04 larger at 100 [m^3/m^2h]. If we are able to increase the heat transfer coefficient inside the collector medium channel this much, the thermal efficiency of the panel would thus be significantly better.
A disadvantage of the addition of fins is that the pressure drop inside the channel will increase. The net collector efficiency (the red line in figure 4.6 and 4.7) will therefore initially be larger than that of a finless collector. The pressure drop will however increase more rapidly, by which the net collector efficiency will reach its maximum earlier and from that point decrease more rapidly. In chapter 5 the addition of fins to the absorber(s) will be treated to determine whether or not it may have a positive influence on collector performance.

5 Addition of fins inside the collector

In this chapter the base two-absorber model from chapter 3 will be altered, as the second absorber will be equipped with fins. First a brief introduction on continuous and offset fins will be given. After that the differences for both types of fins on the model will be introduced, with respect to heat transfer and pressure drop. Finally the model results will be compared to the original two-absorber model using a base case for both types of fins.

5.1 Continuous and offset plate fins

To increase the thermal performance of the PV/T-panel defined in chapter 3 and 4 we will increase the heat transfer inside the collector medium channel. Heat transfer can be augmented via rough surfaces, displacement devices, continuous fins and offset fins. The main disadvantage of the application of these methods is that they also induce an increased pressure drop over the collector medium channel. Whether this pressure drop increase has a major influence on the total pressure drop remains to be seen.
We will limit the heat augmentation to continuous and offset strip fins. The working principle of these two fin types is different as continuous fins provide an increased heat transfer area and offset fins provide a combination of increased area and the vanishing and redeveloping of laminar boundary layers. This will be explained in more detail in § 5.1.2.
Both types of fins will be attached to the second absorber only, since fixed fins to the first absorber would block the transmitted solar irradiance of the first absorber. Since the results from § 4.3.7 , where the transmission and absorption coefficients of the first absorber were varied, show that the absorption coefficient and the resulting first absorber temperature should be minimized we will not influence the total absorbed irradiance of the first absorber.

5.1.1 Continuous fins

Heat transfer
In § 2.1.3 the addition of continuous fins to the second absorber was treated briefly. The addition of these fins inside the collector medium channel provides a larger area for heat exchange than a channel without fins. The fins are placed parallel with the direction of the collector medium. Figure (5.1) shows the geometrical parameters used when working with continuous fins.

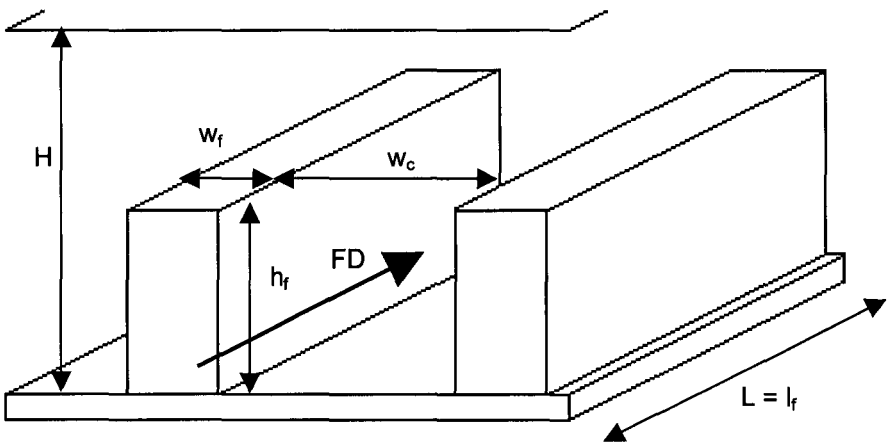

Figure 5.1 Geometrical parameters for a finned absorber.

Here h_f, w_f and l_f are the height, width and length of the fins and H, w_c and L are the height, width and length of the channel. FD shows the flow direction of the collector medium, in this case parallel to the fins. We speak of continuous fins when the fin length is equal to the collector

length ($l_c = l_f$ in figure 5.1). One can now see the extra area the fins provide inside the collector medium channel is equal to:

$$A_{fins} = 2n_{tf} h_f l_f \tag{5.1}$$

where n_{tf} is the total number of fins. The factor 2 is added because the fin has two sides.
We will now define the fin efficiency, which is a dimensionless parameter that describes how well the fin functions as an extension of the base surface of the fin:

$$\eta_{fin} = \frac{q_b}{h_{c,b-cm} p_{topfin} H_{cf} (T_b - T_{cm})} \tag{5.2}$$

Here q_b represents the actual heat transfer rate of the fin and the denominator the maximum heat transfer rate when the entire fin is at the local back plate temperature, p_{topfin} is the perimeter of the top of the fin:

$$p_{topfin} = 2(l_f + w_f) \tag{5.3}$$

and H_{cf} is the corrected fin length defined as:

$$H_{cf} = h_f + \frac{w_f}{2} \tag{5.4}$$

The corrected fin length is used to modify the fin length for a fin with heat transfer through the tip. With the corrected fin length a larger fin with an insulated tip is created, which has the same total heat transfer rate as the original fin. In this way we can use the theory of a finite-length fin with insulated tip as noted in Bejan (1993, chapter 2.7).
The denominator in formula (5.2) is greater than q_b, because the real fin temperature decreases along the fin. Consequently the actual convective heat flow that crosses the wetted surface of the fin is smaller than the maximum value of the denominator. This means the fin efficiency will always be smaller than one. To calculate the fin efficiency we must first define the heat transfer rate of the fin. The heat transfer rate of the fin with corrected fin length can be written as (Bejan 1993):

$$q_b = (T_b - T_{cm})(kA_{tf} h_{c,b-cm} p_{topfin})^{1/2} \tanh(nH_{cf}) \tag{5.5}$$

where *n* is defined as:

$$n = \left(\frac{h_{c,b-cm} p_{topfin}}{kA_{tf}} \right)^{1/2} \tag{5.6}$$

Here p_{topfin} is the perimeter of the top of the fin, k is the thermal conductivity of the fin and A_{tf} is the area of the top of the fin. We can now combine formula (5.2) and (5.5) and rewrite the efficiency of the fin:

$$\eta_{fin} = \frac{\tanh(nH_{cf})}{nH_{cf}} \tag{5.7}$$

With the fin efficiency we can now derive what extra amount of heat is transferred through the increased area of the fins. The total heat transfer rate from the back plate to the collector medium is the original amount of heat over the collector area plus the total amount of heat transferred through the finned area:

$$q_b = h_{c,b-cm} A_{coll} (T_b - T_{cm}) + h_{c,b-cm} A_{fin} \eta_{fin} (T_b - T_{cm}) \tag{5.8}$$

Here A_{coll} is the area of the collector without fins and A_{fins} is the extra area provided by the fins, as was formulated in formula (5.3). Formula (5.8) can now be rewritten as:

$$q_b = h_{c,b-cm} \left(1 + \frac{A_{fins}}{A_{coll}} \eta_{fin} \right) A_{coll} (T_b - T_{cm}) = h_{c,b-cm} \psi_{cont} A_{coll} (T_b - T_{cm}) \tag{5.9}$$

where

$$\psi_{cont} = 1 + \frac{A_{fins}}{A_{coll}} \eta_{fin} \tag{5.10}$$

We can see from formula (5.10) the increased heat transfer from the back plate is determined by the area of the fins A_{fins} and the fin efficiency η_{fins}.
The heat transfer coefficient $h_{c,b-cm}$ will be calculated using the formulas from § 3.2.4.3 and a hydraulic parameter defined with:

$$D_{h,cf} = \frac{4(A_i - (n_{tf} w_f h_f))}{(2h_c + 2w_c) + 2n_{tf} h_f} \tag{5.11}$$

where A_i is the finless inflow area of the collector channel. One can see from formula (5.10) that the influence of the fins on the heat transfer will depend on the heat transfer area and efficiency of the fins.

Pressure drop
The incorporation of fins however also induces an increased pressure drop over the collector medium channel. This increased pressure drop is caused by an increase in perimeter and a decrease in collector inflow area. This means the hydraulic diameter of the channel, as defined in formula (5.11), will decrease, which will induce an increased pressure drop. The calculation of this new pressure drop will be done using the formulas from § 3.2.5 and the hydraulic diameter from formula (5.11). Whether the increase is large compared to the pressure drop of a finless channel will be examined in § 5.4.

5.1.2 Offset fins

The addition of offset fins to the second absorber will increase the heat transfer rate not only through an increase in area, but also through an increased heat transfer coefficient. The fins can be presented as small plane walls along which an external flow is driven. When the fins, placed parallel to the flow direction, are kept small, the thermal boundary layers that will develop along the fins will remain laminar. In the laminar range, the heat transfer coefficient decreases with $x^{-1/2}$, while in the turbulent range this value is $x^{-1/5}$. This means that when the fin length is made sufficiently small, the averaged heat transfer coefficient along the fin will be very large. The averaged shear stress along the fin however also increases with the same values, causing the pressure drop to increase with decreasing fin length. This is illustrated by this figure from Bejan (1993, chapter 5.4):

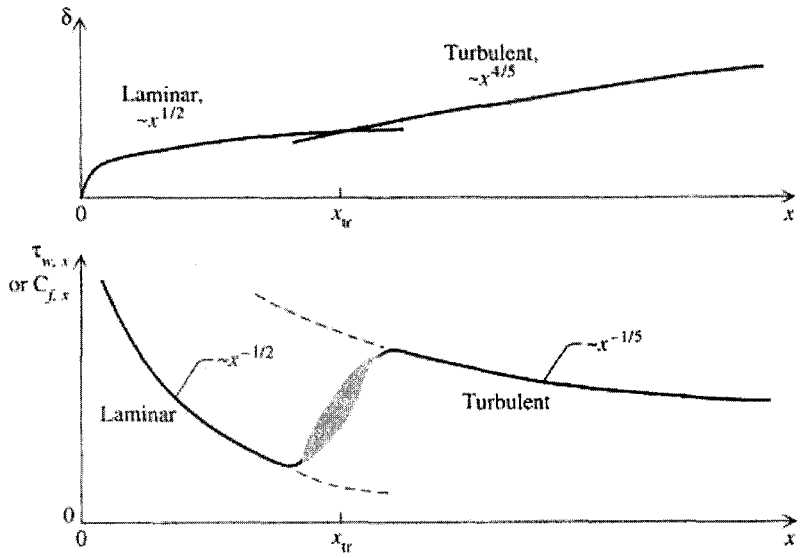

Figure 5.2: The behavior of the boundary layer thickness and wall shear stress in the laminar and turbulent sections of the boundary layer over a plane wall.

In figure (5.2) we can see the shear stresses along the fin increase very fast with decreasing fin length. This means the resulting pressure drop will be very large too. Whether the resulting increased fan power is as large as the resulting increased heat transferred to the collector medium remains to be seen. To what extend the net and thermal efficiencies are influenced we will determine in § 5.4. First we will show the changes the model from chapter 3 experiences when the offset fins are added to the second absorber.

Heat transfer

We can present one single fin as a flat plate with air passing alongside of it. When the fin length is small, the boundary layer will remain laminar. Bejan (1980) gives the averaged Nusselt number over a fin with length *x* as:

$$\overline{Nu}_x = 0.664 \Pr^{1/3} \mathrm{Re}_x^{1/2} \qquad (\Pr \geq 0.5) \tag{5.12}$$

To obtain a constant heat transfer coefficient over the length of the panel, the offset fins will be connected to the backplate as shown in figure (5.3), where l_f is the fin length, l_{bf} is the space between the fins in the flow direction and L_c is the collector length.

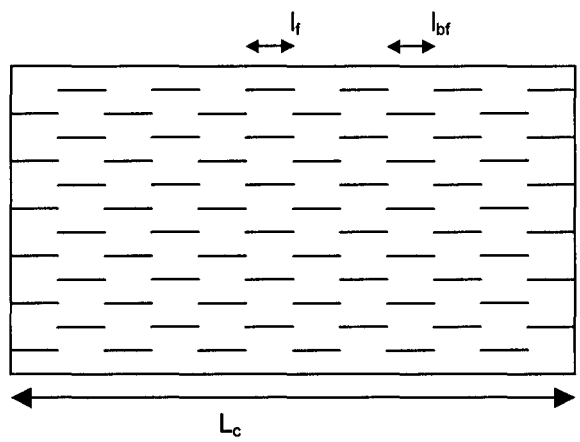

Figure 5.3: Schematic top view of the second absorber with offset strip fins.

The main advantage of this staggered configuration is that the total heat transfer area is equal to that of a continuous fin configuration. If the fins are placed in-line, the area would be smaller. An additional advantage model-wise is that the heat transfer coefficient over the length of the channel will remain constant when we work with the averaged Nusselt number over the fin from formula (5.12).

If we now use the fin efficiency defined in formula (5.2) the heat transfer rate can be defined similar to that in formula (5.8):

$$q_b = h_{c,b-cm} A_{coll} (T_b - T_{cm}) + h_{fin} A_{fins} \eta_{fin} (T_b - T_{cm}) \tag{5.13}$$

where A_{fins} is again defined in formula (5.1), h_{fin} is the averaged heat transfer coefficient over a fin calculated with the Nusselt number from formula (5.12), A_{fin} is the total area of the fins and η_{fin} is the fin efficiency as defined in formula (5.1). The difference between the formulas (5.8) and (5.13) is that the heat transfer coefficient of the fins is different from that of a flat plate.
Based on (5.13), the total heat transfer rate from the back absorber to the collector medium can now be written as:

$$\begin{aligned} q_b &= \left(1 + \frac{h_{fin}}{h_{c,b-cm}} \frac{A_{fins}}{A_{coll}} \eta_{fin}\right) h_{c,b-cm} A_{coll} (T_b - T_{cm}) \\ &= \psi_{offset} h_{c,b-cm} A_{coll} (T_b - T_{cm}) \end{aligned} \tag{5.14}$$

where:

$$\psi_{offset} = 1 + \frac{h_{fins}}{h_{c,b-cm}} \frac{A_{fins}}{A_{coll}} \eta_{fin} \tag{5.15}$$

The thermal profit of the offset fins is thus concealed in a larger heat transfer coefficient over the length of the channel and an enhanced heat transfer area. The influence of the heat transfer coefficient is however strongly dependent of the fin length and velocity of the collector medium.

Pressure drop
The pressure drop over the channel will increase because the addition of the fins will induce an additional skin friction. This extra pressure drop behaves similar to the behavior of the heat transfer coefficient in that it will be large for small fins and small for large fins. This was illustrated earlier in figure (5.2).
The average shear stress along the fin can be evaluated with the dimensionless average skin friction coefficient as defined in Bejan (1993):

$$\overline{C}_{f,x} = \frac{\overline{\tau}_x}{\frac{1}{2}\rho v^2} = 1.328 \mathrm{Re}_x^{-1/2} \tag{5.16}$$

The resulting pressure drop over the channel can be divided into a pressure drop over the fins and a pressure drop over the original finless channel.

$$\Delta P A_{Dh} = \overline{\tau}_{x\,fin} A_{fins} + \Delta P_{finless} A_{channel} \tag{5.17}$$

Here $\Delta P_{finless}$ is the pressure drop over the original finless channel and $A_{channel}$ is the total area inside the collector medium channel without fins.

It has to be noted that a few assumptions have been made during the incorporation of the fins inside the model.
First we assume the pressure drop over the channel can be calculated by adding the extra pressure drop over the fins to the pressure drop of a finless channel. This is a very simple approach, which will not be entirely true. The fins do not only provide a thermal boundary layer but also a velocity boundary layer, which locally influences the velocity of the flow. If the velocity boundary layer from the previous fin has not yet fully disappeared the incoming flow velocity of the next fin will be slightly different. Also the fins are fixed to the back absorber only. Since the fins provide an extra flow resistance, the velocity over the height and width of the channel will differ. Both influences will however not be great when the space between the fins (l_{bf}) in the flow direction and over the width of the absorber (w_c) are kept sufficiently high. The incorporation of fins will thus lead to some two-dimensional influences. Since it is very hard to predict to what extend these two-dimensional influences influence the results for the one-dimensional model and only little research has been conducted on the incorporation of fins in a solar panel we will assume the influences can be ignored.

5.2 Definition of the sensitivity analysis parameters

In this sensitivity analysis the parameters that influence the heat transfer from the absorbers to the collector medium will be varied. First a base case for both the collector with continuous fins as the collector with offset fins will be defined. After that a sensitivity analysis will be performed, which compares both finned collectors to a finless one.

5.2.1 Defining the base case

All parameters defined for the finless model in § 4.1 will be taken as the base case parameters. This is done in order to compare the results with the finless model. The model must however be extended with the fin parameters for both continuous and offset fins. These parameters and their base case value are summarized in table 5.1:

Parameter	Description	Value for continuous fins	Values for offset fins
h_f	Height of the fin	0.01 [m]	0.01 [m]
w_f	Width of the fin	0.005 [m]	0.005 [m]
l_f	Length of the fin	5 [m]	0.02 [m]
w_c	Space between fins	0.045 [m]	0.045 [m]
H	Channel height	0.02 [m]	0.02 [m]

Table 5.1: Base case values for fin parameters.

The height, width and length of the fins are those shown in figure (5.1). The space between the fins is defined as w_c in the same figure. This parameter determines, together with the fin width, what amount of fins there will exist over the width of the channel.
The fins will be made of aluminum, because it has a high thermal conductivity. This means the fin efficiency will be high.

To obtain an idea of the influence of the fins we will compare a few results of the base case model for finless and both types of finned collector medium channels. We will compare the averaged heat transfer coefficient of the back plate $\overline{h}_{c,c-cm}$, the averaged heat transfer coefficient inside the collector medium channel $\overline{h}$ and the averaged total heat loss coefficient from the first absorber $\overline{U}_L$. We will also compare the pressure drop in all three panels. Finally we will compare the thermal and net efficiency in base case scenarios:

Parameters	Finless channel	Continuous fins	Offset fins
$\overline{h}_{c,b-cm}$ [W/m^{2}K]	18.4	57.4	54.1
$\overline{h}$ [W/m^{2}K]	22.3	28.3	26.9
$\overline{U}_L$ [W/m^{2}K]	4.7	4.6	4.7
Δp_{total} [Pa]	108.1	167.2	140.0
η_{th} [-]	0.553	0.570	0.568
η_{net} [-]	0.545	0.558	0.555

Table 5.2: Comparison of model parameters for three kinds of second absorber types.

We can see that for both kinds of fins the increase in heat transfer coefficient from the second absorber (back plate) is fairly large. When we look at the averaged heat transfer coefficient inside the channel we can see these values have also increased with 6 and 4.6 [W/m2K]. This leads to an increase in both thermal end net efficiency, although the increase at base conditions is not very large.

5.2.2 Varied parameters

The parameters that will be varied can all in some way influence the heat transfer inside the collector medium channel. We will first define the parameters that can influence the heat transfer inside the collector medium channel. This means channel height, mass flow rate and geometric fin parameters. It has to be noted that the fin length will of course only be varied in the case of offset fins. The parameters and their variation are summarized in table (5.3):

$\dot{m}$	Mass flow of the collector medium	0 - 0.25 [kg/s]
g	Height collector channel	0.003 – 0.1 [m]
h_f	Height of the fin	0 – 0.018 [m]
w_f	Width of the fin	0.001 – 0.01 [m]
l_f	Length of the fin	0.01 – 0.2 [m]
w_c	Space between fins	0.005 – 1 [m]

Table 5.3: Varied parameters that directly influence the convective heat transfer coefficient inside the channel.

Next we define the parameters that influence the radiative heat transfer inside the collector medium channel directly. Since we concluded in chapter 4 that the emission coefficient from the bottom of the first absorber is difficult to influence, this will not be varied. The emission coefficient of the second absorber will however be varied, especially since with the incorporation of fins the second absorber temperature can become smaller than that of the first absorber. In that case a large emission coefficient would be beneficial.
Another way of altering the radiative heat transfer inside the channel is a variation in absorption and transmission of the first absorber and a variation in solar irradiance. These parameters will change the temperature of both absorbers directly, which in its turn influences the radiative heat transfer. The parameters and their variation are shown in table (5.4)

ε_3	Emission of the second absorber	0.05 – 0.95 [-]
α_2	Absorption coefficient first absorber	0.05 – 0.76 [-]
τ_2	Transmission through first absorber	$\alpha_2 + \tau_2 = 0.76$[-]
I_s	Irradiance on the collector	0 – 1000 [W/m^2]

Table 5.4: Varied parameters that influence the radiative heat transfer inside the collector medium channel.

Since all parameters and the variation of a selected number of them are now known, we can start the sensitivity analysis of the varied parameters.

5.3 Sensitivity analysis

5.4.1 Varying the mass flow

Variation in mass flow will induce a variation in specific flow. The increased heat transfer area and, in the case of offset fins, the varied heat transfer coefficient of the fins can increase the thermal output of the collector. It will however also increase the pressure drop over the channel, causing the net collector efficiency to drop faster than in the case of a finless channel. When we vary the mass flow at base case conditions the following results are obtained:

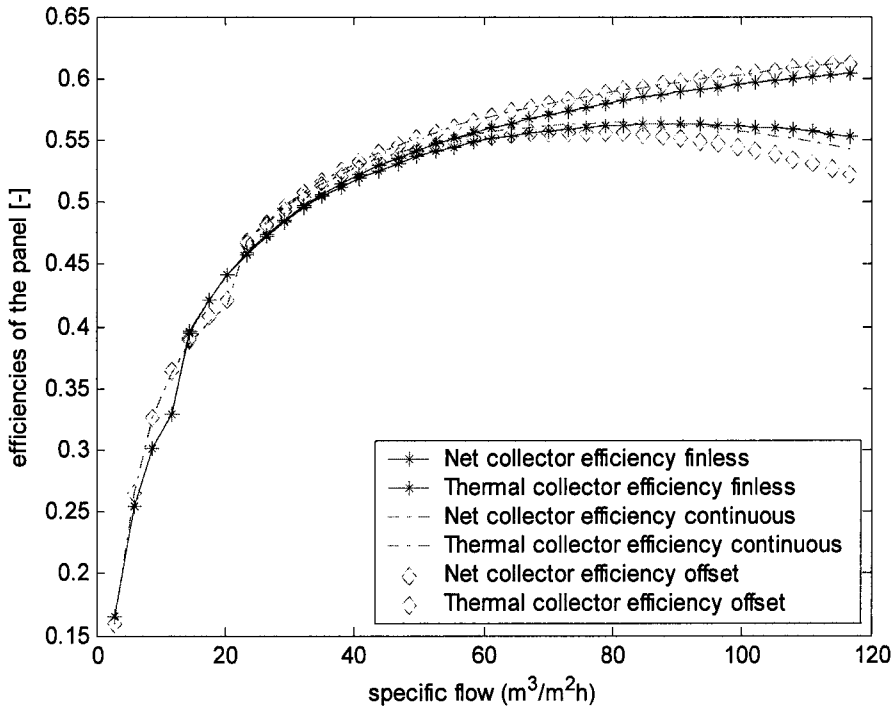

Figure 5.4: Efficiencies for continuous, offset and finless channels vs. specific flow.

Figure (5.4) shows in the laminar range the fins have a fairly large effect on heat transfer. At a specific flow of 12 [m^3/m^2h] the difference between the finned and finless configurations is about 0.04. When transition occurs in the finned configurations, the laminar to turbulent effect is smaller then for the finless configuration.
From this point we see the thermal efficiencies do not differ much. The difference with a finless channel is no more than 0.01 for both continuous fins and offset fins.
The net efficiency of the continuous fins however reaches its maximum at 85 [m^3/m^2h], which is only slightly smaller than the finless configuration at 90 [m^3/m^2h]. This is also the point the two lines intersect. The net efficiency of the offset fins reaches its maximum at 78 [m^3/m^2h], but already intersects the finless line at 72 [m^3/m^2h]. The influence of fins at these base conditions in the turbulent range is thus fairly small.
One reason for this small influence is the small radiative heat transfer coefficient, caused by the small emission coefficient of the second absorber. Since the heat transfer coefficient of the

second absorber with fins is now considerably larger compared to the finless situation, more incoming irradiance can be transferred per m^2. This means the second absorber temperature will become smaller than that of the first absorber. It would therefore be beneficial in finned configurations to create a large emission coefficient.

The emission coefficient of the second absorber will therefore be made 0.9 for finless channels and continuous and offset fins. The thermal and net efficiencies are plotted in figure (5.5).

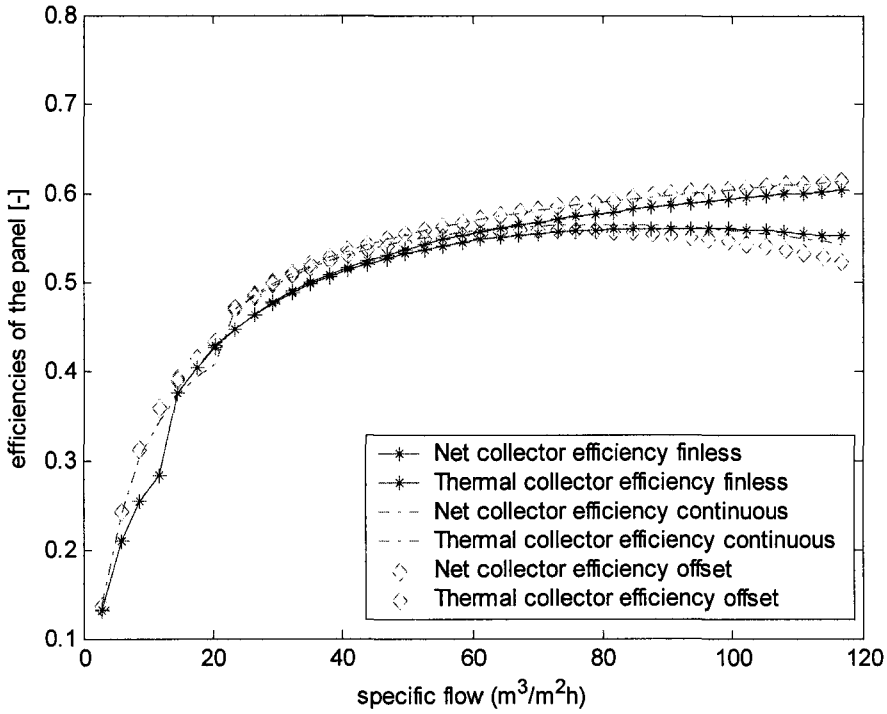

Figure 5.5: Efficiencies for continuous, offset and finless channels vs. specific flow at ε = 0.9.

Figure (5.5) shows the influence of both continuous fins and offset fins is considerable. In the laminar range the efficiencies differ as much as 0.12 at a specific flow of 12 [m^3/m^2h]. In the turbulent range, the thermal efficiency difference gradually decreases from 0.025 at 25 [m^3/m^2h] to 0.01 at 110 [m^3/m^2h]. The intersection points of the net efficiency with the finless channel lies at 85 [m^3/m^2h] for the offset fins and at 95 [m^3/m^2h] for the continuous fins. The specific flow in basic solar air collectors, as treated by Hastings (1999), is usually between 40 and 60 [m^3/m^2h]. In this range the net efficiency of the finned configurations is slightly larger than that of the finless one. The introduction of fins inside the channel thus seems to have a positive effect on the efficiency of the panel within a certain range for the specific flow. The influence is however strongly dependant on the velocities inside the collector. For an indication of the pressure drops experienced in the finned and finless collector medium channel table 5.5 was made:

Collector type	Pressure drop support system [Pa]	Pressure drop collector medium channel [Pa]
Finless channel	67.7	40.4
Continuous fins	67.7	99.5
Offset fins	67.7	110.6

Table 5.5: Pressure drop over the channel and support system at a specific flow rate of 60 [m^3/m^2h].

We can see that although the pressure drop over the channel is somewhat higher for finned channels. The influence on the fan power will however be small compared to the yield of the

collector. At larger specific flow rates we can see an increase of the influence of the fan power (figure (5.5)).

5.4.2 Varying the height of the channel

The channel height cannot be reduced under 0.01 [m], because this is equal to the fin length in the base case. Since the collector medium velocity will decrease with increasing channel height, the heat transfer in a finless channel will decrease rapidly. The influence of the augmentation of fins would therefore be larger under these circumstances.

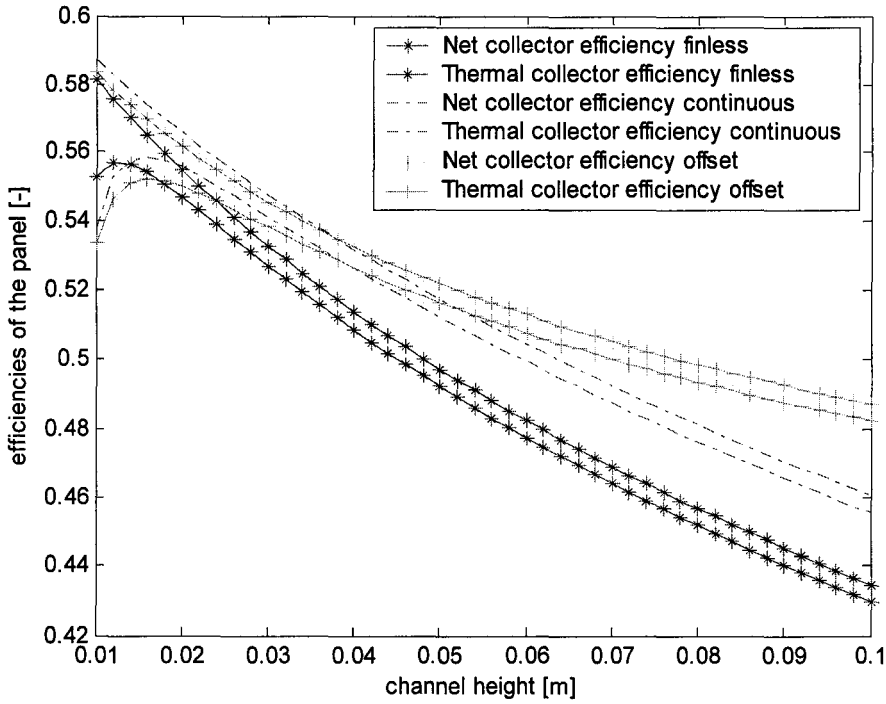

Figure 5.6: Efficiencies for continuous, offset and finless channels vs. channel height.

Figure (5.6) can be compared to figure (5.5) in the way that it shows the same trend. The net collector efficiency for a finless channel is highest for very small values of the channel height. After that the net efficiency of both the continuous fins and offset fins is larger. When the collector medium velocity decreases with an increasing channel height, the offset fins intersect the continuous fins. A similar patron can be distinguished in figure (5.5).

We can thus conclude that for small velocities the offset fins perform best. For very large velocities a finless channel is preferred and for specific flows that are normal in air collectors continuous fins would be beneficial under these base case conditions.

5.4.3 Varying the fin height

The fin length and the resulting fin area determine both the increasing heat transfer from the second absorber as the increased pressured drop induced inside the channel. When the fin height is varied and we regard the resulting efficiencies we can determine whether an optimum fin length exists. The results are plotted in figure (5.7):

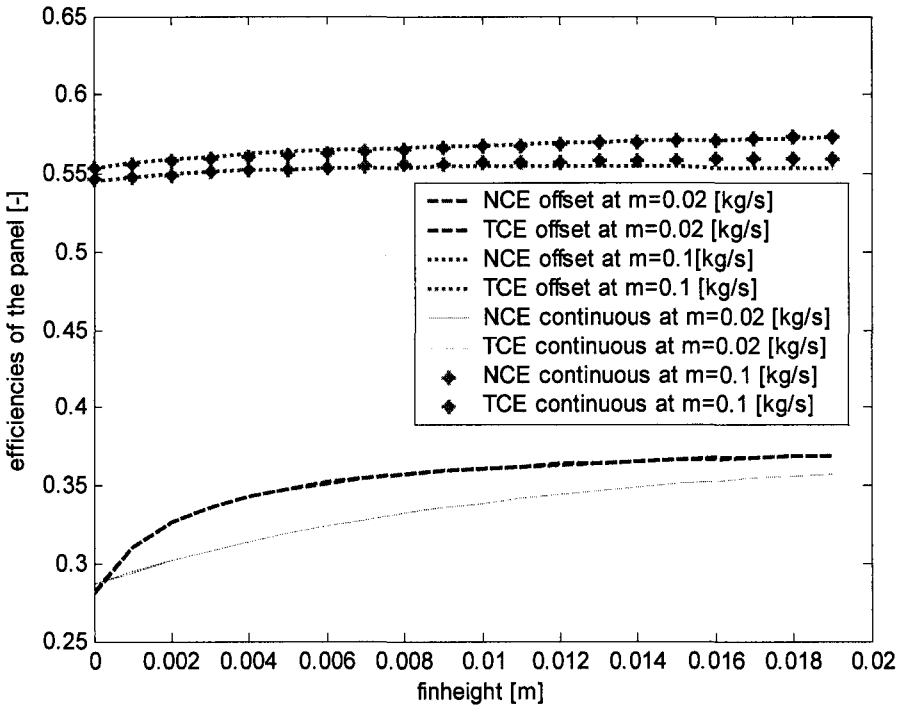

Figure 5.7: Efficiencies for continuous, offset and finless channels vs. fin height.

Figure (5.7) shows the net collector efficiency for offset fins reaches a maximum at a fin height of 0.013 [m]. Continuous fins however do not reach a maximum for this channel height. We can see that at a mass flow rate of 0.1 [kg/s], the heat transfer of continuous fins is larger than that of the offset fins. This means the laminar boundary layers along the fins have developed so much that the averaged heat transfer coefficient of the finned back plate is smaller for offset than for continuous fins.
For a smaller mass flow rate of 0.02 [kg/s] and the resulting small velocity we can see that initially the efficiency for offset fins grows very fast. Since the effect of increasing the heat transfer coefficient has a limiting effect and the fin efficiency is not equal to one we can see the thermal and net efficiency to approach the thermal limits at this collector medium speed. The rise of thermal efficiency for continuous fins has a much more consistent increase.
It seems that at high collector medium velocities, the influence of adding fins inside the channel is only small. This means that at high velocities the heat transfer inside a finless channel is already good, thus reducing the effect the fins have on the thermal output of the collector. For small velocities the influence of the fin height and resulting increase in area is much larger, because the influence on the heat transfer coefficient is much larger relatively.

5.4.4 Varying the fin length

Variation of the fin length will only be performed for offset fins. The fin length is very important for both the heat transfer and pressure drop over the fins, as explained in § 5.2. In this case it would be of more interest see to what amount the heat transfer coefficient of the back plate is influenced by the fin length. For comparison the heat transfer coefficients of continuous fins and no fins are added to the figure.

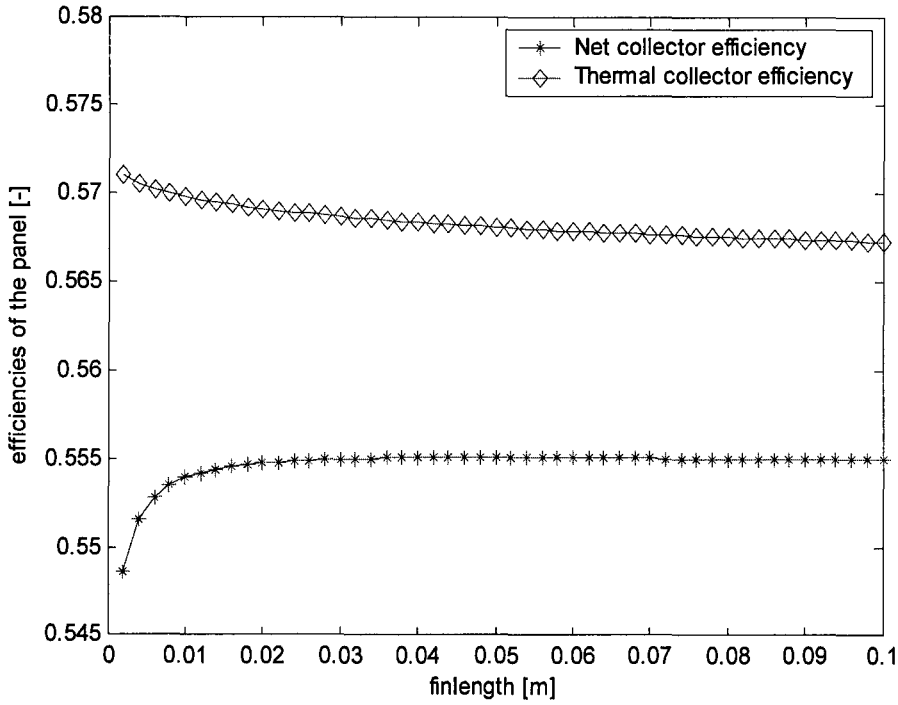

Figure 5.8: Heat transfer coefficient of the back plate for varied fin length.

Figure (5.8) shows that at the base value of 0.05 [m] the offset fins thermally perform slightly less good than continuous fins but much better than a finless channel. This is confirmed by figure (5.5), where at the base value of the mass flow rate (m = 0.1 [kg/s]) the thermal efficiencies are ranked in the same order. To perform equal to the continuous fins, the offset fin length should be reduced to 0.037 [m]. Since this would bring an increase in pressure drop and the net efficiency is already smaller than that of the continuous fins this would not be a good idea.
It seems varying the fin length can have a large influence on the heat transfer coefficient. Reducing the fin length is however only beneficial when the collector medium velocities and the additional heat transfer rate is fairly small. Offset fins are thus beneficial in low-speed PV/T-applications.

5.4.5 Varying the emission coefficient from the bottom absorber

The emission coefficient of the bottom absorber was changed from 0.1 to 0.9 in § 4.5.1. The reason was that the enhanced heat transfer augmented by the fins provided a smaller second absorber temperature than that of the first absorber. Since all heat losses to the environment are suffered from the first absorber it would be interesting to see what influence this emission coefficient, and therefore the radiative heat transfer inside the channel, has on the performance of the various panel configurations.

Figure (5.8) shows the thermal and net efficiency of both finned panels rises with an increasing emission coefficient. The finless panel however shows a decrease in efficiencies, which clearly shows the second absorber temperature is indeed larger than that of the first absorber. We can also see that the thermal efficiency does not vary much with the emission coefficient. The difference between the finned and finless configuration for both thermal and net efficiency does however increase with increasing emission coefficient. Since a large emission coefficient is easily reached by painting the absorber black this would be recommended. When the temperatures of both absorbers are different (for example by increasing the absorption coefficient of the first

absorber), the efficiency lines of the finless channel follow the same trend as that of the finned configurations.

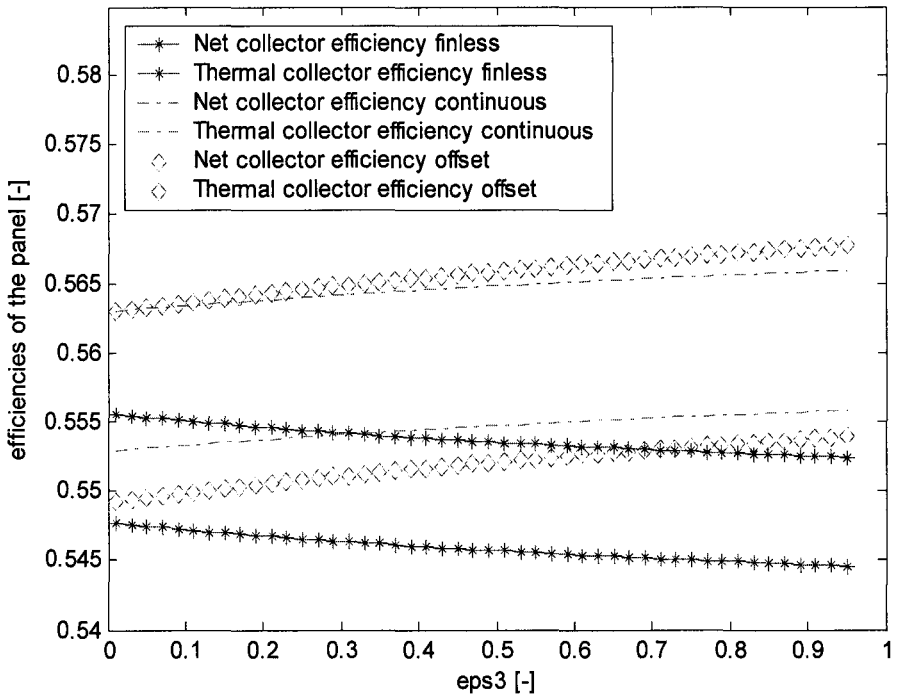

Figure 5.9: Efficiencies for continuous, offset and finless channels vs. emission coefficient of the back absorber.

5.4.6 Varying α_2 and τ_2 of the second absorber

The absorption coefficient of the first absorber α_2 will be varied between 0.76 and 0, as in § 4.3.7. The maximum value of 0.76 is the total value of the sum of the transmission and absorption coefficient for an untextured amorphous silicon solar cell material with semi-transparent back. The transmission coefficient will therefore again be noted as $\tau_2 = 0.76 - \alpha_2$. The transmission and absorption coefficients for a large part determine the temperature of the first and second absorber. The results are plotted in figure (5.10).

Both efficiencies of both finned configurations remain equal or larger than that of a finless channel over the entire absorption domain. The difference between the net and thermal efficiency of the continuous and offset fins and the finless channel remains constant at approximately 0.015 each. For the rest we can see that the trend is almost linear compared to a finless channel.

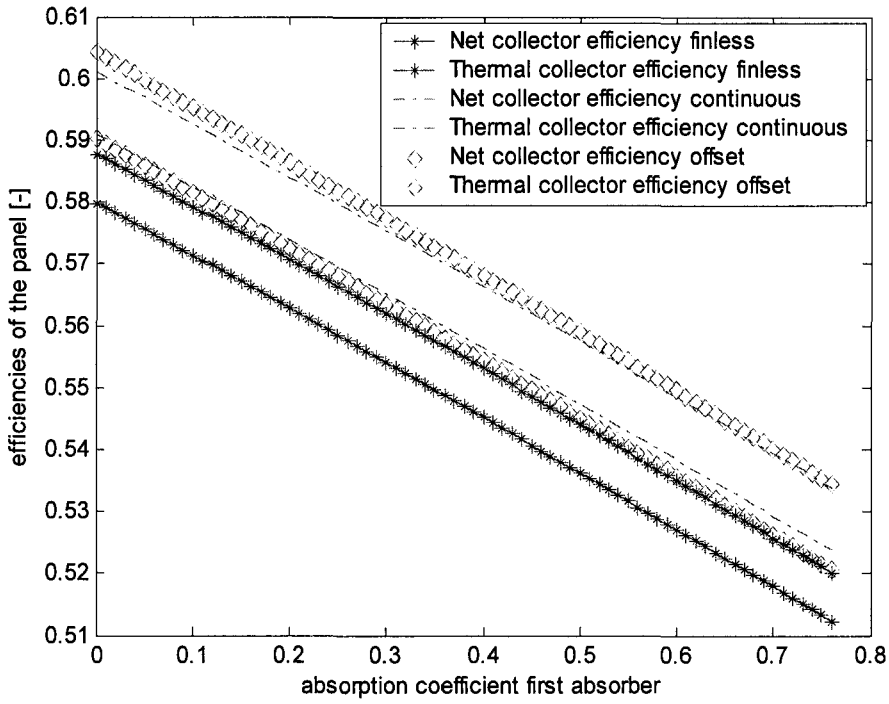

Figure 5.10: Efficiencies for continuous, offset and finless channels vs. absorption coefficient of the first absorber.

5.4.7 Varying the solar irradiance

The solar irradiance on the collector will be varied between 0 and 1000 [W/m^2]. In this case we would expect a similar trend as was plotted in § 4.3.8. It is however expected that the maximum net collector efficiency will be reached at a different solar irradiance value, because of the changes in heat transfer and pressure drop. The results are plotted in figure (5.11).

At very small solar irradiance values the finless channel provides the best net efficiency. This means that in this range the induced fan power by the fins is smaller than the additional thermal power the fins provide. This changes when the solar irradiance reaches 100 [W/m^2] for continuous fins and 150 [W/m^2] for offset fins. From these values the finned collector channels provide a larger net efficiency, which increases to a difference of 0.01 and 0.02 for offset and continuous fins respectively. Also the maximum net efficiency is reached much later for finned channels. The additional heat transfer by the fins keeps the first absorber temperature smaller, thus reducing the thermal loss coefficient from the absorber.

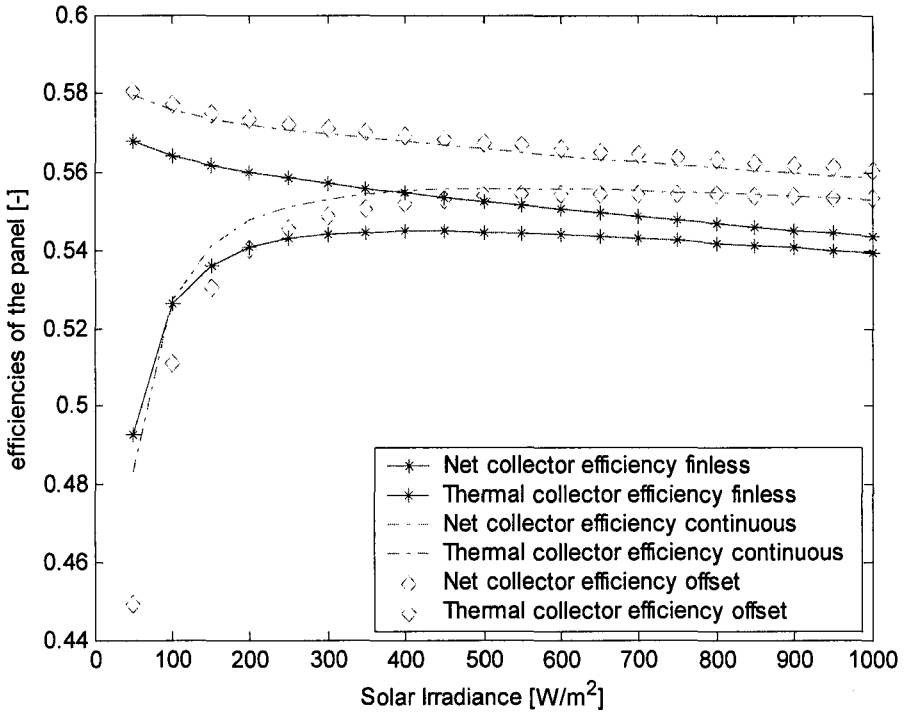

Figure 5.11: Efficiencies for continuous, offset and finless channels vs. solar irradiance.

5.5 Conclusions regarding the application of fins

The sensitivity analysis points out that adding fins to the back absorber would be an easy way to increase the thermal efficiency, especially in the low-velocity range. The biggest problem is the fin area cannot be increased to a large extend, since the channel height for effective solar air thermal collectors is very small.

For continuous fins the heat transfer is increased with every increase fin surface. The incorporation of fins however lowers the hydraulic diameter of the channel considerably, thereby also increasing the pressure drop over the system. In the range of specific flows as common in collectors using air as the collector medium (to approximately 80 [m^3/m^2h], we can see from figure (5.5) the net efficiency is constantly, though decreasingly, larger than that of a finless channel.

Predictions regarding the incorporation of offset fins are slightly more difficult, since the performance is highly dependent on the fin length and the resulting laminar thermal boundary layer development. Figure (5.8) shows the heat transfer coefficient can increase dramatically with decreasing fin length. Whether this has a large influence depends on the velocity off the collector medium, since the difference in heat transfer rate between the fins and the absorber is highly dependable of this parameter. The pressure drop however develops in a similar way to the heat transfer coefficient. Offset fins therefore seem most useful in panels where low collector medium velocities dominate.

It is also hard to influence the first absorber temperature by adding fins to the second absorber. There will off course be an increased radiative heat transfer the first and second absorber when the second absorber temperature is smaller through the addition of fins, but this influence is only marginal. It is therefore recommended to try and add fins to the first absorber and look at the influence this has on the radiative and convective losses through the top.

6 Discussion, conclusions and recommendations

6.1 Discussion

In the preceding chapters we have set up a design for a simple, but effective configuration for the transfer of heat inside a PV/T solar air panel. We have created a one-dimensional model for the heat transfer and pressure drop inside this configuration. The model has been subjected to a few simple tests in order to validate its reliability. After the model was considered reliable, a sensitivity analysis was performed in order to find out what parameters can influence the performance of the panel in what way. After a careful evaluation of the ways to influence the performance positively, it has been found that, especially in the low-speed range, the heat transfer inside the channel has considerable influence on the efficiency of the collector. In the large speed range however the influence is very small.

An important way to compare the energy yield of the panel is to check the thermal and net efficiency of the panel. These efficiencies are plotted in figure (6.1). We can see that, particularly in the low speed range, both efficiencies are very small. This means the losses inside the system are large in this range. When the collector medium velocity increases, we can see an increase in efficiencies. We will compare the thermal yield of the panel with the thermal losses at 10 [m^3/m^2h] and 100 [m^3/m^2h].

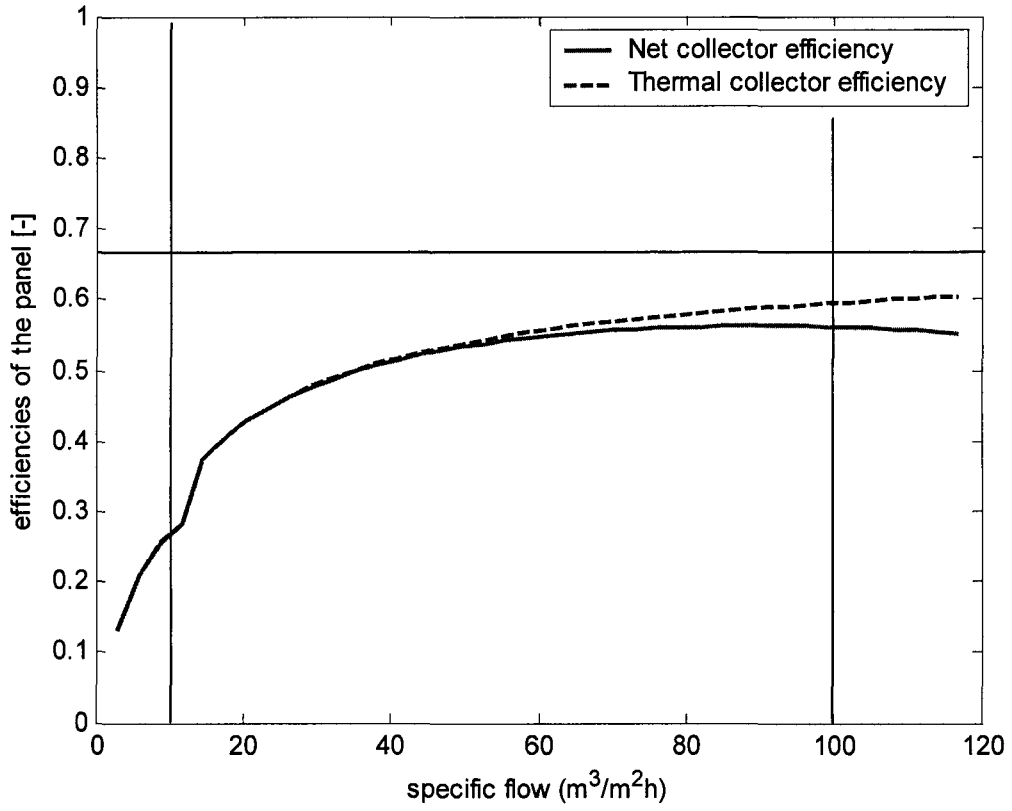

Figure 6.1: Thermal and net efficiency vs. specific flow.

In figure (6.1) the horizontal line marks the optical efficiency at 0.686 (As calculated in § 4.2).

In figure (6.2) the yield and losses at both specific flow rates are schematically represented. We can also see what processes they consist.

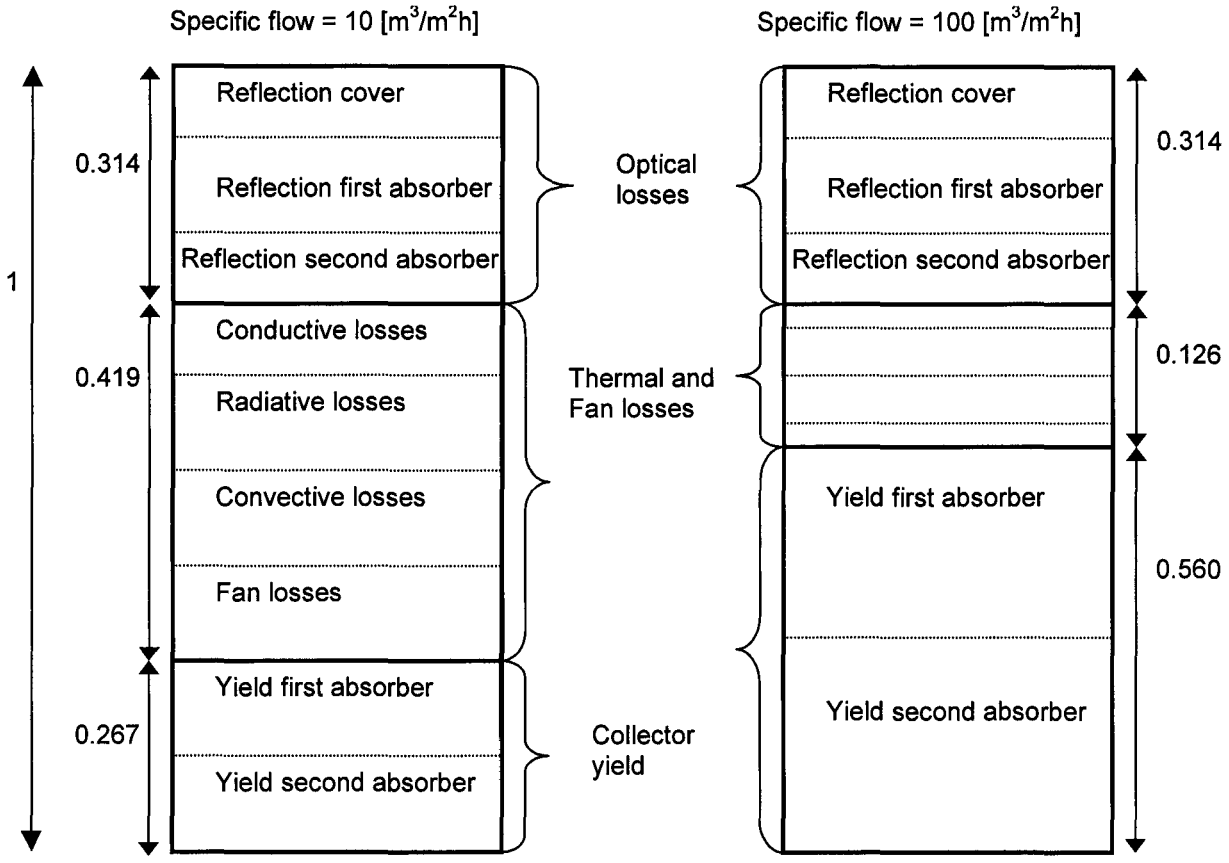

Figure 6.2: Schematic representation of the relative yield and losses inside the panel at 10 and 100 [m³/m²h] respectively.

We will now discuss the yield and losses and the processes they consist of.

The optical losses
The optical losses of the panel consist of three components (§ 2.2). These are the reflection from the cover (ρ_1), the reflection from the first absorber (ρ_2) and the reflection from the second absorber (ρ_3) (Figure 2.8). We can quantify these optic losses at each collector component when we know what amount of irradiance reaches each component. The optic losses at the cover and first and second absorber can be written as:

$$OL = \rho_1 + \tau_1\rho_2 + \tau_1\tau_2\rho_3 \qquad (6.1)$$

Here OL are the optical losses and τ is the transmission coefficient. The optical losses from figure (6.2) can be subdivided into reflection losses from the cover, first absorber and second absorber. We can quantify each of the three components of formula (6.1) by substituting the optical properties from tables (4.2), (4.3) and (4.4) into formula (6.1), see figure (6.3).
The only way to influence the optical losses is to change the optical coefficients of the collector components. This means either the material can be changed or other measures most be taken, like texturing the first absorber.

Since we wish to research thin-film amorphous solar cells this material cannot be changed. The cover and second absorber material can be changed but the reflection coefficients of the materials used are already very small. In this research we use the optical coefficients as was reported by van Poppel (2002).

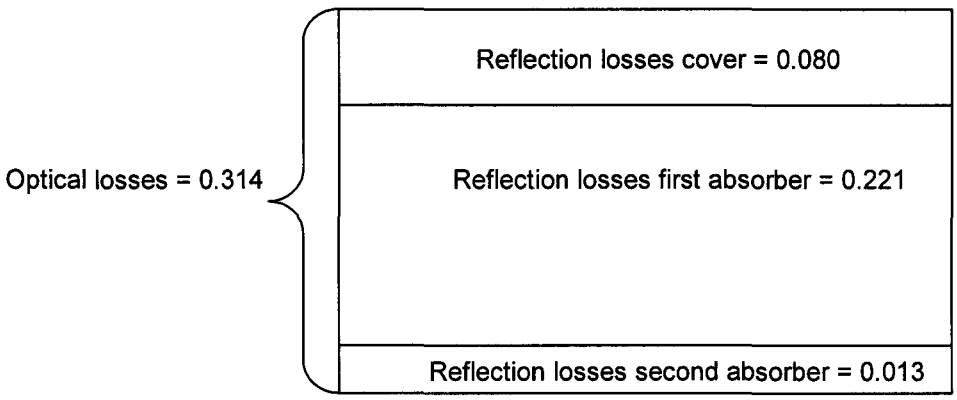

Figure 6.3: Schematic quantification of the optical losses inside the panel.

These values are however only valid for planar amorphous silicon solar cells. When textured cells are used the reflection coefficient of the cell is be approximately 0.1 smaller, which will be contributed to the absorption coefficient. The optical losses due to reflection and the first absorber temperature due to absorption would thus be very different. The amount of optical losses would of course decrease. Due to the increased absorption factor the first absorber temperature, and therefore the thermal losses through the top, would however also be larger.

Thermal and fan losses

A very important aspect of designing a PV/T-panel is to identify and try and control the losses induced by the fan and through convection, conduction and radiation (figure 6.2).
Figure (6.4) features a schematic quantification of the heat and fan power losses the panel suffers at specific flow rates of 10 and 100[m^3/m^2h]. We can see that even at high flow velocities, here at a specific flow of 100 [m^3/m^2h], most losses are still suffered through the top of the panel.

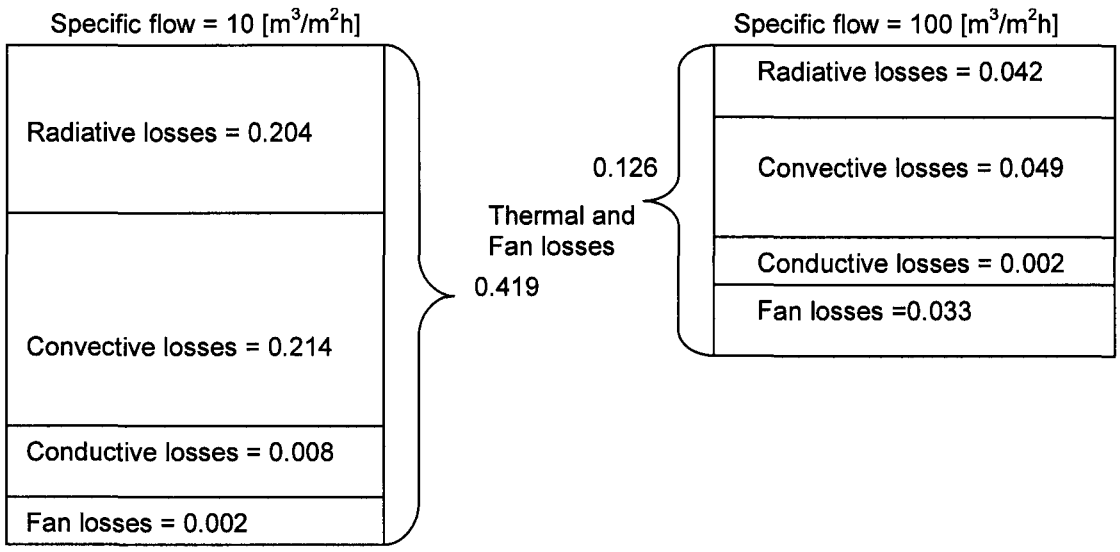

Figure 6.4: Schematic quantification of the thermal and fan losses inside the panel at a specific flow rate of 10 and 100 [m^3/m^2h].

As was mentioned in § 4.5 the conductive heat losses through the back and edges do not play a huge part if the insulation thickness is made sufficiently thick. The convective and radiative heat losses however are much harder to be controlled. They depend on the first absorber temperature, which determines the cover temperature of the panel. We cannot afford to add another cover to decrease the heat losses, because both the irradiance that hits the first absorber and the electrical output would decrease with it. Since the amount of heat losses in the interesting specific flow range is already small due to the addition of the first cover, a second cover would thus not be beneficial.
This means the heat losses through the cover can hardly be influenced. Only by lowering the absorption coefficient of the first absorber, while keeping the same electric output, can the heat losses be directly reduced.
An indirect way of lowering the heat losses is to increase the heat transfer rate to the collector medium.

Collector yield
The yield of the panel consists of electrical output and heat output. In this report the electric efficiency of the cells was put to zero, which means all absorbed irradiance was used for the generation of heat.
The yield of the collector consists of the heat transferred to the collector medium by the first and second absorber. We have seen in this report that the heat transfer to the collector medium can be changed in two ways: varying the collector medium velocity with the mass flow or collector medium height and a change in heat transfer coefficient through the use of fins or other heat transfer inducing devices. Both ways have the disadvantage that the pressure drop over the collector medium channel and thus the fan power increases with every attempt to increase the heat transfer.
The influence of the variation in velocity is represented schematically in figure (6.5).

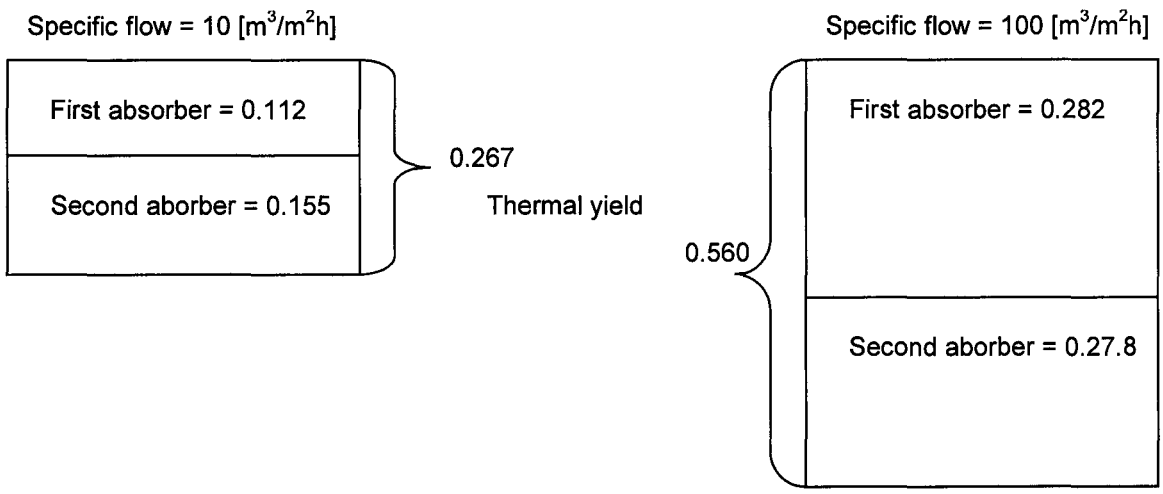

Figure 6.5: Schematic quantification of thermal yield of the first and second absorber at a specific flow rate of 10 and 100 [m^3/m^2h].

Another way to influence the thermal profit of the collector, especially in the low speed range, is to add fins to the second absorber. The advantage of fins is that the second absorber temperature will decrease. This means more heat can be transferred to the collector medium. Another advantage is the fact that the radiative heat transfer from the first to the second absorber will increase, thus decreasing the first absorber temperature. This means the thermal losses, which

depend on the first absorber temperature, decrease. As said before the disadvantage will be an increase in fan power. As long as the increase in heat output is bigger than the extra pressure drop compared to a finless channel, the fins have a positive effect on the net efficiency of the panel.
Fins however are not effective enough to obtain a reasonable heat transfer gain at specific flows usually used in solar air collectors.

6.2 Conclusions

- A good functioning model has been constructed to describe the energy flows inside a two absorber PV/T air panel. It has been proven to be very adequate for describing the loss mechanisms in a PV/T air panel.
- Good efficiencies require high specific flows to obtain good heat transfer. The incorporation of fins to the second absorber has only a small influence on the collector performance.
- The energy/power loss caused by pressure drop over the collector channel and its support system is relatively small.

6.3 Recommendations

For future research a few recommendations can be made.

- The influence of porous materials that can be used as second absorber and the configuration with three absorbers as proposed by Tripanagnostopoulos (2001) can be modeled as a replacement of the two-absorber channel that was treated here.
- More research of the processes that occur when fins are placed inside the collector medium channel and its influence on both the heat transfer and pressure drop must be performed.
- The influence of fixing (thin) fins to the first absorber and its influence on the absorber temperature and resulting thermal losses inside the system.
- The addition of swirls to the first absorber.

Bibliography

Adel, A. H., *Comparative study of the performances of four photovoltaic/thermal solar air collectors*, Energy Conversion and Management, Volume 41, Issue 8, May 2000, Pages 861-881

Bejan, A, Heat transfer, John Wiley & Sons, New York, 1993

Churchill, S.W., *Comprehensive Correlating Equations for Heat Mass and Momentum Transfer in Fully Developed Flow in Smooth Tubes,* Ind. Eng. Chem. Fundam., Vol. 16, No. 1, pp.109-I 16, 1977

Coventry, J.S., K. Lovegrove, *Development of an approach to compare the 'value' of electrical and thermal output from a domestic PV/Thermal system,* Solar Energy vol75, pp 63-72, 2003

Duffie, J.A., W.A. Beckman, *Solar engineering of thermal processes*, John Wiley & Sons, New York, 1980

Fechner, H., O. Bucek, *Solar Air collectors - Investigations on several series produced collectors*, ISES - Solar World Congress, Jerusalem July 1999

Garg, H.P., R. S. Adhikari, *Conventional hybrid photovoltaic/thermal (PV/T) air heating collectors: steady-state simulation*, Renewable Energy, Volume 11, Issue 3, July 1997, Pages 363-385

Garg, H.P., R. S. Adhikari, *System performance studies on a photovoltaic/thermal (PV/T) air heating* collecto, Renewable Energy, Volume 16, Issues 1-4, January-April 1999, Pages 725-730

Goswami, D.Y., F. Kreith, J.F. Kreider, Principles of solar engineering, Taylor & Francis, 2000

Hastings S.R., *Solar Air Systems - Built Examples* , James and James 1999

Kakac, S., Shah, R.K and Aung, W., *Handbookof Single-Phase Convective Heat Transfer*, John Wiley & Sons, New York, 1987

Kotcioglu, I., T. Ayhan, H. Olgun, B. Ayhan, *Heat transfer and flow structure in a rectangular channel with wing-type vortex generator*, Tr. Journal of engineering and environmental science, Volume 22, 1998, pages 185-195

Lienhard IV, J.H., J.H. Lienhard V, *A heat transfer textbook, Phlogiston press*, Massachusetts, 2003

Moummi, N., S. Youcef-Ali, A. Moummi, J. Y. Desmons, *Energy analysis of a solar air collector with rows of fins*, Renewable Energy, Volume 29, Issue 13, October 2004, Pages 2053-2064

Poppel, S.J. van, *Analysis of transmission and absorption of solar cell devices for application in photovoltaic/thermal combi-panels*, University of Eindhoven, 2002

Sandnes, B., J. Rekstad, *A photovoltaic/thermal (PV/T) collector with a polymer absorber plate. Experimental study and analytical model*, Solar Energy, Volume 72, Issue 1, January 2002, Pages 63-73

Swinbank W.C., *Long-wave radiation from clear skies*, Q. J.R. Meteor. Soc., 89, 339–348, 1963

Tripanagnostopoulos, Y.,Th. Nousia, M. *Souliotis Low cost improvement to building integrated air cooled hybrid PV-thermal systems*, In Proceedings 16th EPSEC, Glasgow, 2000

Tripanagnostopoulos, Y., Th. Nousia, M. Souliotis, *Test results of air cooled modified PV modules*, In Proceedings 17th EPSEC, Munich, (2001)

Vries, D.W. de, *Design of a photovoltaic/thermal combi-panel*, Reportnumber WET 2002.07, University of Eindhoven, 1998

Youcef, A.S., *Study and optimalization of the thermal performance of the offset rectangular plate fin absorber plates, with various glazing*, Renewable Energy, Volume 30, Issue 2, February 2005, Pages 271-280

Zolingen, R.J.Ch. van, *Zonnecellen*, University of Eindhoven, 2003

Zondag, H.A., W.G.J. van Helden, *PV-Thermal domestic systems*, World conference on photovoltaic energy conversion, Osaka, Japan, may 2003

World wide web | interesting links

http://www.appliedfilms.com/Precision2/11_photovoltaic/photovoltaic_02.html

http://www.courses.ait.ac.th/ED06.22/course1/lecs/

http://hyperphysics.phy-astr.gsu.edu/hbase/solids/pnjun.html

http://www.mysolar.com/mysolar/pv/techorient.asp

http://www.novem.nl/generalroutines/OphDocument.asp?ID=2647&DeelsIte=I

List of figures

Appendix A

```
clear all
close all
format short


%%%% Definiton of the matrices %%%%
Z=[]; BETA=[]; GETA=[]; FRETA=[]; RE=[]; NU=[]; NU1=[]; NU2=[]; NU3=[]; TPM=[]; TCM=[]; U=[];
UE=[]; UB=[]; UL=[]; FF=[]; QP=[]; QU=[]; QB=[]; QV=[]; DELTAP=[]; WP=[]; H=[];
UTOT=[]; UEE=[]; UBB=[]; UTT=[]; HH=[]; HUE=[]; HUEUB=[]; HUEUBUT=[];
HCATOT=[]; HPCTOT=[]; FRIC=[]; QUUU=[]; TCC=[]; TCMM=[]; TBB=[]; TPMM=[];
GZ=[]; NUpflam=[]; NUpfturb=[]; NUPFlam=[]; XTH=[]; HCA=[]; HCCA=[]; Qp=[]; Qb=[];
TT=[]; TV=[]; RE1=[]; ETANET=[]; LCOND=[]; LRAD=[]; LCONV=[]; QNET=[]; TCCCC=[]; QCX=[]
HCBF=[]; HRPB=[]; HCPF=[] HCPC=[]; HRPC=[]; HCCA=[]; HRCA=[]; HCCA=[]; QA1=[]; QA2=[];

%%%% First loop to vary the collector parameter %%%%

for m=0:0.01:0.1;        %mass flow rate [kg/s]
   Z=[Z,m];              %matrix varieted pararmeter
   META=length(Z);       %length of matrix varieted pararmeter

%%%%%%%%%%%%% Varieted model parameter %%%%%%%%%%%%%%%%
l=0.04;                  %heigth between cover and absorber [m]
g=0.02;                  %heigth of the channel [m]
V=2;                     %windspeed
epsp1=0.9;               %emission quotient of the top of the plate
epsp2=0.9;               %emission coeffient from the bottom of the plate
epsb=0.9;                %emission quotient of the backplate

%%%%%%%%%%%%% Constant model parameters %%%%%%%%%%%%%%%%
L=5;                     %length of collector
w=1  ;                   %width of collector
epsc=0.9;                %emission quotient of the cover
sigma=5.67e-8;           %Stefan_Boltzmann constant
cp=1006;                 %specific heat at constant pressure of air
k=0.026;                 %conduction coefficient of air at 30 degrees celcius
alfa=0.64577;            %corner withthe earth in which the collector is situated (in rad:
(alfa/360)*2*pi)
beta=37;                 %inclined angle
ki=0.045;                %insulation conductivity of back and edge collector
ti=0.1;                          %thickness of the insulation
Ac=w*L;                  %area of the collector
Pr=0.72;                 %Prantl number for air

%%%%%%%%%%%%% Calculation Hydraulic diameter %%%%%%%%%%%
Ad=w*g;                  %area of the inflow duct
p=2*w+2*g;               %perimeter of the inflow duct
Dh=4*Ad/p;               %hydraulic diameter of the inlow duct

%%%%%%%%%%%%% Stepsize and number of loops %%%%%%%%%%%%%
dx=0.01;                 %stepsize of increments over L
n=L/dx;                  %number of increments over L
loop=10;                 %number of loops that is repeted in the calculation
```

```
%%%%%%%%%%%%% initial conditions %%%%%%%%%%%%%%%%%%%%%%
Tpm=zeros(loop,n);  Tb=zeros(loop,n);  Tcm=zeros(loop,n);  Ts=zeros(loop,n);
Tc=zeros(loop,n); hrpc=zeros(loop,n); hrca=zeros(loop,n); Ul=zeros(loop,n);  hrpb=zeros(loop,n);
hcpc=zeros(loop,n); Nupc=zeros(loop,n); F=zeros(loop,n);   h=zeros(loop,n);

Tpm(1,1:n)=380;         %initial temp of the collector plate [K]
Tb(1,1:n)=360;          %initial temp of the back plate [K]
Tcm(1,1:n)=283;         %temp of the collector medium at the inlet [K]
Tamb=283;               %ambiant temp outside the collector [K]
Tc(1,1:n)=320;          %temperature of the cover plate [K]
Ts=0.0552*Tamb^1.5;             %skytemperature [K]

%%%%% Second loop, which counts the number of iteration loops %%%%%%
for     b=1:loop-1;             %number of loops to calculate the temperatures and efficiencies
        X=[];                   %matrix with increment position from x=0

   %%%%%% Third loop over all the increments dx %%%%%%
   for  a=1:n;          %number of increments over the length of the collector
        x=dx*a;         %position of increment from x=0
        X=[X,x];        %filling of matrix X

     %%%%% abs, trans, refl %%%%%%%%%%%%%%%%%%%%%%%%%
    ac=0;               %absorption coeficient cover
    tc=0.92;            %transmission of the cover
    rc=1-tc;            %reflection coefficient cover

    ap1=0.4;            %absorption coeficient of the first absorber
    tp1=0.36;           %transmission of the first absorber
    rp1=1-ap1-tp1;        %reflection coefficient of the first absorber


    ap2=0.96;           %absorption coeficient of the second absorber
    tp2=0;              %transmission of the second absorber
    rp2=1-ap2-tp2;      %reflection coefficient of the second absorber


     as=tc*ap1;                 %amount of irradance absorbed by first absorber
     as2=tc*tp1*ap2;            %amount of irradance absorbed by second absorber

     %%%%% Irradiance and amount absorbed %%%%%%%%%%%%%%%%%%%
     Is=500;            %amount of solar irradiation  [W/m^2]
     Ha=as*Is;           %amount of power received by first absorber [W/m^2]
     Hb=as2*Is;          %amount of power received by second absorber [W/m^2]

     %%%%% Averaged temp cover to first absorber %%%%%
     Td=(Tpm(b,1)+Tpm(b,a))/2;
     Tf=(Tc(b,1)+Tc(b,a))/2;
     Tg=(Td+Tf)/2;

     %%%%% Averaged temp cover ambient %%%%%%%%%%%%%
     Tr=(Tf+Tamb)/2;

     %%%%% Averaged temp first to second absorber %%%%%%%%%%%%%%%
     Tw=(Tpm(b,1)+Tpm(b,a))/2;
     Tq=(Tb(b,1)+Tb(b,a))/2;
```

```
Te=(Tw+Tq)/2;

if          Tw-Tq>0
            Tgf=Tw-Tq;
            else Tgf=Tq-Tw;    %loop to check which absorber has the largest temp
end
%%%%% Averaged temperature collector medium (CM) %%%%%%%%%%%%
Ttr=(Tcm(b,1)+Tcm(b,a))/2;

%%%%% Calculation temp dependent Rayleigh number %%%%%%%%%%%%
n1=1.0e+009 * 1.48772802867131;
n2=1.0e+009 *-0.00769661818182;
n3=1.0e+009*0.00001019510490;

Racon11=(n1+n2*Tg+n3*Tg^2)*(Td-Tf)*l^3;    % Rayleighnumber first absorber and cover
Racon1=real(Racon11);                      % Rayleighnumber first absorber and cover
Racon22=(n1+n2*Te+n3*Te^2)*(20)*l^3;       % Rayleighnumber first and second absorber
Racon2=real(Racon22);                      % Rayleighnumber first and second absorber

Racov1=(n1+n2*Tr+n3*Tr^2)*(Tf-Tamb)*L^3;       % Rayleighnumber cover to ambient
Racov=real(Racov1);                            % Rayleighnumber cover to ambient

%%%%% Calculation temp dependent dynamic viscosity %%%%%%%%%%
y1=1.0e-006*0.76480282935467;
y2=1.0e-006 *0.06930327144120;
y3=1.0e-006 *-0.00003460906909;

muu=(y1+y2*Ttr+y3*Ttr^2);                  % dynamic viscosity of the air inside the channel
mu=real(muu);                              % dynamic viscosity of the air inside the channel
muamba=(y1+y2*Tamb+y3*Tamb^2);                   % dynamic viscosity of the ambient air
muamb=real(muamba);                        % dynamic viscosity of the ambient air

REA=V*L/muamb;

%%%%% Calculation temp dependent density %%%%%%%%%%%%%%%%%%%%
p1=3.71251987032125;
p2=-0.01276695549661;
p3=0.00001436402678;

rhop=(p1+p2*Ttr+p3*Ttr^2);                 % density of air inside channel
rho=real(rhop);                            % density of air inside channel

rhoambs=(p1+p2*Tamb+p3*Tamb^2);            % density of ambient
rhoamb=real(rhoambs);                      % density of air inside channel

%%%%% Calculation temp dependent thermal conductivity %%%%%%%%
l1=0.03493255244755;
l2=-0.00012531468531;
l3=0.00000031468531;

kpcp=l1+l2*Tg+l3*Tg^2;                     % thermal conductivity of air cover and absorber
kpc=real(kpcp);                            % thermal conductivity of air cover and absorber

kcmc=l1+l2*Ttr+l3*Ttr^2;                   % thermal conductivity of air inside channel
kcm=real(kcmc) ;                           % thermal conductivity of air inside channel
```

```
%%%%% Velocity of the collector medium %%%%%%%%%%%%%%%%%%%%%%
v=(m/rho)/Ad;                    %velocity of the collector medium

%%%%% specific flow %%%%%%%%%%%%%%%%%%%
FG=(Z/rho)*3600/Ac;              %specific flow

%%%%% Calculation of pressure drop support system %%%%%%%%%%%
L1=5;                            %length support system
Dh1=0.1;                         %diameter system
A1=Dh1^2*pi/4;                   %area system
v1=(m/rho)/A1;                   %velocity system
Re1=Dh1*v1/mu;                   %Reynoldsnumber system
B1=(pi*(Dh1^2)/4)/A1;
Cb1=16*exp(0.294*B1^2+0.068*B1-0.318);
ks=0;
if          real(Re1) < 2300
                fric1=Cb1/Re1;
                deltaP1=(1/2)*fric1*(4*L1/Dh1)*rho*v1^2;
elseif      2300 <= Re1 <= 1e4
                fric1=0.079*Re1^(-1/4);
                deltaP1=(1/2)*fric1*(4*L1/Dh1)*rho*v1^2;
elseif      Re1 > 1e4
                fric1=0.046*Re1^(-1/5);
                deltaP1=(1/2)*fric1*(4*L1/Dh1)*rho*v1^2;
end

%%%%% Calculation of the pressure drop over the collector %%%%%
Ref=rho*v*Dh/mu;
Re=real(Ref);                    %Reynoldsnumber inside the channel
B=(pi*(Dh^2)/4)/Ad;
Cb=16*exp(0.294*B^2+0.068*B-0.318);
ks=0;
if          real(Re) < 2300
                fric=Cb/Re;
                deltaP2=(1/2)*fric*(4*L/Dh)*rho*v^2;
elseif      2300 <= Re <= 1e4
                fric=0.079*Re^(-1/4);
                deltaP2=(1/2)*fric*(4*L/Dh)*rho*v^2;
elseif       Re > 1e4
                fric=0.046*Re^(-1/5);
                deltaP2=(1/2)*fric*(4*L/Dh)*rho*v^2;
end

%%%%% calculation of total fan power %%%%%%%%%%%%%%%%%%%%%%%
deltaP=deltaP1+deltaP2;          %Total pressure drop over the system
etac=0.45;                       %fan efficiency
Wp=(1/etac)*(m/rho)*deltaP;      %Total power of the fan
Replate=rhoamb*V*L/muamb;        %Reynoldsnumber at the top of the cover


%%%%% Calculation of heat transfer coefficients %%%%%%%%%%

    %%%%% Radiative heat transfer coefficients %%%%%%%%%%%%%%%%%%
hrca(b,a)=epsc*sigma*((Ts^2+(Tc(b,a)^2))*(Ts+Tc(b,a)));     %riadiative h.t.c. cover and ambient
hrpc(b,a)=sigma*(Tpm(b,a)+Tc(b,a))*(Tpm(b,a)^2+Tc(b,a)^2)/((1/epsp1)+(1/epsc)-1);   %radiative
h.t.c. between plate and cover
```

```
hrpb(b,a)=sigma*(Tpm(b,a)+Tb(b,a))*(Tpm(b,a)^2+Tb(b,a)^2)/((1/epsp2)+(1/epsb)-1);
%radiative h.t.c. from plate to back plate

    %%%%% Convective heat transfer coefficients %%%%%%%%%%%%%%%%%

      %%%%% cover to ambient %%%%%%%%%%%%%%%%%%%%%%%%
    if      Racov<=1e7
                Nuccalam=0.59*Racov^(1/4);
    else    Nuccalam=0.13*Racov^(1/3);
    end

    Nuccaturb=0.036*REA^(4/5)*Pr^(1/3);
    Nucca=(Nuccalam^4+Nuccaturb^4)^(1/4);
    hcca(b,a)=Nucca*k/L;

    %%%%% convection first absorber to cover %%%%%%
    sa=(1708/(Racon1*cos(alfa)));
    SA=1-sa;
    if  SA<=0;
            SA=0;
    end

    ga=(Racon1*cos(alfa)/5830)^(1/3);
    GA=ga-1;
    if  GA<=0;
            GA=0;
    end

     ja=(sin(1.8*alfa)^(1/6)*1708)/(Racon1*cos(alfa));
    Nupc=1+1.44*(SA)*(1-ja)+(GA);    %Nusselt number between cover and absorber
    if  Nupc<=1;
            Nupc=1;
    end
    hcpc(b,a)=Nupc*kpc/l;          %Convective h.t.c. from first absorber to cover

      %%%%% first and second absorber to CM %%%%%%%%%
      Xth=0.05*Re*Pr*Dh;          %thermiche inlooplengte
      Gz=(pi/4)*((x/Dh)/(Re*Pr))^-1;          %Graetz number

      Nupflam1=4.364*((1+(Gz/29.6)^2)^(1/6));
      Nupflam2=(1+(Pr/0.0207)^(2/3))^(1/2);
      Nupflam3=(1+(Gz/29.6)^2)^(1/3);
      Nupflam4=(1+((Gz/19.04)/(Nupflam2*Nupflam3))^(3/2))^(1/3);

      Nupflam=Nupflam1*Nupflam4;          % Nusselt number for laminar flow, with
thermal entrance length effect

    Nupfturb=(Pr*0.0192*(Re^(3/4)))/(1.22*(Re^(-1/8))*(Pr-2)+1);    %Nusselt number for
developed turbulent flow

    if  Re<=2300
            Nupf=Nupflam;
    else
            Nupf=Nupfturb;
    end
```

```
hcpf(b,a)=Nupf*kcm/Dh;          %Convective h.t.c. first absorber to CM
hcbf(b,a)=Nupf*kcm/Dh;          %Convective h.t.c. first absorber to CM

hcatot(b,a)=hcca(b,a)+hrca(b,a);
hpctot(b,a)=hcpc(b,a)+hrpc(b,a);

%%%%% total h.t.c. under the first absorber %%%%%%%%%%%%%%%%

h(b,a)=hcpf(b,a)+(1/(1/hrpb(b,a)+1/hcbf(b,a)));

%%%%% Calculation of collector loss coefficients %%%%%%%%%%%%

Ut(b,a)=(1/(hcpc(b,a)+hrpc(b,a))+(1/(hcca(b,a)+hrca(b,a))))^-1;    %Top loss coefficient
Ubr(b,a)=ki/ti;                                  %Back loss coefficient
Ue(b,a)=((l+g)*w*2+(l+g)*L*2)*(ki/ti)/Ac;                  %Edge loss coefficient

Ub(b,a)=Ubr(b,a)+Ue(b,a);                  %Integration of back with edge losses

Ul(b,a)=Ut(b,a)+Ue(b,a)+Ubr(b,a);          %Total Loss coefficient of the solar collector

%%%%% Calculation of collector efficiency factor %%%%%%%%%%%%
F(b,a)=h(b,a)/(Ul(b,a)+h(b,a));                    %Collector efficiency factor

%%%%% Calculations of temperatures over the absorber %%%%%%%%

%Temperature of the collector medium

   Tcm(b+1,a)=(Ha/Ul(b,a)+(1/(Ul(b,a))+(hcbf(b,a)/(hcbf(b,a)+hrpb(b,a)))/(h(b,a)))*Hb+Tamb
   )-1/Ul(b,a)*(Ha+(1+(hcbf(b,a)/(hcbf(b,a)+hrpb(b,a)))*(Ul(b,a)/h(b,a)))*Hb-
   Ul(b,a)*(Tcm(1,1)-Tamb))*exp(-Ul(b,a)*F(b,a)*x/((m/w)*cp));

   %Temperature of the plate
   Tpm(b+1,a)=(Ha+Ul(b,a)*Tamb+h(b,a)*Tcm(b,a)+(Hb*(hrpb(b,a)/(hrpb(b,a)+hcbf(b,a)))))/
   (h(b,a)+Ul(b,a))   ;

   %Temperature of the back plate
   Tb(b+1,a)=(hrpb(b,a)*Tpm(b,a)+hcbf(b,a)*Tcm(b,a)+Hb)/(hrpb(b,a)+hcbf(b,a));

   %Temperature of the cover
   Tc(b+1,a)=Tpm(b,a)-((Ut(b,a)*(Tpm(b,a)-Tamb))/(hcpc(b,a)+hrpc(b,a)));

Tk(b,a)=Tc(b,a)-Tamb;
Tk1(b,a)=Tpm(b,a)-Tcm(b,a);
Tk2(b,a)=Tb(b,a)-Tcm(b,a);

end

  %%%% Calculation averaged values %%%%%
hcpff=sum(hcpf')/n;
tpm=sum(Tpm')/n;   %averaged Tpm
tcm=sum(Tcm')/n;   %averaged Tcm
tb=sum(Tb')/n;     %averaged Tb
tre=sum(Ul')/n;    %averaged Total loss coefficient
ytr=sum(Ut')/n;    %averaged Top loss coefficient
ue=sum(Ue')/n;
ub=sum(Ub')/n;
```

```
y=sum(F')/n;        %averaged value of air collector afficiency factor
hh=sum(h')/n;
ht=sum(Ul')/n;
hcatot1=sum(hcatot')/n;
hpctot1=sum(hpctot')/n;
hcbff=sum(hcbf')/n;
hrpbb=sum(hrpb')/n;
Tcc=sum(Tc')/n;
hccaa=sum(hcca')/n;


hccaaa=hccaa(1,b);
Tccc=Tcc(1,b);
tyu=tre(1,b);
ytre=ytr(1,b);
uee=ue(1,b);
ubb=ub(1,b);
f=y(1,b);
u=ht(1,b);
tpmm=tpm(1,b);
tcmm=tcm(1,b);
tbb=tb(1,b);
Hh=hh(1,b);
hcpfff=hcpff(1,b);
hcatot2=hcatot1(1,b);
hpctot2=hpctot1(1,b);
hcbfff=hcbff(1,b);
hrpbbb=hrpbb(1,b);
%%%%% Calculation of the yield losses and efficiencies %%%%

qu=m*cp*(Tcm(b,a)-Tcm(1,1));    %Total heat power output
eta=qu/(Ac*Is);                 %Thermal efficiency of the collector
etanet=(qu-Wp)/(Ac*Is);
BETA=[BETA,eta];
GZ=[GZ,Gz];
qnet=qu-Wp;
Qb=m*cp*(tbb-Tamb);
Qp=m*cp*(tpmm-Tamb;
qcond=Ac*ki/L*(tpmm-Tamb);
qconv=Ac*hccaaa*(Tccc-Tamb);
qrad=Ac*epsc*sigma*((Tccc^4)-(Ts^4));
 Akk=dx*w;
qcx=hcca(b,1:n)*Akk*Tk(b,1:n)';
qa1=hcpf(b,1:n)*Akk*Tk1(b,1:n)';
qa2=hcbf(b,1:n)*Akk*Tk2(b,1:n)';
q1=qu+qcond;
q2=qu+qcond+qcx;
q3=Is*Ac*(1-(rc+tc*rp1+tc*tp1*rp2));

end

%%%% Filling the matrices %%%%%
LCOND=[LCOND,q1];
LCONV=[LCONV,q2];
LRAD=[LRAD,q3];
HCCA=[HCCA,hccaaa];
```

```
QCX=[QCX,qcx];
QA1=[QA1,qa1];
QA2=[QA2,qa2];
HCA=[HCA,hcca(b,a)];
XTH=[XTH,Xth];                %Thermal entrance length
QU=[QU,qu];                   %Total heat output
QNET=[QNET,qnet];
U=[U,ytre];                   %Top loss coefficient
UE=[UE,uee];                  %Edge loss coefficient
UB=[UB,ubb];                  %Back loss coefficient
UL=[UL,tyu];                  %Total loss coefficient
FF=[FF,f];                    %Collector efficiency factor
H=[H,Hh];                     %Total heat transfer coefficient inside the CM-channel
HCATOT=[HCATOT,hcatot2];
HPCTOT=[HPCTOT,hpctot2];
QUUU=Ac*(Ha+Hb-Ut(b,a)*(Tpm(b,a)-Tamb)-Ub(b,a)*(Tb(b,a)-Tamb));
ETA=BETA;                     %Collector efficiency
FRIC=[FRIC,fric];             %Friction coeff inside the CM-channel
DELTAP=[DELTAP,deltaP];       %Pressure drop over the fan
WP=[WP,Wp];                   %Fan power
Qtot=QU-WP;                   %Total power output
TCMM=[TCMM;Tcm(b,1:n)];       %Collector medium temp
TPMM=[TPMM;Tpm(b,1:n)];       %First absorber temp
TBB=[TBB;Tb(b,1:n)];          %Second absorber temp
TCC=[TCC;Tc(b,1:n)];          %Cover temp
RE=[RE,Re];                   %Reynolds number inside the collector medium channel
RE1=[RE1,Re1];
TCM=[TCM,tcmm];
TPM=[TPM,tpmm];
TCCCC=[TCCCC,Tccc];
QB=[QB,Qb];
QP=[QP,Qp];
TT=[TT,Tcm(b,a)];
ETANET=[ETANET,etanet];

end

TV=[TV,TT];
ULL=(U*(tpmm-Tamb)+UB*(tbb-Tamb))/(tpmm-Tamb);  %Altered loss coefficient
pool=loop-1;
KETA=ETA(pool:pool:META*pool);     %Collector efficiency
HHH=(TPM-TCM);
HHh=HHH'*H;
HH=diag(HHh);
HhH=(TPM-Tamb);
UBB1=HhH'*UB;
UBB=diag(UBB1);
UTT1=HhH'*(U);
UTT2=diag(UTT1);
HUEUB=Ac*(HH+UBB);
HUEUBUT=Ac*(HUEUB+UTT2);
```

Dankwoord

Bij deze wil ik alle mensen bedanken die mij hebben geholpen bij de tot stand koming van dit afstudeerproject. Allereerst wil ik Ronald bedanken voor zijn grote inzet en steun tijdens het project, vooral tijdens de moeilijke periodes die ik, net als de meeste mensen, heb meegemaakt. Ook wil ik Camilo en Herbert bedanken voor hun begeleiding tijdens het project. Zij hebben ervoor gezorgd dat ik steeds met groot enthousiasme ben blijven werken om het afstuderen tot een goed einde te brengen.

Ook wil ik alle mensen bedanken die ik tot mijn vrienden ben gaan rekenen in de zes en een half jaar dat ik op de universiteit heb doorgebracht. In het bijzonder wil ik hier noemen Roel, een vriend tijdens mijn gehele periode hier, Ilona, waarvoor hetzelfde geldt, het duo Maartens, waar ik na het kiezen van de richting Thermal Fluids Engineering een mooie vriendschap mee heb opgebouwd en vooral veel ondersteuning en lol van gehad heb. Ditzelfde geldt voor verschillende andere mensen die ik tijdens mijn studie en in "de zaal" en later op " de gang" heb leren kennen.

Van de mensen naast mijn studie wil ik mijn ouders, mijn twee broers, vrienden en huisgenoten bedanken voor de geweldige tijd die ik tijdens mijn studie heb mogen beleven. En als laatste zou ik graag mijn vriendin Elke bedanken voor de ondersteuning tijdens mijn laatste jaren en vooral de laatste maanden, waarin ik erg hard heb moeten werken en weinig tijd voor haar had, maar waarbij ze me steeds bleef ondersteunen.

Met vriendelijke groeten

Hans Mollen